CO_2 Compression for Capture-Enabled Power Systems

By Rajat Suri

B. A. Sc. Chemical Engineering, University of Waterloo, 2007

B. A. Economics, University of Waterloo, 2007

Submitted to the Department of Chemical Engineering
in partial fulfillment of the requirements for the degree of

Masters of Science

at the

MASSACHUSETTS INSTITUTE OF TECHNOLOGY

January 2009
[Feb]

Author .....

Rajat Suri
Department of Chemical Engineering
15th January 2009

Certified by .....

Gregory J. McRae
Hoyt C. Hottel Professor of Chemical Engineering
Thesis Supervisor

Accepted by .....

William M. Deen
Professor of Chemical Engineering
Chairman, Committee for Graduate Students

Carbon Dioxide Compression for Capture-Enabled Power Systems

by

Rajat Suri

Submitted to the Department of Chemical Engineering
on 15th Jan 2009 in partial fulfillment of the
requirements for the Degree of Masters of Science in Chemical Engineering

Abstract

The objective of this thesis is to evaluate a new carbon dioxide compression technology – shock compression – applied specifically to capture-enabled power plants. Global warming has increased public interest in carbon capture and sequestration technologies (CCS), but these technologies add significant capital and operating cost at present, which creates a significant barrier to adoption.

Carbon dioxide compression technology makes up a high proportion of the additional cost required, making it a focal point for engineering efforts to improve the economic feasibility of carbon capture. To this effect, shock compressors have the potential to reduce both operating and capital costs with supporting compression ratios of up to 10:1, requiring less stages and theoretically allowing for the possibility of heat integration with the rest of the plant, allowing waste heat to be recovered from hot interstage compressed carbon dioxide.

This thesis first presents a technical context for carbon dioxide compression by providing an overview of capture technologies to build an understanding of the different options being investigated for efficient removal of carbon dioxide from power plant emissions. It then examines conventional compression technologies, and how they have each evolved over time. Sample engineering calculations are performed to model gas streams processed by these conventional compressors.

An analysis of shock compression is carried out by first building a background in compressible flow theory, and then using this as a foundation for understanding shock wave theory, especially oblique shocks. The shock compressor design is carefully analyzed using patent information, and a simulation of the physics of the shock compressor is created using equations from the theory section described earlier.

A heat integration analysis is carried out to compare how conventional compressor technologies compare against the new shock compressor in terms of cooling duty and power recovery when integrated with the carbon dioxide capture unit. Both pre-combustion IGCC using Selexol and post-combustion MEA configurations are considered and compared.

Finally an economic analysis is conducted to determine whether shock compression technology should be attractive to investors and plant managers deciding to support it. Key factors such as market, macroeconomic and technical risk are analyzed for investors, whereas a comparison of capital and operating cost is carried out for plant managers. Relevant risks associated with new compression technologies are also analyzed.

It is found that there is no significant operating cost benefit to the shock compressor over the conventional compressor, both costing $3,700/hr for an IGCC plant. Power recovery is simply too low to justify the high power requirements in operating a shock compressor with a 10:1 ratio. The technical claims of the shock compressor (such as projected discharge temperature and pressures) seem reasonable after basic modeling, which shows a higher temperature and pressure than claimed by Ramgen.

Thesis Supervisor: Gregory McRae
Title: Hoyt C. Hottel Professor of Chemical Engineering

Acknowledgements

I would like to thank Randall Field and Professor Gregory McRae for the guidance they provided during the production of this thesis. I would like to thank the Carbon Sequestration Initiative and BP for the financial support they provided.

Contents

List of Figures

List of Tables

Chapter 1

Introduction

1.1 Global warming can have harmful effects on human life

Global warming has been well-documented in both academic and popular literature, both of which have strongly influenced policy-making in developed countries around the world. The basic issues will be recapped in the following sections to allow the analyses and conclusions of this study to be understood in context.

1.1.1 Increases in surface temperature have accelerated

It is a fact that the temperature of the Earth has been increasing rapidly in the industrial age. Historical climate data show that global temperatures have risen by about 0.2 C per decade for the last 30 years, which means the mean temperature of the world is now near its peak for the last 12,000 years (see Figure 1-1) [1]. In addition, the ten warmest years on record have taken place after 1990, showing the recent upswing in global temperatures. This sharp change in climate has also been perceived in ecological systems. Several types of animal and plant species have been moving poleward by an average of 6 km a decade for the last 40 years. Seasonal events such as egg laying occur 2-3 days earlier each decade in the Northern hemisphere.

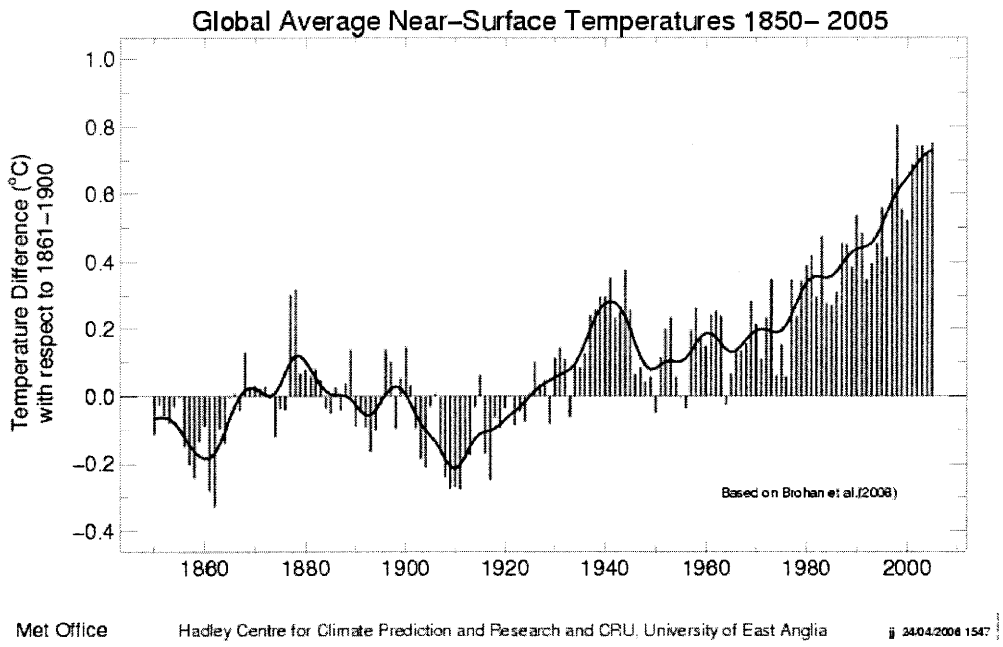

Figure 1-1: Temperature chart showing how the earth has warmed 0.7 C since 1900 [1]

However, it must be noted that these increases in temperature have not occurred uniformly or consistently across the world. Temperature has varied sharply in different parts of the world (see although there is a clear trend in an overall upward direction).

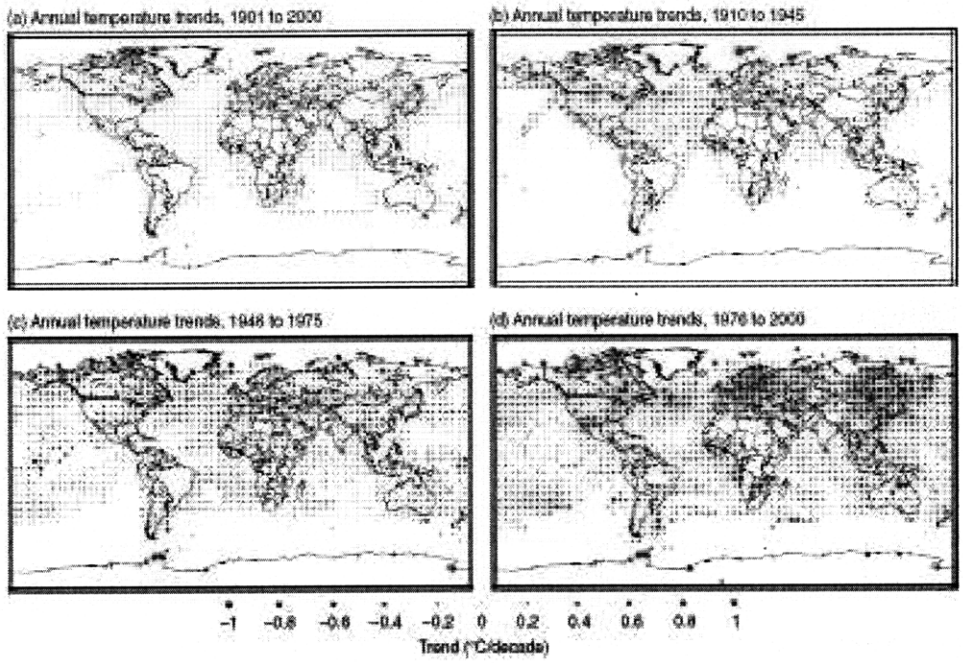

Figure 1-2: Regional temperature trends over different periods of the 20th century [2]

Other significant changes that have taken place as a result of this perceived warming of the globe include a 10% decrease of snow cover since the 1960s as well as an increase in total water vapor in the atmosphere by several percent [2]. Most famously, sea levels have also been rising by about 1-2 mm a decade due to the expansion of water due to the warming, in addition to the melting of polar ice caps. Another well-known conclusion of the Third Assessment Report of the Inter-governmental Panel for Climate Change (IPCC) is that the variability of extreme precipitation events such as hurricanes has increased in the past decades.

1.1.2 Carbon Dioxide emissions are to blame for increases in surface temperature

The increase in temperature of the Earth can be explained by first understanding the technical details of the greenhouse effect. Radiant energy has two main sources – the Sun and the Earth itself. The significant difference in temperature between the two

bodies (some 5700 K) means that each body emits energy in different sections of the electromagnetic spectrum. For example, radiation from the Sun is at 2000 – 50000 cm^{-1}.whereas radiation from the Earth ranges from 50 – 2500 cm^{-1}. This is important because radiation in the atmosphere can be absorbed by gas molecules, increasing their kinetic energy and causing them to collide with a greater impact with other gas molecules.

The greenhouse effect can be more comprehensively understood by examining Figure 1-3. The greenhouse gas layer can be modeled as a slab of glass, reflecting radiation in some wavelengths and transmitting others. Short-wave radiation from the Sun is transmitted, heating the earth to a temperature T. The Earth then emits long-wave radiation according to Stefan-Boltzmann's law: $U = \sigma T^4$, where U is the upward flux of long-wave radiation. The amount of radiation reflected back to space is called albedo. The average albedo is about 0.3, meaning 30% of the radiation from the sun is reflected back into the atmosphere[3]. In the diagram, U = 0.3 I.

A model can be constructed to depict the energy balance of the atmosphere as follows:

$$\frac{S}{4}(1-A) = \varepsilon\sigma T^4 \qquad (1.1)$$

In this equation A represents albedo (0.3), S represents solar constant of 1840 $W/m^2/K$, σ represents the Stefan Boltzmann constant 5.67 x 10^{-8} $W/m^2/K$, ε represents atmosphere constant due to the greenhouse effect and T is the temperature in Kelvin. If we assume the atmospheric constant is 0.612, the average temperature of the Earth in the zeroth order is around 288 K or 59 F [4].

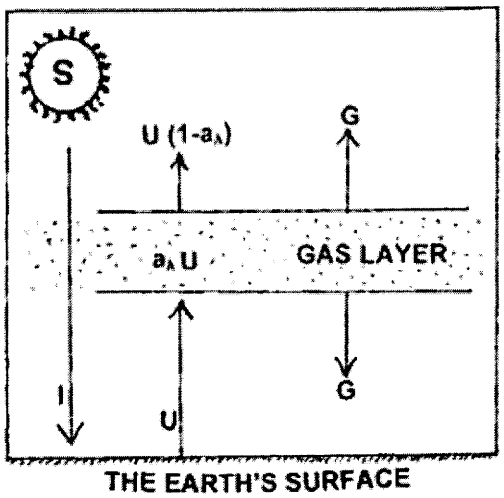

Figure 1-3: The greenhouse effect [5] G represents the flux of radiation from the atmosphere upwards and downwards and a represents the proportion of albedo absorbed by the atmosphere

There are many different greenhouse gases (or 'forcing' agents), but carbon dioxide is the main absorber in the range of wave numbers from 500 to 800 cm^{-1}. This is considered long-wave radiation, and is absorbed mostly by gases produced by humans such as methane. Other atmospheric gases such as nitrogen and ozone absorb radiation at much shorter wavelengths. Ozone is especially important since it absorbs a high proportion of incoming short-wave radiation. However, carbon dioxide is considered the most important gas in the atmosphere in terms of impact on the increase in temperature observed in the last few decades (see Figure 1-4).

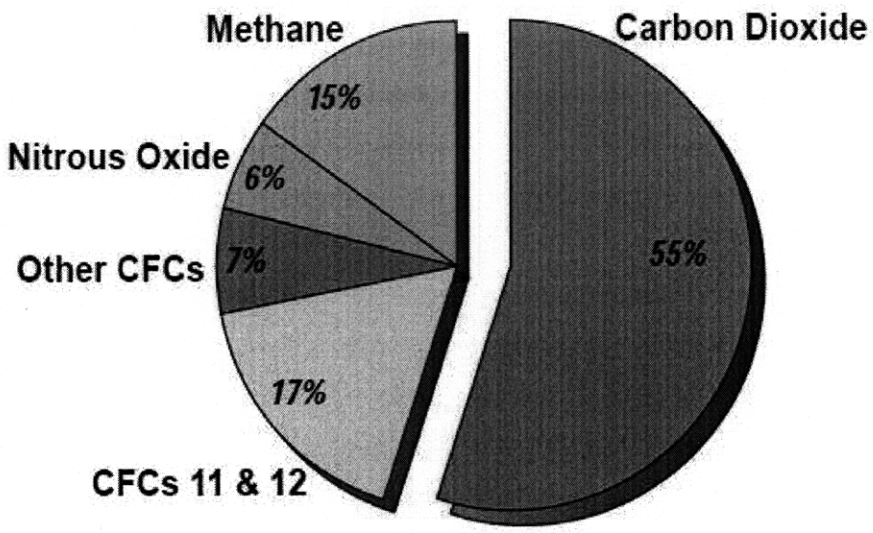

Figure 1-4: Relative contributions to additional radiation forcing (thus increasing the temperatures at the surface) between 1980 and 1990 [1]

Thus, the consensus in the mainstream scientific community is currently that the sharp growth in carbon dioxide levels in the atmosphere is due to human activity [1 2]. Carbon dioxide is currently at a concentration of 367 parts per million in the atmosphere . This is a significant increase from 285 ppm in 1750 (see Figure 1-5). It is thought that these levels of carbon dioxide have not been seen in the atmosphere for the last 20 million years. The sharp increase in the last few centuries and the corresponding decrease in oxygen suggest that these increases are due to the fossil-fuel combustion for energy purposes or possibly land-use changes from deforestation. [2] In addition the concentration of carbon dioxide in the air trapped in the ice cores has dramatically increased since 1980. [2]

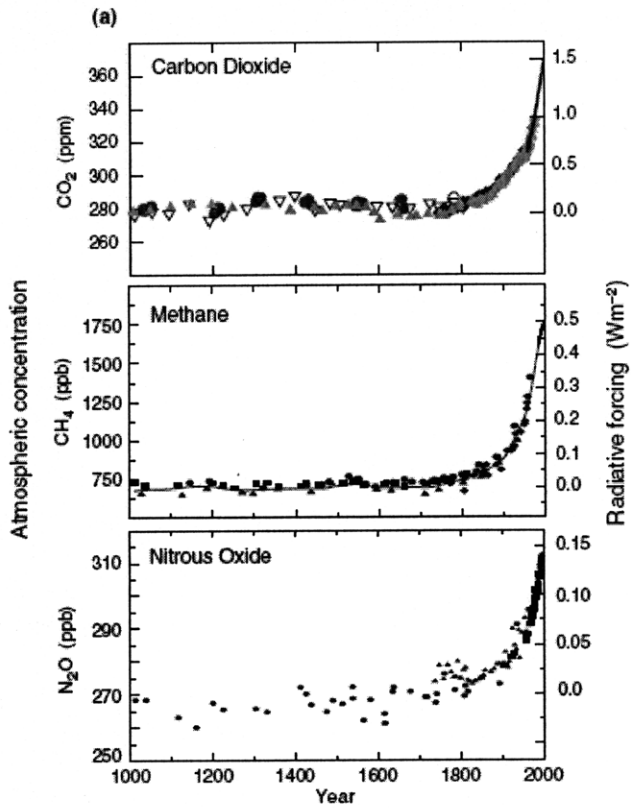

Figure 1-5: Concentrations of various forcing agents over time and corresponding 'radiative forcing' (amount of energy absorbed per unit area) [2]

The Kaya equation tries to formulate a relationship between carbon emissions and human activity by expressing net carbon emissions in terms of energy efficiency, economic efficiency and carbon intensity in energy sources used. It is best used to understand the breakdown of the wider global warming problem into four distinct smaller issues that can targeted separately by policymakers.

$$C = [GDP * E / GDP * Cg / E] - S \qquad (1.2)$$

Where

C = Net Carbon Emissions

GDP = Gross Domestic Product

E = Total energy use

Cg = carbon emissions generated in CO_2

S = Natural or induced sequestration of carbon

This equation shows how carbon emissions are directly related to various factors such as economic activity (GDP), overall energy efficiency in the economy (E/GDP) and carbon intensity of the energy (Cg/E). To provide some benchmarks, the energy intensity of the US economy from 1985 to 1996 was around 17 MJ per dollar of GDP (in 1987 dollars). This equation provides a useful framework in section 1.2 where each specific factor is examined in turn.

1.1.3 Consequences of global warming are disastrous

Naturally, a sudden change in global conditions can have sharp adverse effects on various worldly systems. Computer models predicting these changes have been developed by the IPCC, and they have released their forecasts complete with confidence levels (see Table 1-1).

Table 1-1: Changes in phenomenon due to global warming and the probability they will occur [2]

Confidence in observed changes (latter half of the 20th century)	Changes in Phenomenon	Confidence in projected changes (during the 21st century)
Likely	Higher maximum temperatures and more hot days over nearly all land areas	Very likely
Very likely	Higher minimum temperatures, fewer cold days and frost days over nearly all land areas	Very likely
Very likely	Reduced diurnal temperature range over most land areas	Very likely
Likely, over many areas	Increase of heat index[a] over land areas	Very likely, over most areas
Likely, over many Northern Hemisphere mid- to high latitude land areas	More intense precipitation events[b]	Very likely, over many areas
Likely, in a few areas	Increased summer continental drying and associated risk of drought	Likely, over most mid-latitude continental interiors (Lack of consistent projections in other areas)
Not observed in the few analyses available	Increase in tropical cyclone peak wind intensities[c]	Likely, over some areas
Insufficient data for assessment	Increase in tropical cyclone mean and peak precipitation intensities[c]	Likely, over some areas

Broadly speaking, there are several risk factors, but perhaps the biggest one is the possibility of a positive feedback loop, where global warming causes even more greenhouse gases to be emitted to the atmosphere, further aggravating the problem. This could be because of the permafrost thawing, thus releasing large quantities of

methane into the air, or else because higher temperatures enable plants and soils to take up less carbon from the atmosphere. The water cycle might become more volatile and lead to more extreme situations, worsening problems such as drought in some parts of the world while producing more violent and damaging storms in other parts. Ocean and wind circulation patterns might be drastically and suddenly altered, harming species that cannot evolve fast enough. Finally and most famously, the oceans may rise significantly due to the melting of the Greenland or West Antarctic ice sheets, flooding several land areas.

Clearly these shifts could be catastrophic to an ecology used to changes occurring at a much more moderate pace. Thus, many countries have decided to focus efforts on mitigating climate change by reducing greenhouse gas emissions instead of trying to adapt to the problem. One of the chief targets of planned policy efforts has been that of stationary power systems.

1.2 The Importance of Power Systems in the effort to reduce global warming

Because electric power generation relies on fossil fuels so heavily, it has become one of the centerpieces of global warming government policy and clean energy initiatives around the world. In fact, 36% of US carbon emissions is solely due to the production of electricity. As mentioned previously, there are three ways of reducing carbon emissions from stationary power – increasing energy efficiency (reducing E/GDP in the Kaya equation), reducing carbon intensity of energy (Cg/E) or increasing sequestration (S).

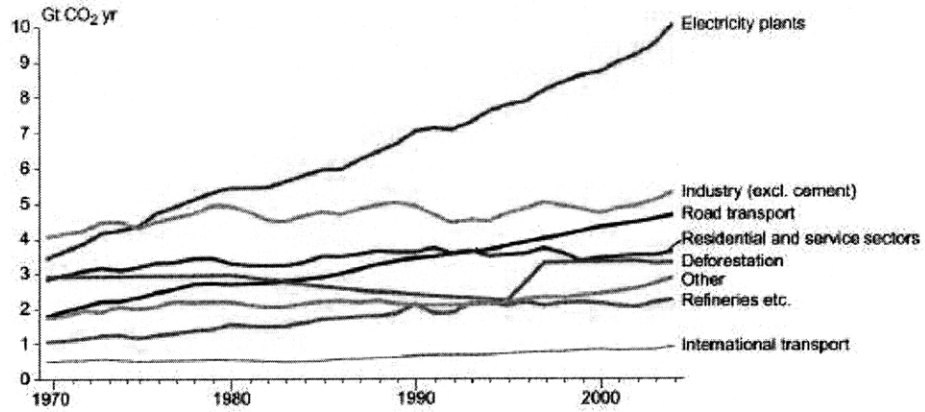

Figure 1-6: Sources of global carbon dioxide emissions over the past 30 years [6]

1.2.1 Increasing Energy Efficiency

It is thought that the most straightforward way of reducing carbon emissions is by improving the efficiency of the operations that burn carbon-heavy fuels. Half of all the electricity produced in the United States is generated from coal. There have been major gains in efficiency in both coal and gas power plants in the past few years, but the low price of these fuels discourages their replacement by other fuels, or even upgrades of plant facilities to modern, more efficient equipment. Hence, the actual mean carbon emissions per power plant is far higher than what could potentially be observed if all plants used current standards for technology. What this means in practice is that carbon emissions per MWh generated could be dramatically reduced in the US with efficiency gains. See

Table 1-2 for examples of thermal efficiencies for different fossil fuels in the US.

Table 1-2: Thermal Efficiencies of Modern Emission Systems [7]

Power System	Thermal Efficiency (percent)
Coal: Integrated Gasification/ Combined Cycle (IGCC)	42-52
Coal: Integrated Gasification/ Fuel Cells (IGFC)	47-64
Coal: High Performance Power Systems (HiPPS)	51-54
Coal: Pressurized Fluidized Bed (PFB)	42-50
Natural Gas: Combustion Turbine/Steam Turbine Combined Cycle	55-60
Natural Gas: Fuel Cell/Combustion Turbine Combined Cycle	65-67

To put the table into context, the current average thermal efficiency for a power plant in the US is about 33%. Most of the power systems listed also use multiple power cycles instead of normal steam and Rankine cycles that only consist of one cycle each.

1.2.2 Reducing Carbon Intensity

The carbon intensity (defined above) of methane (CH_4) which is a chief component of natural gas is less than that of coal (see Table 1-3), which is why so many efforts to reduce the carbon intensity of power plants have revolved around the increased usage of natural gas. Natural gas can also be used in higher efficiency combined cycles, where waste heat from a gas turbine is used to generate steam to drive another turbine. However, natural gas is typically more expensive than coal if the energy density of each fuel is taken into account. In addition reserves of natural gas are not as plentiful and accessible as those of coal, implying that a scale up of natural gas consumption may drastically impact price. One bright prospect might be the production of natural gas from hydrates, which will significantly increase supply.

Table 1-3: Carbon intensity of Fossil Fuels

Fuel	Carbon Intensity (gC/MJ)
Coal	23-26
Oil	19
Natural Gas	13

Other ideas to reduce the carbon intensity of fossil fuel power plants include the co-firing of coal with biomass. Biomass is conventionally thought to have zero carbon intensity since plants fix carbon dioxide from the atmosphere, and burning plants is considered to be simply releasing that carbon back into the atmosphere (therefore adding zero net carbon).

1.2.3 Carbon Capture & Sequestration (CCS)

Perhaps the most technologically advanced method of reducing the carbon emissions from stationary power systems is the set of technologies that embody sequestration – the term given to the trapping of carbon dioxide produced by combustion within subterranean repositories instead of releasing it into the atmosphere. These natural bodies are generally contained within the ground; for example, depleted oil and gas fields or subterranean saline aquifers are potential sites for carbon sequestration. Other possible sinks that could be used for sequestration are deep parts of the ocean as well as coal seams.

The overall process for sequestration involves capturing the carbon dioxide at the point of its generation, pressurizing it to a supercritical state and then transporting it for sequestration. All of these steps tend to add significant cost to the power-generation process, and so there has been a lot of research into figuring out how to reduce their cost.

But there is evidence that the popularity of CCS as a method of mitigating global warming and reducing carbon dioxide emissions is growing. There are projects of varying scales and national origins that have been launched in the past decade (see Table 1-4). The increase in popularity and scale of the projects shows that CCS is increasingly being acknowledged as a viable solution throughout the world. In the US alone it was a major focus of the 2008 presidential election and a central part of the energy platform that President Barack Obama campaigned on [8]

Table 1-4: Summary of planned and operating CCS projects [6]

Project	Location	Operator	Storage Type	Injection Start Date	Annual Injection Rate	Total Planned Storage
Sleipner	North Sea	StatoilHydro	Aquifer	1996	1 Mt/y	20 Mt
Weyburn	Saskatchewan, Canada	EnCana	EOR	2000	1.2 Mt/y*	19 Mt
In Salah	Sahara, Algeria	Sonatrach, BP, StatoilHydro	Depleted Gas Reservoir	2004	1.2 Mt/y	17 Mt
Salt Creek	Wyoming, USA	Anadarko	EOR	2006	2.2 Mt/y~	27 Mt
Snohvit	Melkøya, Norway	StatoilHydro	Aquifer	2007	0.7 Mt/y	
Gorgon	Barrow Island, Australia	Chevron	Aquifer	2009§	3.2 Mt/y	>100 Mt

* Average annual delivery rate over 15 year CO_2 contract
~ Peak annual storage rate
§ Planned date

1.3 Objectives and Organization of Thesis

This thesis will focus on the capture and compression components of CCS, in both pre-combustion capture and post-combustion capture situations. The broad purpose of this thesis is to evaluate a new compression technology – shock compression – in the context of the technological developments in capture-enabled power plants and com-

pressors. The evaluation will be technical as well as economic – the objective is to communicate to the inexperienced reader how the new technology works, why it's important and what potential it actually has to be the 'game-changer' it is claimed to be. There has been no published work that performs this type of in-depth analysis of this new and potentially ground-breaking compressor.

There are six chapters to this thesis, including this introductory one. Chapter 2 explains carbon capture in more detail, discussing both the technical options available as well as performing a basic comparison between the accepted alternatives. Chapter 3 delves into compression technologies and how they have evolved in design and popularity, with some sample calculations to illustrate how properties of a gas change due to compression. Chapter 4 specifically investigates shock compression, a new technology being developed by Ramgen to lower the costs of compression in capture-enabled systems. Chapter 5 involves a detailed energy balance of the Rampressor system, using both basic hand calculations as well as a detailed Aspen model in order to quantify the benefits of the Ramgen technology and compare it to conventional compressors. Chapter 6 offers an economic analysis using base cases to compare costs between conventional and Ramgen compressors, and also states the conclusions of this thesis and future work to be done.

Chapter 2

CO_2 Capture Technologies

2.1 Background

As discussed in the previous chapter it has been shown that the problem of global warming is directly related to the increase in emissions of carbon dioxide (CO_2), mostly because of increasing fossil fuel and changes in land use [2]. Thus, there is a political movement to regulate carbon emissions from high carbon content fuels like coal. However, carbon regulation is expensive; it reduces the energy efficiency of the power generation process and increase capital cost of the plants. The same can also be said of carbon dioxide compression technologies. These are geared either towards transportation to an underground location where carbon dioxide can be stored (a process called geological sequestration) or towards transportation to enhanced oil recovery (EOR) fields. Hence, there is an intensive research effort focused on the discovery and improvement of carbon capture and compression technologies used in the process to improve their economic feasibility.

The purpose of this chapter is to provide an overview of the different categories of carbon capture technologies in power plants and provide a context for the subsequent discussion of how new compression technologies can be combined with capture methods to drive down plant costs and thus help mitigate the problem of global warming.

2.2 CO_2 Capture

The efficient separation of CO_2 from the gas streams produced by the burning of coal requires sophisticated technology. Currently there are various means for achieving this separation, of which five have gained significant prominence [9 10]:

- Post-combustion
- Post-combustion Chilled Ammonia
- Pre-combustion IGCC
- Oxy-Fuel Combustion
- Chemical looping combustion

2.2.1 Post-combustion

Post-combustion CO_2 separation applies to the removal of CO_2 from the flue gas streams of a power plant by methods such as adsorption (chemical/physical) or membranes. Chemical solvents such as amines are especially cost-effective in natural-gas sweetening and hydrogen production applications.

One of the basic processes is as follows: flue gases from the power plant are chilled first and then stripped of SO_x and NO_x contaminants. A fan is used to account for pressure drops in the system, after which the stream passes through an absorption unit where a lean amine solution such as monoethanolamine (MEA) contacts the gas to absorb the CO_2. Subsequently, the clean gas stream is removed via the stack, whereas the CO_2 rich amine stream moves to a stripper to separate the amine from the CO_2. The latter process is powered by steam used to heat a reboiler. Further separation can be achieved by condensing the stream emerging from the top of the stripper column to separate the CO_2 phase, after which it is sent for drying and compression.

A post-combustion generation plan with CO_2 as shown in Figure 2-1 produces 500 MW of power requires 37% more coal per day than a generation plant without CO_2. The efficiency is reduced from 34% to 25% due to the additional energy required for CO_2 capture. [9]

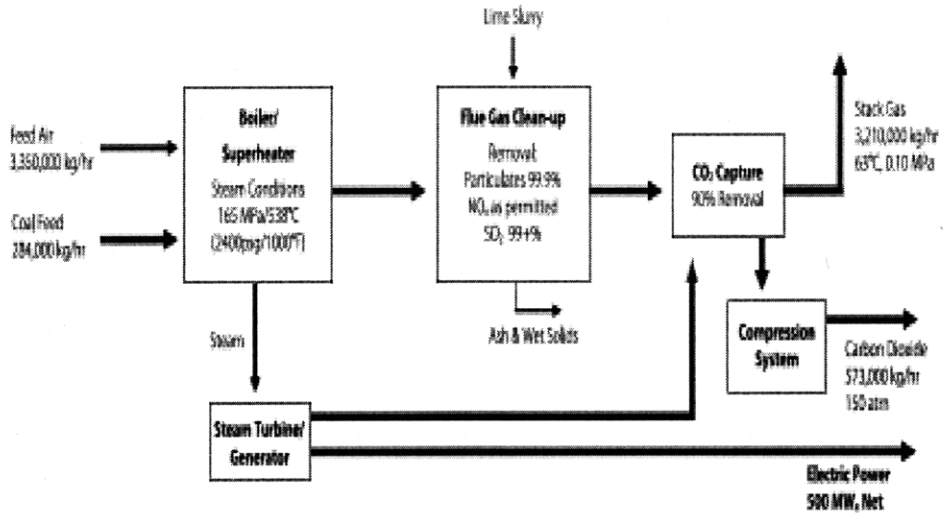

Figure 2-1 – Post-combustion capture of CO_2 [9]

The benefit of this process is that it is well-understand and verified under field conditions. The disadvantages of post-combustion capture are:

- The energy penalty is high for the solvent regeneration step in the stripper
- The equipment used in this process is at risk of corrosion and so maintenance costs are high
- Certain expensive solvents evaporate into the vapor stream and so must be replaced

2.2.2 Post-combustion chilled ammonia

Chilled ammonia as a solvent is similar to an amines solvent, except with a slightly lower absorption rate. Used in CO_2 absorbers, it contains a mixture of dissolved and suspended ammonium carbonate that counter-currently contact the incoming flue gas (chilled to 1.6 C). The chilled ammonia solvent is expected to capture upwards of 90% of the CO_2 present in the incoming flue gas. It can then be regenerated under a high pressure to reduce the energy required for compression and liquefaction of the CO_2. On the other hand, the clean gas is emitted through the stack, containing only a low amount of CO_2, some oxygen and some nitrogen.

This process remains experimental, as there have not been any commercial plants launched using this process (although Alstom is developing a pilot test). Hypothesized advantages of the process are a potentially lower energy requirement, lower ammonia emissions, high absorption efficiency of CO_2, low degradation of the ammonia solvent, and a potential overall cost that is lower than half of the next-lowest CO_2 capture process currently being studied.

In contrast, there are thought to be several disadvantages as well. The concentration of dissolved ammonia in the liquid CO_2 stream may not allow for carbonate formation. In addition, more packing and absorber vessels are needed to account for the slower absorption rate, which drives up the capital cost. Finally, the only advantage in this process is from the reduction of the CO2 compression energy requirements with the use of high-pressure solvent regeneration.

2.2.3 Pre-combustion

IGCC refers to an Integrated Gasification Combined Cycle process, where electric power is made from syngas (a combination of hydrogen and carbon monoxide) which in turn is made from coal in a gasification unit. A materials flowsheet of a typical IGCC process without carbon capture can be found in Figure 2-2. Electricity is produced from the combustion of the syngas, which provides exhaust heat to boil water and produce steam. This steam can be used to generate electricity in a steam turbine system.

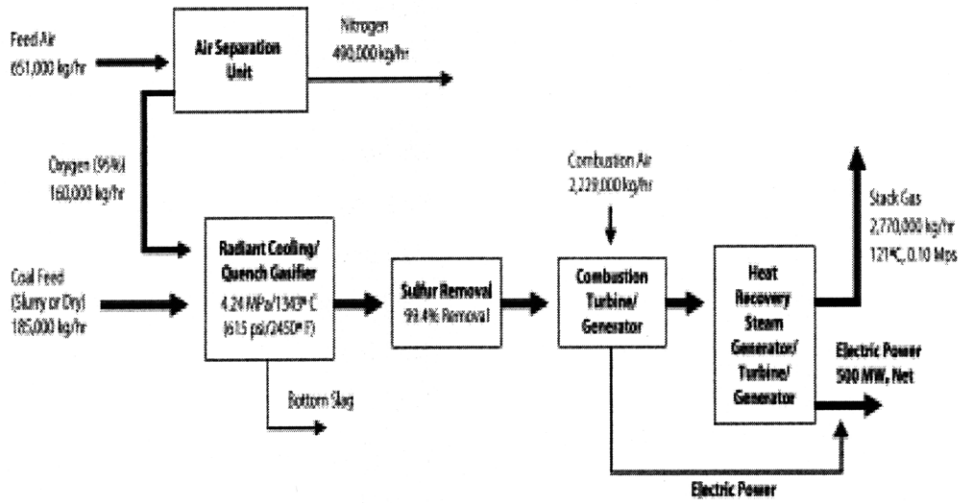

Figure 2-2 – A depiction of an IGCC process without carbon capture [9, 11]

In an IGCC process with carbon capture (Figure 2-3), a water-gas-shift reaction converts most of the water and carbon monoxide in the syngas produced by the gasifier into CO_2 and H2 respectively. This syngas is treated in an Acid Gas Removal process where a physical solvent like Selexol or Rectisol is used to capture the CO_2 and H2S from the syngas. The Selexol is regenerated via a stripping process that re-

moves most of the H_2S and sends it to a Claus unit for sulfur recovery (to be sold on the market). The H_2 is also removed in this process and sent to a gas turbine to be burnt for electricity. The CO_2 is flashed off at various pressures, compressed and sent into a pipeline system. The number of shift steps in the process determines the maximum amount of CO_2 captured and H_2 recovered.

Operating an IGCC plant with carbon capture adds 23% to the daily coal feed requirements, compared to 37% for a post-combustion plant. The overall generating efficiency is higher, however, at 31.2% when compared to 25% for a post-combustion plant.

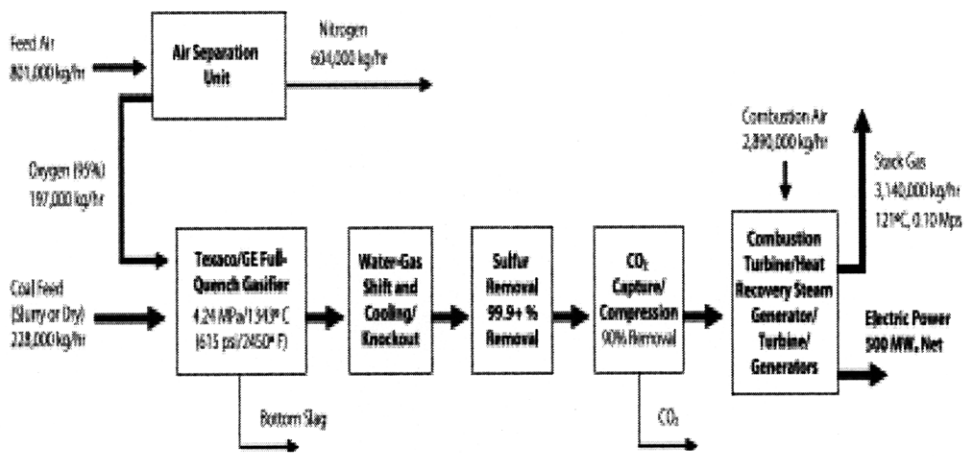

Figure 2-3: IGCC process with Carbon Capture using a Selexol process [9]

The major advantage of this IGCC pre-combustion process is the lower amount of fluid that needs to be treated (just the syngas versus the entire flue gas stream in a post-combustion unit). In addition, similar to post-combustion capture, the energy required in the AGR unit consists mostly of the pump energy and the steam needed in the reboiler of the H_2S stripper. As IGCC technology matures, many of the disadvantages can be eradicated with careful engineering. For example, earlier in IGCC development plant availability was a significant issue due to design and materials prob-

lems. However these issues were taken care of and now it is thought that with economics of scale the IGCC may prove to be economically feasible one day. [9]

2.2.4 Oxy-Fuel Combustion

Instead of resorting to a water-gas shift reaction to produce CO_2, oxygen gas can be used in place of air to combust the coal. This produces extremely pure streams of CO_2 that is easier to capture at a low cost. There is far less volume of flue gas leaving the boiler than that of an air-fired process, simply because of the lower amount of inert N2 in the stream.

An air-separation unit (ASU) is required to separate the oxygen from the nitrogen in air. Novel membrane and ceramic technologies are helping to reduce the high electricity requirement imposed by oxygen recovery from air. Oxy-fuel is considered to have great potential, and many theoretical offshoots are being developed such as a Graz cycle where the fluid following the combustion is made up of three quarts steam and one quart oxygen.

The main benefit of oxy-fuel processes is that the high purity of CO_2 in the flue gas stream means that capture costs have been significantly reduced. The low volumes of gas needed also reduce the required boiler size; combustion is more efficient with such high purity oxygen. Finally NO_x emissions are also reduced due to the insignificant presence of N_2 in the gas stream.

On the downside, the ASU requires a high amount of energy (up to 20% of power output). Also infiltration of air into the process is a difficult problem to overcome since it reduces the efficacy of the process and may force further distillation to purify the CO_2 emerging from the combustion process.

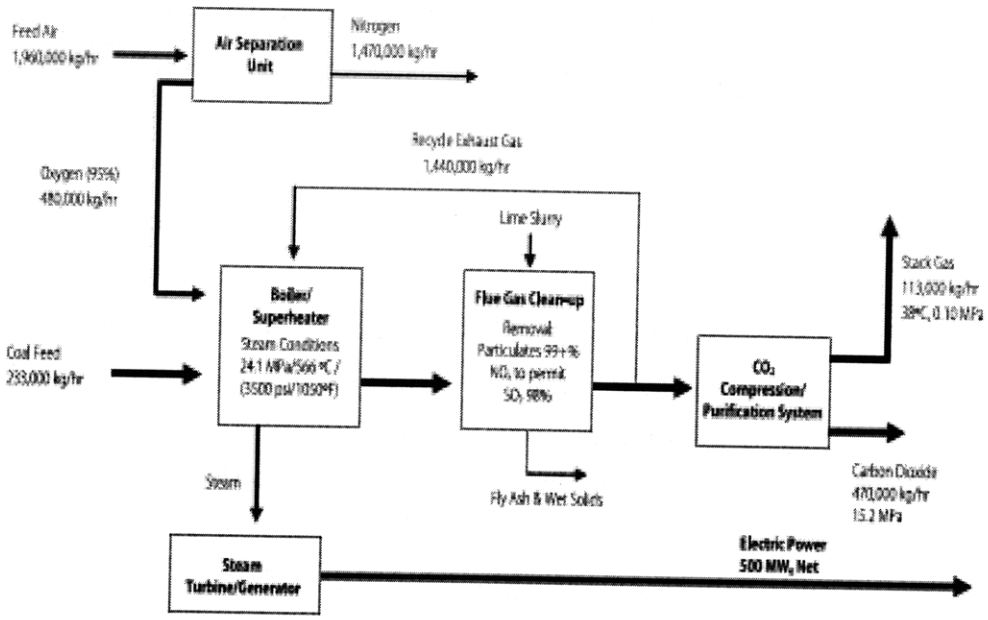

Figure 2-4: 500 MW Oxy-fuel generation plant [9]

2.2.5 Chemical Looping Combustion

Chemical looping combustion, also known as CLC, uses an oxide solid to transport oxygen from the air used for combustion to a fuel such as syngas, natural gas or refinery gas. This prevents direct contact between the air and the fuel, and the flue gas will have a lower volume since the nitrogen is kept separate from air. The oxidation reaction in air is exothermic, and the oxide retains the heat for the endothermic reduction reaction with the fuel. The net heat produced is roughly the same as regular combustion with full direct contact. In a pulverized coal application, the particulates in the flue gas are subsequently removed, yielding a high purity CO_2.

The benefits of such a process include the fact that no energy needs to be consumed to separate oxygen in an ASU unit, and a high purity CO_2 is rendered in the

flue gas. Carbon capture is tremendously efficient, and capture rates of up to 98% are economically feasible. Also, retrofitting is relatively straightforward.

The drawbacks of this system include limited experience, especially with coal processes, limited range of metal oxides that can be used and the possibility of solid carbon deposition as well as the formation of carbon monoxide. [10]

2.3 Thermophysical properties

In order to understand compression of carbon dioxide, it is imperative that good physical data of its thermodynamic properties be available. The following section presents a brief overview of the salient physical properties of CO_2.

Table 2-1: Carbon Dioxide Thermodynamic Data [11]

Molecular Weight	0.097 lb
Triple Point Temperature	- 70 F
Triple Point Pressure	75 psia
Normal Boiling Point Temp	-109 F
Freezing Point Temp	- 70 F
Critical Pressure	155 psia
Critical Temperature	87.53 F
Critical Volume	0.094 m^3/mol
Critical Compressibility	0.274
Accentric Factor	0.239
Enthalpy of Formation (25 C)	-373 BTU/ mol
Gibbs Energy of Formation (25C)	-374 BTU/mol
Heat of Vaporization	14.5 BTU/mol

Understanding the supercritical phase properties of carbon dioxide is vital to working with CO_2 compression technology. The critical point of carbon dioxide was mentioned in Table 2-1 to be 87.53 F and 155 psia. Above this temperature and pressure, carbon dioxide enters a phase characterized by a high density gas, solubility attributes similar to that of a liquid and diffusivities similar to that of a gas [12]. In addition, mass transfer properties and viscosities mimic that of a normal gas. is the phase diagram.

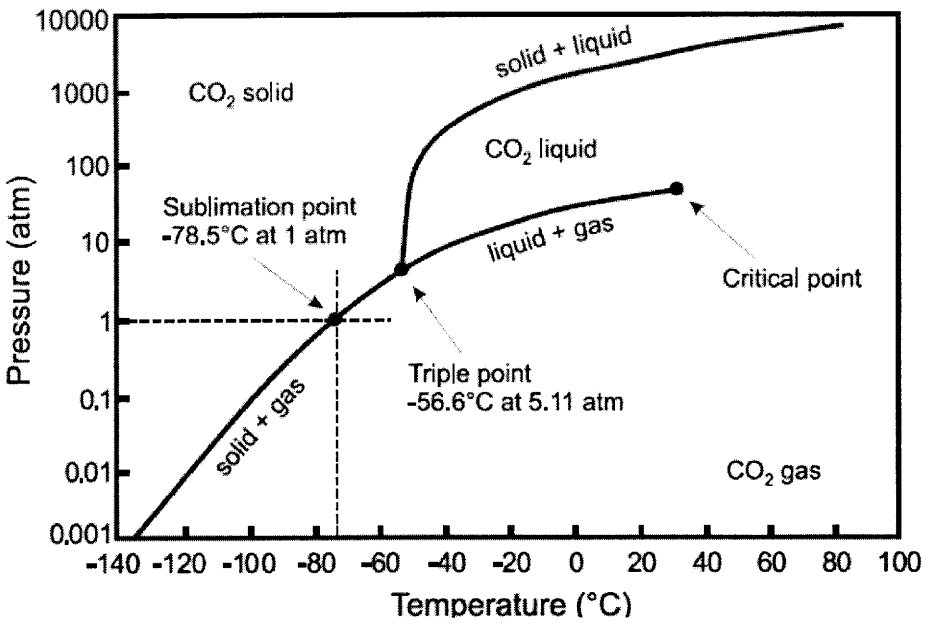

Figure 2-5: Phase Diagram for Carbon Dioxide [13]

Chapter 3

Compression Technology

The purpose of this chapter is to understand the various challenges in continuously pressurizing large volumes of CO_2 and present background information that will be critical to the analysis of new types of compressors. First, an overview of compression will be presented with some basic economic facts about the importance of compression in power systems. After that, a basic technical analysis of how compressors work will be presented, including useful equations to determine heat evolved and power requirements. Next, the evolution of compression technologies from conception to the state-of-the-art will be described in order to set the stage for a comprehensive study of current widely-used compressor technologies. Also basic data concerning the specifications for the compression section will be listed.

3.1 Compression costs are high in capture-enabled power systems

CO_2 compression is a key step in any capture process as a conduit between capture and transportation for geological injection or enhanced oil recovery. It is currently a major obstacle in addressing CO_2 capture needs, simply because of the high energy requirements needed for compression. The compression penalty is around 8-12% of the power requirement of a pulverized coal (PC) plant [14], and around 4% of the gross

power for a coal fueled integrated gasification combined cycle (IGCC) plant [Rao]. Also in the case of 90% capture and compression up to 2200 psia, auxiliary power load is increased by 40% relative to the case with no capture. Of this increase, approximately half is due solely to the load of CO_2 compression.

A more detailed cost breakdown for CO_2 compression based on \$/tonne CO_2 is 10.48 for power, 0.88 for Operations & Maintenance and 3.30 for Capital Cost (based on an electricity price of 10 cents per kilowatt-hr) [15].

Given this significant energy penalty and thus high cost relative to other incremental capture technologies, it is necessary that we also have a detailed understanding of how compression technology works.

3.2 Compressor Theory

A compressor is a machine that pressurizes a relatively large volume of gas. Compressor technology relies on basic thermodynamic relationships that describe how gas temperature, pressure and compressor work are interconnected. This section will discuss some of the most important design equations in the compressor industry. The equations will help us understand how the basic properties of a gas – temperature, pressure, mass flow and volume are inter-related and how these are related to important process quantities like work required and heat evolved, which are significant in deciding on the optimal compression technology for CO_2.

The ideal gas law describes how pressure, temperature and volume are related for a gas whose molecules have no attractive or resistive forces between each other. Its basic form is

$$Pv = RT \tag{3.1}$$

where

P = absolute pressure

v = specific volume

R = gas constant

T = absolute temperature

If a real gas is considered, a compressibility factor Z can be introduced, as in the following equation:

$$Pv = ZRT \tag{3.2}$$

These compressibility factors are empirically determined under a wide range of conditions and can be found from compressibility charts.

Another important concept is that of critical temperature and pressure. The critical temperature of a gas is the temperature above which a gas cannot be liquefied regardless of pressure. The critical pressure is the pressure at which the gas liquefies at the critical temperature.

Another basic concept (Dalton's Law) is that the total pressure of a mixture of a gas is the sum of the pressure of each of the gases, or their individual 'partial pressure'. This is in turn equal to the mole fraction of each gas multiplied by the total pressure.

The speed of sound in a specific gas is an important factor in designing a compressor to predict the presence of shock waves within the machinery. Acoustic velocity can be found by

$$c = \sqrt{kRgT} \tag{3.3}$$

Where

c is the acoustic velocity

k is the ratio of specific heats

R is the gas constant

g is the gravitational constant

T is absolute temperature

The Mach number is another standard metric used in the compressor design industry. It is given by

$$M = U / c \tag{3.4}$$

Where M is the Mach number and V is the uniform flow velocity.

The first law of thermodynamics hypothesizes that energy cannot be destroyed or created, but only transformed from one state to another. From this principle, the following general equation can be derived that accounts for a steady flow process:

$$h_1 + \frac{V_1^2}{2g} + z_1 + Q_h = h_2 + \frac{V_2^2}{2g} + z_2 + W \tag{3.5}$$

where

W is shaft work into or out of the system

h is enthalpy

z is height relative to a reference

Q is heat input to a system

In this equation, the velocity term can be incorporated into the enthalpy term to form a total enthalpy term. Thus the equation becomes

$$h_2 - h_1 = -W + Q_h \tag{3.6}$$

The second law of thermodynamics postulates the existence of entropy by stating that heat cannot flow from cold to hot without work being done. The basic equation that is useful for compressor technology is:

$$du = Tds - Pdv \tag{3.7}$$

where

du is the differential of internal energy

ds is the differential of entropy

dv is the differential of volume

From Maxwell's thermodynamic relations, it can be found that

$$dh = vdP + tdS \tag{3.8}$$

For an isentropic process, dS =0. This means

$$dh = vdP \tag{3.9}$$

For an isentropic process that is also adiabatic, the following is true:

$$Pv^k = \text{constant} = C \tag{3.10}$$

Thus the differential of Pressure, dP is given by

$$dP = C\left(-k\right) v^{-k-1}\, dv \tag{3.11}$$

Substituting equation (3.9) in equation (3.11), we get

$$dh = C\left(-k\right) v^{-k}\, dv \tag{3.12}$$

This can be integrated from state 1 to state 2 with the assumption that k remains constant to give

$$h_2 - h_1 = \frac{Cv_2^{1-k} - Cv_1^{1-k}}{k-1} k \tag{3.13}$$

Substituting equation (3.11) in (3.13), we get

$$h_2 - h_1 = \frac{P_2 v_2 - P_1 v_1}{k-1} k \tag{3.14}$$

We can then use the ideal gas law to get this expression in terms of temperature

$$h_2 - h_1 = \frac{R(T_2 - T_1)}{k-1} k \tag{3.15}$$

This expression can be rearranged by factoring out T_1 to provide this expression in terms of temperature ratio:

$$h_2 - h_1 = \frac{RT_1 k}{k-1} \left({}^{T_2}\!/_{T_1} - 1 \right) \tag{3.16}$$

We also know that enthalpy difference for an adiabatic process can be presented as

$$h_2 - h_1 = c_p (T_2 - T_1) \tag{3.17}$$

With the use of algebraic rearrangement as well as equations (3.10) and (3.1), we can find the temperature ratio in terms of pressure ratio

$$\frac{T_2}{T_1} = \frac{P_2}{P_1}^{\frac{k-1}{k}} \tag{3.18}$$

Combining the above equations, an important equation for compressor adiabatic head can be derived.

$$H_a = h_2 - h_1 = Z_{avg} R T_1 (\frac{k}{k-1})(\frac{P_2}{P_1}^{\frac{k-1}{k}} - 1) \tag{3.19}$$

where

H_a is the adiabatic head

Z_{avg} is the average compressibility $(Z_1+Z_2)/2$

For a process that is real or polytropic, the following relation can be derived:

$$H_p = h_2 - h_1 = Z_{avg} R T_1 (\frac{n}{n-1})(\frac{P_2}{P_1}^{\frac{n-1}{n}} - 1) \tag{3.20}$$

Where n is given by

$$\frac{n-1}{n} = (\frac{k-1}{k})\frac{1}{\eta_p} \tag{3.21}$$

η_p is the polytropic efficiency

The adiabatic power, which uses an adiabatic efficiency, can be found by

$$W_a = m H_a / \eta_a \tag{3.22}$$

where m is the mass flow rate

The polytropic power uses a polytropic efficiency and can similarly be found by

$$W_p = m H_p / \eta_p \tag{3.23}$$

In industrial applications, it is common to separate the compression process into stages, with intercoolers in between. The reason for this is that it reduces the discharge temperature after each stage as well as the volumetric flow of the gas stream; this limits the energy required by the process, decreasing overall operating costs.

Intercoolers also help to reduce the required pressure ratio per stage. Indeed, having multiple stages with low pressure ratio per stage may require less operating cost but higher capital cost than a compression train of few stages but high pressure ratio per stage. In many industries, the pressure ratio is only around 1.5:1 or 2:1. In certain applications, however, it might be useful to have a higher discharge temperature so that the heat can be used for any heat-intensive operations in the entire plant process. A careful evaluation must be performed to determine which option is most economically feasible.

Intercoolers can be water-cooled or air-cooled. Cooling water adds significant operating expense whereas air-cooling adds capital cost. Also air-cooling is subject to far more variability in the temperatures of the ambient air, which makes the process difficult to predict and control. If condensation is expected, there must be a way to remove the liquid fraction of the fluid stream, since compressors are sensitive to liquid. The removal of the liquid fraction also changes the volumetric flow rate of the stream, which must be accounted for in the compressor design.

Isothermal compression is a different type of compression than adiabatic or polytropic, and represents the ideal form of compression where there are an infinite number of intercoolers and stages. Understanding isothermal compression is useful as it helps quantify the upper limits of horsepower savings from cooling.

An isothermal process implies

$$Pv = C \tag{3.24}$$

From this and integrating the differential work equation, we find that the theoretical power requirement for an isothermal compression is found by

$$W = wRT \ln\left(P_2 / P_1\right) \tag{3.25}$$

3.2.1 Example calculation

To understand how these equations are used and the effect of intercooling and multiple stages, it will be helpful to trace through an example calculation comparing the effect of different numbers of intercoolers on discharge properties and power requirements.

Assumptions: 100% efficient compression, ideal gas and ideal cooling with no pressure drop and the outlet temperature of the cooling process being the same as the inlet to the first stage. The situation is as follows:

Gas= Carbon Dioxide (Mol Wt = 44 g/mol)
Specific heat capacity ratio, k = 1.4
Inlet pressure = 20 psia
Outlet Pressure = 180 psia
Inlet Temperature = 80 F
Weight flow = 100 lb/min

R = 1545/44 = 35.1 ft-lb/lb °R
T_1 = 140 °R +460 °R = 600 °R
(k-1)/k = 0.286

Base Case– No intercooling

Final temperature as given by equation (3.18)
$T_f = 600\ (9^{0.286})\ -460 = 664$ °F

From equation (3.20)

$H_a = 1 \times 35.1 \times 600 * (9^{0.286} - 1) / 0.286$

$= 64403.87$ ft-lb /lb °R

From equation (3.23)

$W_a = 100 * H_a / 33000 = 195.16$ hp

Case (1) – One intercooler

Final temperature as given by equation (3.18)

$T_f = 600\ (3^{0.286}) - 460 = 361.50$ °F

The compression ratio per stage is calculated as $(P_{final}/P_{inlet})^{1/n}$ where n is the number of stages.

One intercooler implies two stages, so the compression ratio per stage is given by

$r_p = 9^{1/2} = 3$

From equation (3.20)

$H_a = 1 \times 35.1 \times 600 * (3^{0.286} - 1) / 0.286$

$= 27184.17$ ft-lb /lb °R

From equation (3.23)

$W_a = 100 * H_a / 33000 * 2 = 164.76$ hp

This amounts to **84%** of the base case power requirement

Case (2) – Two intercoolers

Final temperature as given by equation (3.18)

$T_f = 600\ (2.08^{0.286}) - 460 = 279.81$ °F

$r_p = 9^{1/3} = 2.08$

From equation (3.20)

$H_a = 1 \times 35.1 \times 600 * (2.08^{0.286} - 1) / 0.286$

$= 17157.91$ ft-lb /lb °R

From equation (3.23)

$W_a = 100 * H_a /33000 *3 = 155.97$ hp

This amounts to **80%** of the base case power requirement

Case (3) – Infinite intercoolers (isothermal compression)

From equation (3.23)

$W_a = 100 * 35.1 * 600 * \ln (9) /33000 = 140.22$ hp

This amounts to **71%** of the base case power requirement

There are several conclusions we can draw from this exercise. First, it's clear that intercoolers reduce the total amount of horsepower required to drive the compressors. However, it's also evident that each additional intercooler has a reduced impact on horsepower savings. The first intercooler saves 16% of the energy, whereas the second only saves 4% extra. After that, an infinite number of coolers only saves an additional 9%. This manifests the decreasing returns of adding extra coolers in a multi-stage compression train.

The effect on the temperature rise is also apparent. The highest temperature difference from the base case is about 300 F in the one intercooler case, whereas adding an additional intercooler only reduces temperature by another 80 F. This is another example of how the additional first intercooler has the bigger overall impact on gas properties.

As mentioned in chapter 2, the critical temperature of CO_2 is around 88 F whereas the critical pressure is 155 psia. This means that the compressed stream of CO2 will at some point become supercritical in phase. This point obviously varies depending on how many stages are present, but care must be taken so that liquid is not formed since many compressors cannot handle liquid. Instead, the discharge stream can easily be cooled into liquid phase and then pumped for sequestration or enhanced oil recovery.

It is also useful to understand how an ideal vapor-compression cycle works, since it bears at least some similarity to compression in industrial applications. Saturated vapor is fed into a compressor, which pressurizes it. The subsequent temperature rise makes the vapor superheated. This vapor is then cooled in a condenser to become a saturated liquid, releasing heat. The liquid is expanded across a valve to produce a mixture of liquid and vapor. This mixture is then heated to reproduce the saturated liquid.

Figure 3-1 depicts the process on a temperature-entropy diagram. Heat is absorbed from step 5 to 1, and heat is rejected from step 2 to 4. The amount of heat can be determined from area under the curve.

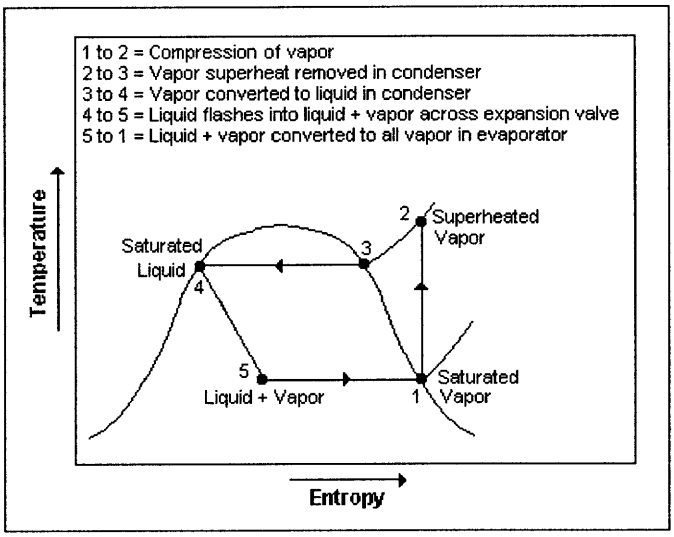

Figure 3-1– Temperature-entropy diagram of an ideal vapor-compression cycle

In a real compression train, the only important steps are 1 to 3, since there is no creation of saturated liquid in a real compressor. 1 to 2 represents one stage of a compressor, and 2 to 3 represents intercooling. Instead, in a normal compressor, the cycle starts again at point 3 as the saturated vapor is pressurized in the next stage.

Figure 3-2 depicts two-stage compression. Saturated vapor is sent to the first compressor stage at point 1, and then compressed to point 2. The gas is then cooled to

point 3 after which it is sent to another compressor stage and pressurized to point 4. The heat rejected in this process is the area under the 2-3 curve.

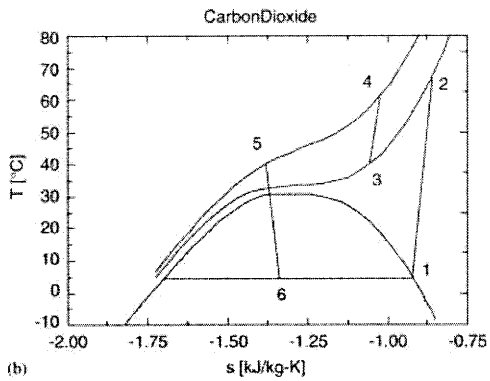

Figure 3-2– Temperature-entropy diagram involving two stage compression [16]

3.3 Turbomachinery Technology Evolution

The history of compressor technology is mostly intertwined with the long process of developing a suitable gas turbine [17, 18]. The main challenge remains attaining a level of compressor efficiency.

The first known fluid-based machinery was a paddle water wheel developed by the Romans over two thousands years ago. The function of these 'impulse' wheels was to grind grain. At around the same time, a Greek inventor named Hero developed the first steam-powered engine. The design consisted steam jets connected tangentially to a small spherical closed vessel, so that the vessel would rotate upon the reaction of the steam jets.

The next major development was much later, in 1551, when an Islamic engineer developed an impulse steam engine that turned a spit. The eighteenth century brought a revolution in turbine technology. In 1705, descriptions of centrifugal pumps and blowers were published. Leonhard Euler investigated Hero's turbine and derived a

version of Newton's law for compressors. This law helped designers methodically plan the building of turbomachinery rather than using a trial and error procedure.

In the nineteenth century, innovations such as the vaneless radial diffuser were introduced to help increase the efficiencies to close to 90 percent. In 1884, the first axial-flow compressor was patented by Charles Parsons by operating a multistage reaction type turbine in reverse. Three years afterwards, he also built a three-stage centrifugal compressor for ventilating ships. He continued working with axial-flow compressors and once designed an 81 stage compressor that had 70% efficiency.

Another important developer of compressor technology was Auguste Rateau who performed research on turboblowers, most notably in an important paper he released in 1892. One of his earliest compressors had a pressure ratio of 1.5 but only had an isentropic efficiency of 56%. He continued to work with compression technology to increase pressure ratio and efficiency.

Gas turbines require compression losses to be low to produce net positive work; however, this was not achieved until the twentieth century. The compressors designed for gas turbine did not use diffusers correctly and so could not produce work efficiently. This problem could be surmounted however with centrifugal compressors.

A 1906 gas turbine design by Charles Lemale used a 25-stage Rateau centrifugal compressor at 4000 rpm, requiring 245 kW and producing a pressure ratio of 3:1. The efficiency of this compressor was about 70%. The first commercially successful gas-turbine engine was produced in 1936 and used a 20-stage axial compressor with an isentropic efficiency of 86%.

The centrifugal compressor is the most popular compressors in use today in terms of capacity or horsepower. It has evolved to replace the reciprocating compressor in the last 60 years as its simple design eliminates the shaking forces of the reciprocator and allows a larger capacity flow. It first found use in the early 1930s in the steel industry as an oxidation air compressor for the blast furnace. Small units also found use as air conditioners, especially since the lack of shaking was a major benefit in the crowded environments of theaters and shopping centers. Although the centrifugal compressor was not that efficient, the availability of cheap energy helped it become

the compressor of choice for large plants in the 1950s. As the oil shock of the 1970s forced energy costs higher, developers focused more funds and effort to improving the efficiency of their installed base of centrifugal compressors, leading to tangible gains in this regard.

Axial-flow compressors have improved significantly over the last 130 years. Originally they were bladed based on propeller theory, which led to low-efficiency designs as the blades were not meant to deal with pressure increases in the same direction as flow. The efficiencies at around the beginning of the twentieth century were about 50 to 60%. World War I sparked an interest in aviation and thus fluid mechanics, leading to significant improvements in axial-flow compressors thanks to isolated air foil theory. Axial-flow compressors reached higher efficiencies at moderate pressure ratios per stage. To improve aircraft performance, increased stage pressures were attempted by changing the blading of the rotors. By the 1950s, the pressure ratios per stage were much higher without losing too much efficiency.

3.4 Compressor Technology

Compression technology is employed to pressurize large volume of gas from pressure of around 10 kPa to many thousands of kPa [19]. Compressors fall into two categories: continuous flow machines and positive displacement machines, the latter have a fluctuating flow instead of a continuous one. Each of these will be explained in turn in the following section.

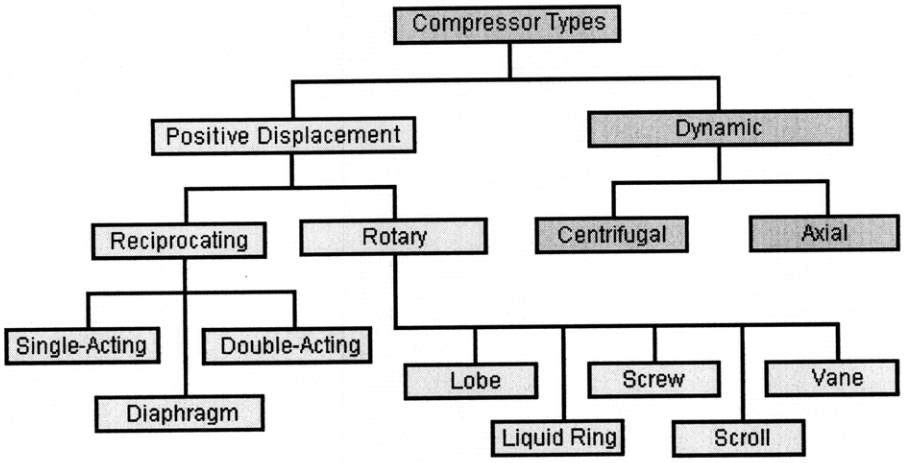

Figure 3-3: The various types of compression technologies [Wikipedia]

3.4.1 Continuous Flow Compressors

Continuous flow compressors, often classified as turbomachines, are used primarily in the chemical and petroleum industry, but also have applications in the iron and steel industry and as pipeline boosters. They have a smaller footprint and produce less vibration than positive displacement machines. This technology is optimal for an inlet flow rate of 1000 cfm to 150000 cfm.

In a centrifugal continuous compressor, the flow enters the impeller axially but departs in a radial direction, being pushed out by the impeller's rotating blades (Figure 3-4). Both the impeller and stationary diffusers are equally responsible for converting the fluid's velocity into pressure. The diffusers consist of passages that diverge, and may contain vanes.

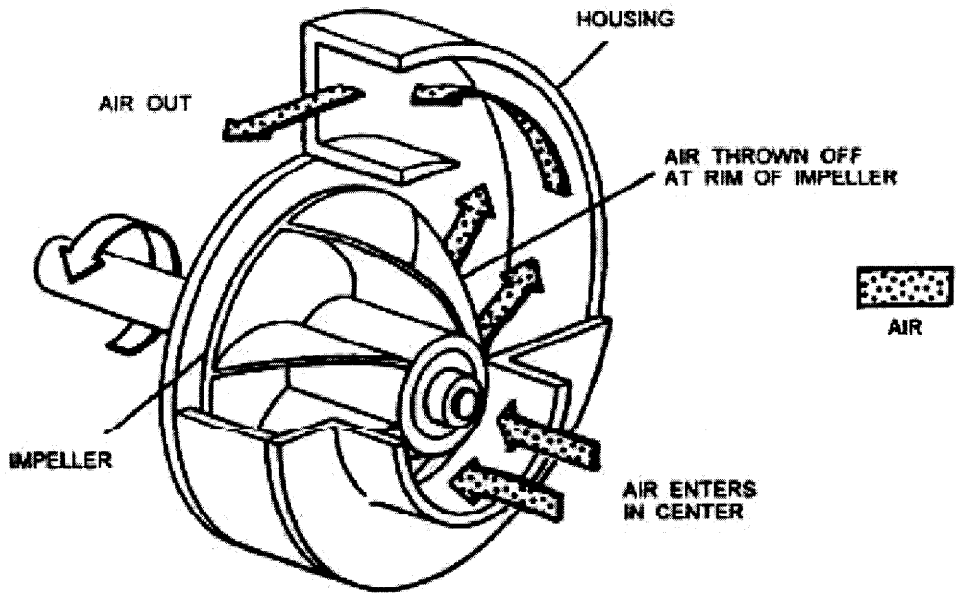

Figure 3-4: Flow of air through a centrifugal compressor

Centrifugal compressors have higher pressure ratios but lower flow rates than axial flow compressors. Pressure ratios in single-stage compressors vary; in the petrochemical industry for example, 1.2:1 is common. In the aerospace industry, pressure ratios are higher and can reach as much as 9:1. Multi-stage machines may have pressure ratios of about 3:1.

Intercoolers are often applied to cool the streams in between stages to reduce the power required. Multiple stages for the casing can also be employed; up to 9 stages per casing is common. Rotation speeds of the impeller go as high as 50,000 rpm.

The flow through a centrifugal compressor at a given operating speed is bound by an upper limit, called the choke, and a lower limit called the surge. Surge refers to the situation where forward flow cannot be maintained and a flow reversal occurs, primarily because of an increase in discharge pressure. After the surge has occurred, the discharge pressure drops again and forward flow resumes [20]. Chokes refers to the op-

posite case where forward flow is too high, implying that the flow channels between the blades are blocked to an extent. This can lead to blade vibrations that damage the compressor [21]. The range between surge and choke is reduced as the number of stages or the pressure ratio per stage is increased. It is critical to keep the flow rate between these limits to reduce mechanical damage to the compressor; however the tradeoff between the range of operating flows and pressure ratios per stage is significant factor in compressor design.

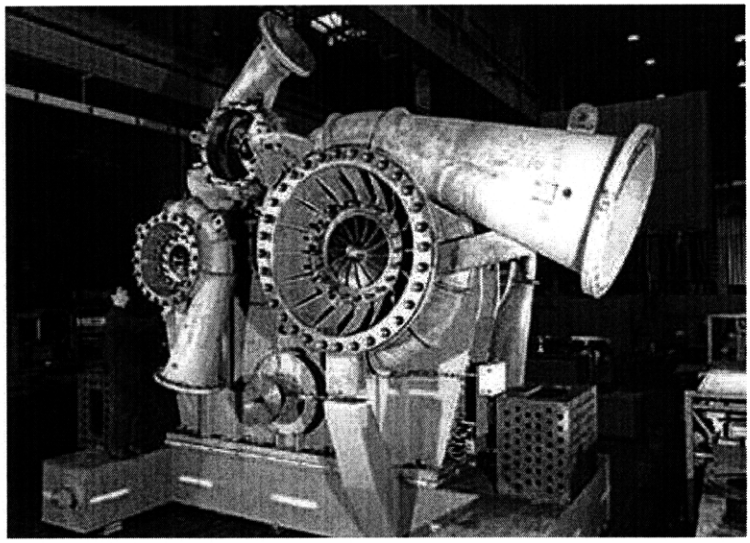

Figure 3-5: Picture of a centrifugal compressor [22]

The design of a centrifugal compressor is dictated primarily by the gas molecular weight, temperature and pressure. Factors that might improve plant performance include having a cold inlet stream to reduce lubrication problems, having a single inlet or having a discharge to reduce external piping issues.

Axial flow compressors have a higher efficiency than centrifugal compressors and are mostly employed as compressors for gas turbines. Pressure ratios per stage tend to be less than that of centrifugal compressors but flow rates are often higher because of a greater area in the fluid flow path. These range from 30,000 cfm to 1,000,000 cfm. A reasonable upper limit for the flow is about 300,000 cfm. Pressure ratios are

about 1:05-1:15 per stage and 1.1-1.2 per stage. Because of the low pressure-ratio per stage, axial-flow compressors are always manufactured as multi-stage machines.

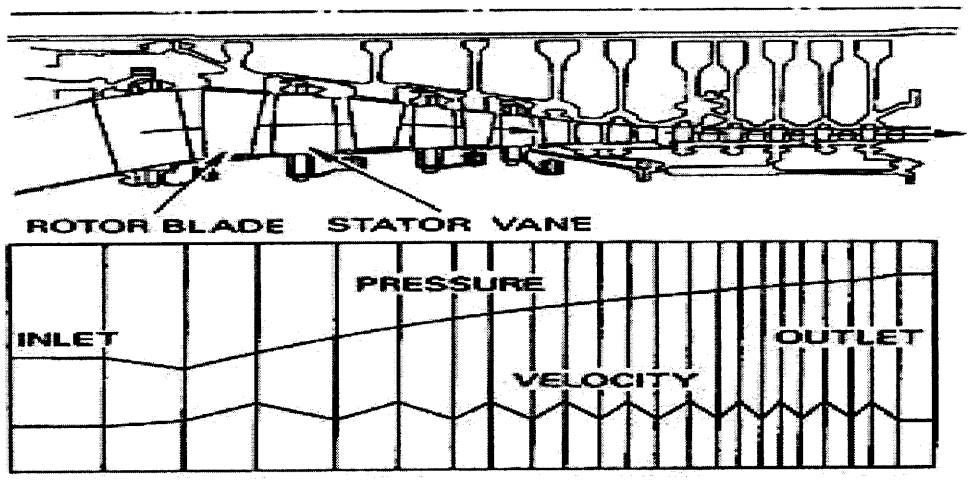

Figure 3-6: The variation of pressure and velocity along the length of an axial flow compressor. The rotors add velocity and the stators convert that velocity into static pressure [9]

Axial flow compressors' performances depend on the rotational speed of the blades and the movement of the rotors due to the flow. Stationary blades called stators convert the velocity of the fluid into static pressure (Figure 3-5). In addition, axial flow compressors have a tighter surge-choke operating range than centrifugal compressors. Primary applications include the steel industry as blast furnace blowers and the chemical industry as nitric acid plants.

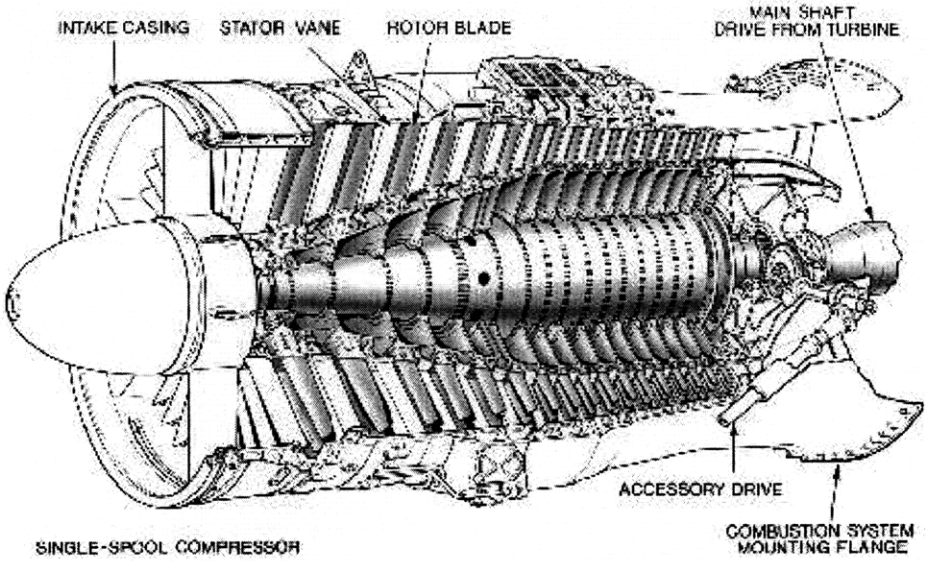

Figure 3-7: An axial flow compressor in use for jet engines [9]

3.4.2 Positive displacement compressors

Positive displacement compressors have fixed volume with variable discharge pressures, and consist mainly of rotary and reciprocating type compressors. Rotary compressors are divided into several different types: straight-lobe, screw, sliding-vane and liquid piston. The volume of rotary compressors can only be varied by changing the speed of the flow or bypassing the casing altogether. Discharge pressure varies with the resistance in the outlet section of the compressor.

Reciprocating compressors are required when a high pressure is desired at a low flow rate. Multiple stages are available if needed by the operating conditions, as determined by the ratio of the outlet pressure over the inlet pressure. Pressure ratios range from 4 to above 8, as determined by the maximum allowable gas temperature at the discharge.

In multistage reciprocating compressors, intercoolers are applied to reduce the temperature of the fluid in between stages. This helps to decrease the volume of the incoming gas stream and so reducing the total power needed for compression. This inter-cooling process also helps to keep the temperature of the gas within the allowable range.

Different control mechanisms can be applied to regulate the performance of a compressor, based on what the desired change is. Pressure, temperature, volume or speed can be regulated. Types of control include constant speed and automatic start-and-stop, to be used when gas demand is not consistent.

Lubrication of the compressor cylinder is a common requirement given the amount of moving parts involved in the technology, but some applications forbid the presence of the most common lubricant – oil. Hence, non-lubricated cylinders with piston rings made of graphite carbon or Teflon are manufactured.

High pressure compressors are increasingly the norm in the chemical industry, with discharge pressures from about 5000 to 25000 psia, and flow rate capacities of 5000 to 25000 cfm. Most often, the applications use barrel-type centrifugal compressor technology. At such high pressures, the deviation from ideality for the gases is significant and the compressors require up to 8 stages.

3.5 Specifications for compression

In order to understand the design conditions for a compression, it helps to know what the purpose of the design is. Specifications for CO_2 compression therefore would be helpful to know what is required from a compressor in a capture-enabled plant. A comparison of three different types of specifications can be found in

Table 3-1.

Table 3-1: A comparison of three different pipeline specifications

Property	Kinder Morgan [23]	DOE [24]	Dakota Gasification [25]
Temperature	<120 F	--	---
Pressure	---	>152 bar	>2700 psig
Carbon Dioxide	>95%	--	>96.8%
Nitrogen	<4%	<300 ppmv	---
Hydrocarbons	<5%	---	1.3%
Argon	---	<10 ppmv	---
Water	>30 lbs/MMCF	233 K Dew point	200 K Dew Point
Oxygen	<10 ppm	< 40 ppmv	---
Glycol	<0.3 gal/MMCF	---	---
H2S	10-200 ppm	---	1.1%

In an IGCC plant, the captured CO_2 must be compressed to a certain pressure to be in a liquid state, making it suitable for pipeline transport. A 'CO_2 Capture Guidelines' report from the DOE has specified the correct discharge pressure from the compression system to be about 152 bar or 2200 psia [DOE].

There is also a purity constraint on the CO_2 incident to the pipeline system. The same report restricts nitrogen, oxygen and argon concentrations in the CO_2 stream to less than 300 ppmv, 40 ppmv and 10 ppmv respectively.

However, a report from the field by Statoil in Norway that recounts their own experience with CO2 compression has slightly different figures. They apply an injection pressure of 62 bara with a suction pressure of 1 bara, using a 4 stage centrifugal compressor [Statoil]. They have had ten years of experience with CO_2 compression, extracting CO2 from an offshore rig mining for gas/condensate and claim their system would be very similar to that used in a power plant. Other discharge pressures reported in the literature are 187 bar for Enhanced Oil Recovery (EOR) [22].

Another real case is the Great Plains Synfuels Plant operated by the Dakota Gasification Company [25]. Here, coal is gasified to produce a synthetic natural gas (SNG)

along with several other byproducts including a carbon dioxide 'waste gas' product. This CO_2 is compressed to 2700 psig to be transported along a 205 mile pipeline for use in enhanced oil recovery in Canada.

Up to 95 million standard cubic feet per day (MMSCFD) are transported along this pipeline. The specifications of the gas produced by the Rectisol capture unit consist of a purity of 96.8 volume percent CO_2 together with a dew point of -100 F. This 'waste gas' also contains 1.1 volume percent hydrogen sulfide, 1 % ethane and 0.3% methane.

The compression system for this plant is made up of two 8-stage compression units, each with a capacity of 55 MSCFD in order to pressurize the gas stream from 3 psig to 2700 psig, at which it is in its supercritical state. The gas is intercooled between the stages with air-cooled heat-exchangers. However, it is imperative that the gas not be allowed to drop out of the supercritical state into the liquid-gas envelope portion of the phase diagram, which occurs at 1000 psig at about 25 C. Hence the intercooling process must be monitored carefully to ensure the integrity of the process.

Another widely cited set of pipeline specifications are those quoted by Kinder Morgan CO_2 Company. These are presented in Table 3-2.

Table 3-2 - Kinder Morgan CO2 pipeline specification [23, 26]

Property	Specification	Condition	Reason
Temperature	120 F	Max	Pipeline Materials
Carbon Dioxide	95%	Min	Minimum Miscibility Pressure (MMP)
Nitrogen	4%	Max	MMP
Hydrocarbons	5%	Max	MMP
Water	30 lbs/MMCF	Max	Corrosion
Oxygen	10 ppm	Max	Corrosion
H2S	10-200 ppm	Max	Safety
Glycol	0.3 gal/MMCF	Max	Hydrate Formation Prevention

Chapter 4

How Shock Compression Works

In the previous chapter we discussed traditional technologies being applied for carbon dioxide compression. These technologies are the focus of many corporations and research institutes world-wide as the struggle to produce a cost-effective clean power alternative continues.

However, there is potentially an idea that may disrupt the industry. Ramgen, a DOE funded company, has invented a new shock compression technology that they believe offers many benefits over the current state of the art. One of these claims is that there is significant scope for heat recovery based on their novel two-stage compression process. This would be highly advantageous in reducing the overall cost of the process since current technology cannot easily achieve any significant energy recovery; however, this claim from Ramgen remains unverified. There is a need to evaluate their claims and examine how this new technology compares against existing forms in the context of carbon-capture enabled power plants. To be able to accomplish this, it is important to fully understand shock compression technology itself in terms of how far it has come and also what challenges remain for this technology to attain full-scale commercialization. This chapter will discuss this point in detail.

4.1 Compressible Flow Theory

To be able to model shock compression and compare it to other types of compression technology, it is critical to understand the theory of thermodynamics and gas dynamics that are at the core of Ramgen technology. This involves having a basic knowledge of the mechanics of shock waves and compressible fluid dynamics. A gas is a compressible fluid that undergoes significantly changes of volume, velocity and temperature within the confines of a compressor. To understand how the intensive properties of temperature and pressure change in this process, the behavior of a compressible fluid must be investigated.

In a Ramgen compressor, the gas being compressed sometimes travels at a speed faster than that of sound and experiences several shock waves. Generally, as an object moves through a medium at a speed faster than sound, waves of molecules ripple away from the object, as they are limited by the speed they can travel in inside the medium. This speed is the speed of sound, and those waves are called shock waves, whose intensity is directly related to the speed and shape of the object relative to the medium.

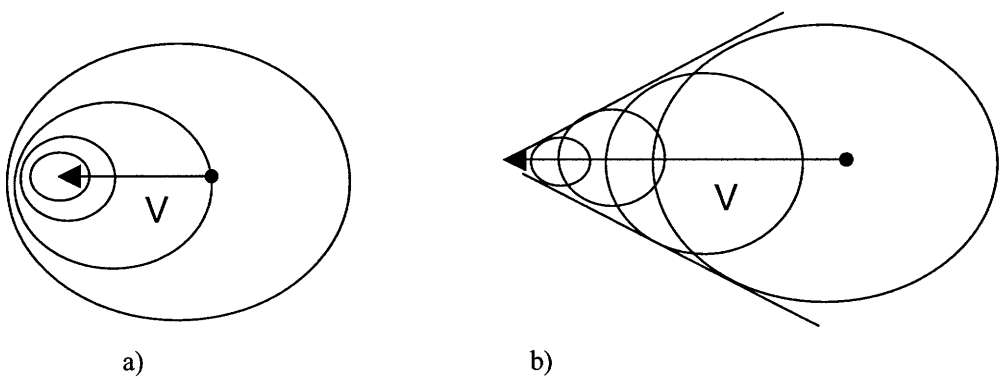

Figure 4-1: How shock waves work. a) represents the subsonic case where the disturbance object (the path of which is represented by the arrow) is always within the sphere of the emitted sound waves. b) represents the situation in which V is higher than the speed of sound and the waves are continually left behind the disturbance object [Redrawn from Anderson]

A shock wave could be understood by thinking of an object emitting some disturbance in a fluid (such as a beeper emitting sound waves).This object is traveling at a certain velocity (see Figure 4-1). If this velocity is below the speed of sound as seen in Figure 4-1a) the waves emitted from the beeper always contain the beeper; that is the beeper cannot travel outside a single wave it emits because it is not moving as fast. However, if the velocity V of the beeper is higher than the speed of sound as in Figure 4-1b), it will always move past the waves it emits, leaving behind a trail of waves it has already emitted. These waves form a wave-front traveling diagonally (or obliquely) to the object's motion [27]. This wave front is of high entropy and so can be seen in some photographs as in Figure 4-2.

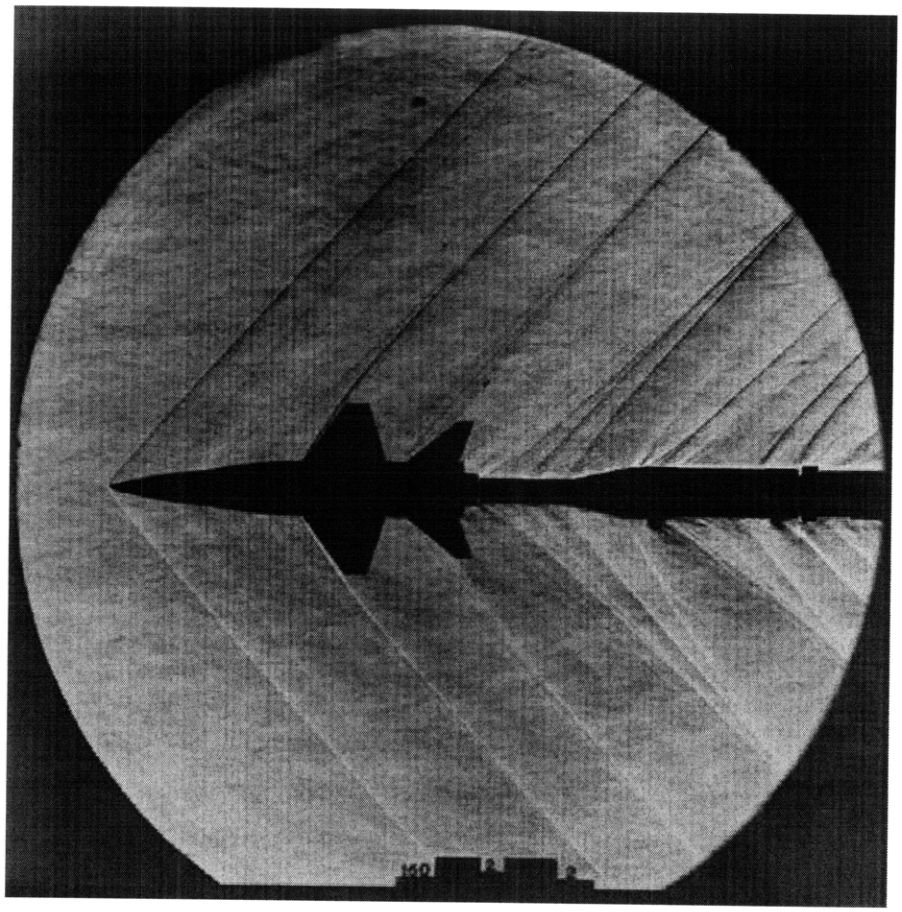

Figure 4-2: Oblique shock waves in a NASA Langley supersonic wind tunnel. The line represents high-entropy wave fronts in a series of ripple-like shock waves

A sound wave is just an infinite weak shock wave[27].The following formula determines the speed of sound in any given ideal medium:

$$c = \left(kRT / MW\right)^{0.5} \tag{4.1}$$

And the speed of sound in a real gas is given by:

$$c = \left(nzRT / MW\right)^{0.5} \tag{4.2}$$

Here c is speed of sound in the medium, k is the ratio of specific heats (C_p/C_v), R is the universal gas constant, T is temperature and MW is molecular weight. n and z represent the real gas first coefficient and compressibility factor respectively. n is given by:

$$n = k\left(\frac{z + T(\frac{\partial z}{\partial T})_P}{z + T(\frac{\partial z}{\partial T})_P}\right) \tag{4.3}$$

Thus the denser the gas, the lower the speed of sound in that gas. CO_2 has a molecular weight of 44 g/mol and an acoustic velocity value of 880 ft/sec. Air on the other hand has a lower molecular weight of 28.9 g/mol and has a speed of sound of 1130 ft/sec.

Ernest Mach was the first to discover that the most important variable determining external supersonic flow was the ratio of the speed of the flow to the speed of sound in the medium. As such, this ratio was coined the Mach number by posterity. Flows at a Mach number less than 1 are termed subsonic, whereas flows at a Mach number higher than 1 are labeled as supersonic or hypersonic.

A concept called stagnation state is applicable in describing compressible flows in shock compression technology such as the Rampressor. This state is a theoretical point at which all flows are brought to a standstill in an isentropic manner without the application of an external force. It is possible to derive useful equations by employing this concept.

Using the energy conservation law, we get

$$h + \frac{U^2}{2} = h_0 \tag{4.4}$$

In this equation, the left hand side represents the total energy of a flow in a moving state (where U is the speed of the flow), whereas the right hand state represents the total energy in a motionless state. Assuming an ideal gas, we can get the following equation

$$C_p T + \frac{U^2}{2} = C_p T_0 \tag{4.5}$$

This equation is more useful as it employs a measurable quantity, temperature. Rearranging by dividing by C_pT and substituting equation (X), we get

$$1+\frac{kU^2}{2C_pc^2}=\frac{T_0}{T} \tag{4.6}$$

Applying the definition of k and knowing that the Mach number M is the ratio of U to c, we obtain the following:

$$\frac{T_0}{T}=1+\frac{k-1}{2}M^2 \tag{4.7}$$

We can also relate the stagnation pressure to static pressure ratio to the temperature due to the isentropic assumption.

$$\frac{P_0}{P}=(\frac{T}{T_0})^{\frac{k}{k-1}} \tag{4.8}$$

When M =1, the pressure ratio is simply a function of k, as in the following expression:

$$\frac{P^*}{P_0}=(\frac{2}{k+1})^{\frac{k}{k-1}} \tag{4.9}$$

The values of stagnation density ratio, pressure ratio and temperature ratio relative to Mach number can be depicted on a chart as in Figure 4-3.

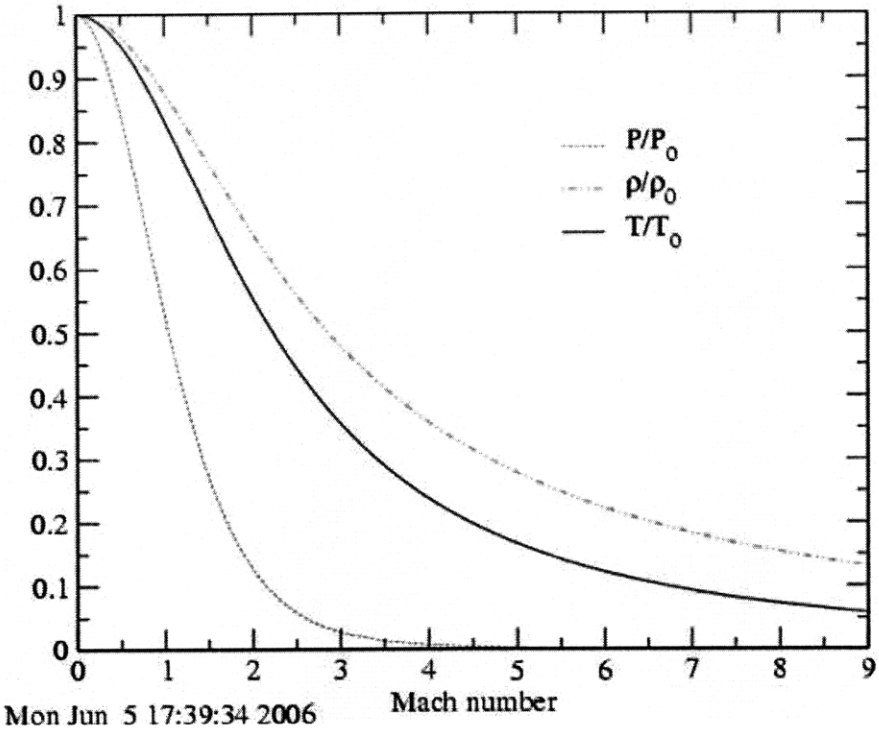

Figure 4-3: Stagnation and static property ratios as a function of Mach number [28]

An important example in the area of compressible flows is the isentropic flow in a converging-diverging nozzle. The two important models are adiabatic and isothermal flow. In adiabatic flow, the stagnation temperature remains constant because there is no heat flow. This means the stagnation pressure also remains the same because of isentropic flow. Hence, if the Mach number is known, all other values should be solvable.

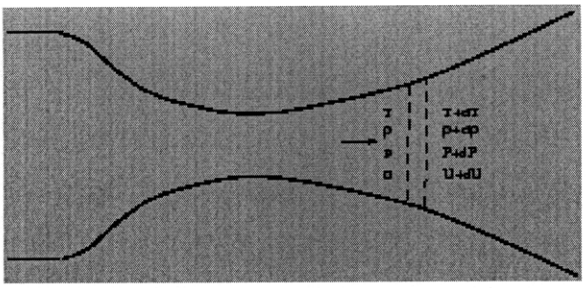

Figure 4-4: Control volume in a converging-diverging nozzle

Since the mass flow rate in a converging-diverging nozzle is constant, we can say that

$$\frac{d\rho}{\rho}+\frac{dA}{A}+\frac{dU}{U}=0 \tag{4.10}$$

And differentiating the ideal gas law gives us

$$\frac{dP}{P}=\frac{dT}{T}+\frac{d\rho}{\rho} \tag{4.11}$$

Also for an isentropic process where ds = 0, we can say

$$\frac{dP}{\rho}+UdU=0 \tag{4.12}$$

Rearranging these equations and remembering that $dP/d\rho = c^2$, we obtain the important expression:

$$\frac{dP}{\rho}(1-M^2)=U^2\frac{dA}{A} \tag{4.13}$$

This equation clearly shows how the critical Mach number is 1, because the relationship between the change in pressure and change in flow area is dependent on how the Mach number is compared to M=1. For flows at subsonic speeds (M <1) the change in pressure (dP) will have the same sign to the change in flow area (dA). For flows at supersonic speeds (M>1), they will have the opposite sign.

The behavior for subsonic flows makes intuitive sense, since it holds for incompressible fluids like liquids as well. If cross-section area increases as a function of

distance, we expect the dynamic pressure to be converted to static pressure (which increases). However, this increase in pressure is higher for compressible fluids than incompressible fluids.

From equation (4.12) we also note that the change in velocity and change in pressure have opposite signs. Hence, if velocity increases, pressure must decrease and vice-versa, as expected.

From equation (4.13), we can also find a relationship between differential temperature and Mach number. Since it is an adiabatic stream, we know that the stagnation temperature does not change and so $dT_0 = 0$. This gives us

$$\frac{dT}{T} = -(k-1)\frac{MdM}{1+\frac{(k-1)}{2}M^2} \tag{4.14}$$

A relationship between Mach number and cross section area can now be found, using the identity

$$\rho U^2 = kMP \tag{4.15}$$

Combining equations (4.13) and (4.14) we obtain the following important equation to relate cross-section area to Mach number

$$\frac{dA}{A} = \frac{(M^2-1)dM}{M(1+\frac{(k-1)}{2}M^2)} \tag{4.16}$$

This equation is important because the area is the main factor that changes within the Ramgen shock compression system as the air is impinged on a supersonic ramp followed by a gas expansion diffuser space. This equation is intuitive for Mach numbers less than 1 – as the cross-section area increases, the velocity of the fluid will decrease and so will the Mach number. The opposite is also true. For Mach numbers greater than 1, as the cross-section area increases the Mach number will also increase, which is counter-intuitive to most people.

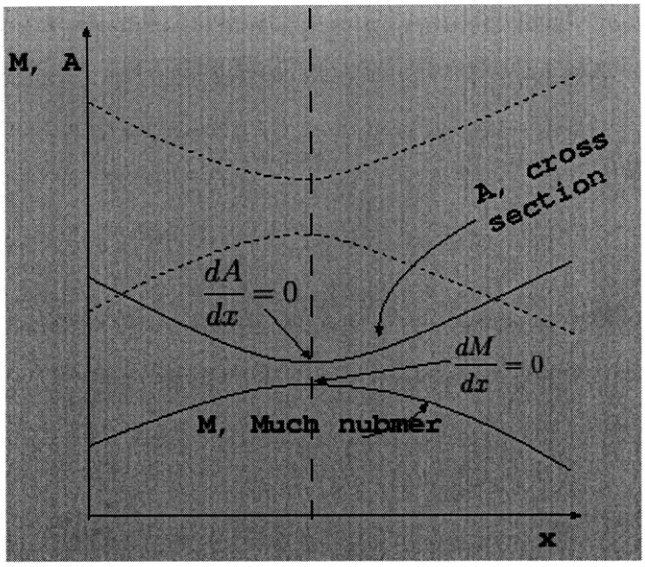

Figure 4-5: Depiction of the change of Area and Mach number with distance for internal flows

4.2 Shock Wave Theory

Understanding shock waves is vital in designing shock compression systems like the Rampressor. Because the Rampressor deliberately forces air moving at supersonic relative speeds to slow down, several shock waves are created within the system. These shock waves have many diverse effects on the structure and function of the compressor; thus, it is imperative that accurate models of their behavior be constructed.

Shock waves are phenomena observed only in compressible fluid flows, and are a result of sharp discontinuities in fluid properties. Another important phenomenon observed in compressible fluids is choking, where downstream variations in the fluid (beyond a certain critical value) do not affect upstream flow.

There are two main types of shock– normal and oblique. And both are found within a Rampressor. A normal shock is when there is an acute disturbance in the downstream properties of a fluid that changes the boundary condition of the fluid, making it react along the direction of the flow. Normal shocks only occur when a wall or surface is completely flat. However, if there is not a flat wall, the deflection angle is increased and the boundary condition changes angle. To suit this new boundary condition, the shock wave changes angle to become an oblique shock wave.

The normal shocks will be examined first. Consider a control volume in a tube as presented in Figure 4-6. The shock wave is very thin and narrow and is a discontinuity in the flow regime between upstream (x) and downstream (y) conditions.

Key equations in a shockwave assume the conservation of mass from x to y:

$$\rho_x U_x = \rho_y U_y \tag{4.17}$$

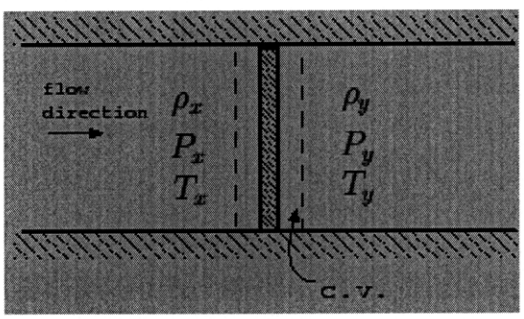

Figure 4-6: Control volume of a normal shock wave in a tube

In addition there will be conservation of momentum:

$$P_x + \rho_x U_x^2 = P_y + \rho_y U_y^2 \tag{4.18}$$

Conservation of energy is also a critical aspect:

$$C_p T_x + \frac{U_x^2}{2} = C_p T_y + \frac{U_y^2}{2} \tag{4.19}$$

For this case, however, we cannot assume isentropic flow. Instead the entropy must increase for the adiabatic case, and so we obtain the following, implying that entropy downstream is higher:

$$s_x - s_y < 0 \tag{4.20}$$

Assuming ideal gases, this means we can say

$$(k-1)\ln(\frac{P_y}{P_x}) - \ln(\frac{T_y}{T_x}) < 0 \tag{4.21}$$

Two different types of flow are important as limiting cases for shock wave solutions, called Rayleigh flow and Fanno flow. Rayleigh flow refers to frictionless flow to which heat is added, whereas Fanno flow is adiabatic but with momentum resistances to flow. Flow in a shock compression system such as the Rampressor is more likely to resemble Fanno flow, as explained below.

Rayleigh flow assumes that the heat exchange with some heat source is relative more significant than any loss to friction (momentum-based losses). See Figure 4-7 for a T-S diagram of this type of flow. It can be seen here that the maximum entropy occurs at Mach number = 1 (ie when the shock wave has just formed). Another important point on the curve is where the derivative dT/ds = 0. At this point, according to the equations described in the compressible flow section, 1- kM^2 = 0. Therefore, M can be solved for as a direct function of k. At this point, if more heat is added to the fluid, the temperature does not increase. Rayleigh flow is not seen as being applicable to real life situations, which often have high losses to friction compared to heat evolved from the fluid.

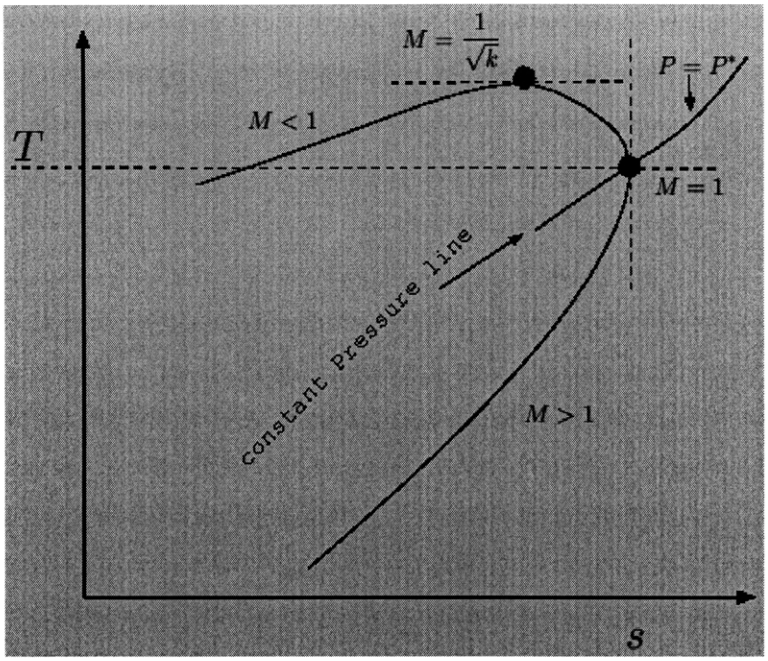

Figure 4-7: Temperature Entropy Diagram for Rayleigh flow [28]

Fanno flow accounts for the case where heat transfer can be neglected. In essence, it describes the situation where the flow is much faster than the heat transfer processes involved. Figure 4-8 describes how temperature changes with entropy in Fanno flow. Notice the difference with Figure 4-8 and Rayleigh flow – there is no point where dT/ds =0, and where heating does not change the temperature of the fluid. This is one reason why Fanno flow is more realistic than Rayleigh flow. In fact, Fanno flow is often used to approximate flow in nozzles, like the exhaust system of an internal combustion engine or compressed air systems. The Fanno flow model actually came about from the need to explain steam flow in turbines. Because Fanno flow is more representative of real processes, including shock compression, it is likely that the Rampressor more closely approximates Fanno flow rather than Rayleigh flow.

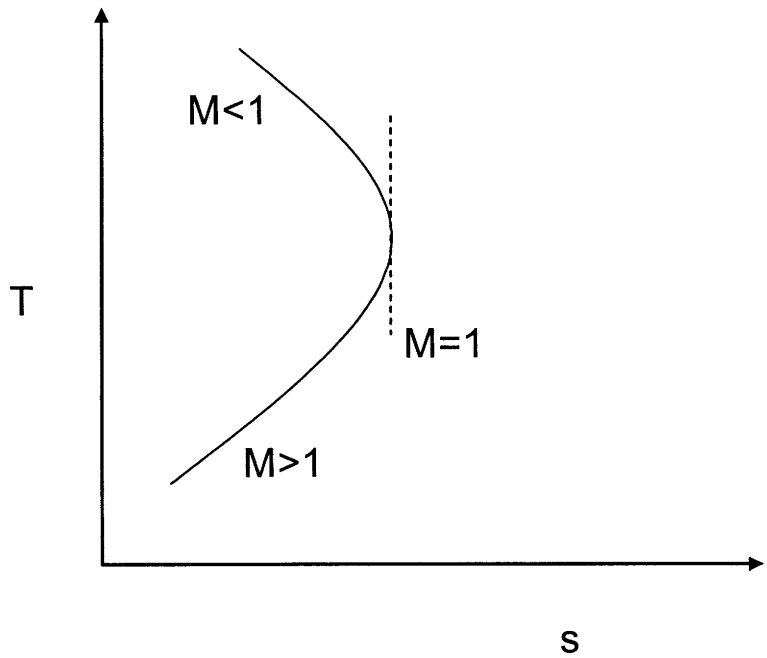

Figure 4-8: Fanno flow temperature-entropy diagram

To account for friction in tubes, the Fanno flow model uses the Fanning friction factor 'f'. A mathematical assumption the model has to make is that the value of 4fL/D remains constant (where L is a characteristic tube length and D is the diameter of the tube), since there is no impact from Mach number, temperature and other properties that are changing in the tube. Converging nozzles are found to only have subsonic flow whereas converging-diverging nozzles may have supersonic flow.

Rayleigh and Fanno flow are both modeled by a set of governing equations that are similar to those described above, but with a few extra limitations characteristic to each individual model. These governing equations can be used to solve for the properties of a normal shock wave. On a temperature-entropy diagram such as Figure 4-8, the behavior of a shock wave can be seen. The real behavior of a shock wave is the intersection of these two solutions, as seen in Figure 4-9.

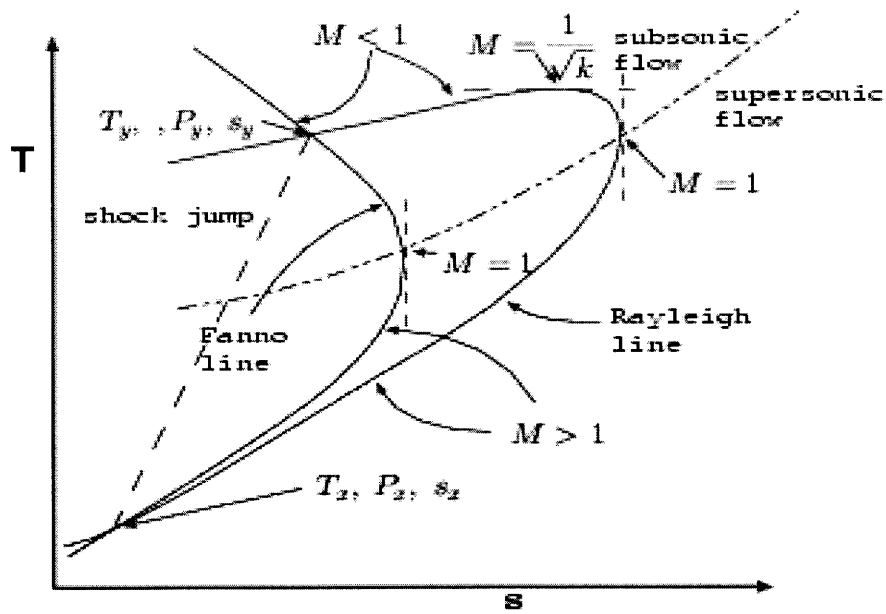

Figure 4-9: Shock wave properties, as determined by the intersection of the solution of Fanno and Rayleigh flow lines. The lines start at point x and move through the shock to point y [28]

If it is assumed that the shock wave is nearly adiabatic, it can be said that the temperatures on either side of the shock are equal; ie $T_{0x} = T_{0y}$. From this fact and equation (4.7), the following expression can be derived

$$\frac{T_y}{T_x} = \frac{\frac{T_y}{T_{0y}}}{\frac{T_x}{T_{0x}}} = \frac{1+\frac{k-1}{2}M_x^2}{1+\frac{k-1}{2}M_y^2} \tag{4.22}$$

This type of equation will be very important when calculating temperature gain in a Ramgen compressor, which further helps to determine potential heat recovery. Since the Mach number is a function of temperature itself, this equation can be solved numerically given a relationship between the two Mach numbers upstream and downstream of the shock wave. To do this, we can combine the continuity equation, the ideal gas law and the definition of the Mach number to obtain the relation:

$$\frac{T_y}{T_x} = \frac{M_y^{\,2}}{M_x^{\,2}} \frac{P_y^{\,2}}{P_x^{\,2}} \tag{4.23}$$

Substituting equation (4.23) for the temperature ratio, we arrive at the following expression relating pressure and Mach number:

$$\left(\frac{P_y M_y}{P_x M_x}\right)^2 = \frac{1 + \frac{k-1}{2} M_x^{\,2}}{1 + \frac{k-1}{2} M_y^{\,2}} \tag{4.24}$$

Also the momentum expression given in equation (4.24) can be written as the following, using the identity $\rho U^2 = kPM^2$

$$P_x + kP_x M_x^{\,2} = P_y + kP_y M_y^{\,2} \tag{4.25}$$

The stagnation pressure ratio can be found by the relationship provided in equations (4.8) and (4.24) (with the same assumption of isentropic behavior upstream and downstream of the shock wave). However, the main equations we require are the ones with pressure and Mach number terms, equations (4.24) and (4.25), which are combined to give the relation:

$$\left(\frac{1 + kM_x^{\,2}}{1 + kM_y^{\,2}}\right) = \left(\frac{M_x}{M_y}\right)^2 \frac{1 + \frac{k-1}{2} M_x^{\,2}}{1 + \frac{k-1}{2} M_y^{\,2}} \tag{4.26}$$

This equation has two analytical solutions that can be interpreted to understand the physics of a shock wave. The first solution is

$$M_x = M_y \tag{4.27}$$

This is the trivial solution which represents the lack of a shock wave between points X and Y, with temperatures and pressure remaining equal. The second solution can be analytically solved by rearranging the expression into a fourth order polynomial and find a solution of the form:

$$M_y^{\,2} = \frac{M_x^{\,2} + \dfrac{2}{k-1}}{-1 + \dfrac{2k}{k-1} M_x^{\,2}} \tag{4.28}$$

This relationship is true for the case in which a shock wave exists between points X and Y. It can be a very powerful tool, as it allows us to express property ratios in terms of the upstream Mach number as such:

$$\frac{P_y}{P_x} = \frac{2k}{k+1} M_x^{\,2} - \frac{k-1}{k+1} \tag{4.29}$$

These expressions become especially useful in the cases where property values are extreme. For example, for very high upstream Mach numbers, the downstream Mach number is simply

$$M_y^{\,2} = \frac{k-1}{2k} \tag{4.30}$$

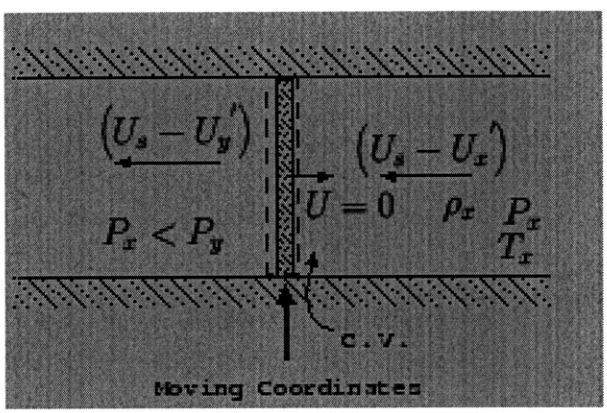

Figure 4-10: Special coordinate system for moving shocks. The apostrophes indicate a stationary frame

The situation where a shock wave is propagating upstream or downstream is called a moving shock. This case is common in industrial settings; indeed it may be relevant to consider either the lower or upper wall of the Rampressor as moving with the shock downstream of the supersonic ramp (see Ramgen Design section). To explain this

situation, it is necessary to develop a set of appropriate coordinates for an ideal case where the shock wave velocity is more or less constant. Figure 4-10 explains how these coordinates are similar to that of the static coordinates.

Assumptions made to generate a model for this case include the fact that 'moving' temperature and static temperature are equal ($T_x = T_x'$). Similar assumptions can be made for pressure. Since the speed of the sound at point x and point y is a function of temperature, we can say it remains constant. The static Mach number can be defined as

$$M_x' = \frac{U_s - U_x}{c_x} = M_{sx} - M_x \tag{4.31}$$

The subscript 's' here defines the shock wave properties. A relationship between upstream and downstream Mach numbers can be found as:

$$\frac{U_s}{c_x} = \frac{U_s}{c_y}\frac{c_y}{c_x} \tag{4.32}$$

which can be translated to

$$M_{sx} = M_{sy}\sqrt{\frac{T_y}{T_x}} \tag{4.33}$$

Although the stagnation temperatures in the moving coordinates upstream and downstream are equal, the stagnation temperatures in the static coordinates remain different. The derivation is not expressed here but involves realizing that the moving stagnation temperature expression is the same as the static expression for a normal static wave as in equation (4.22). The moving Mach numbers can then be substituted in this expression to give

$$T_{0y}' - T_{0x}' = U_s\left(\frac{T_x}{c_x}\frac{k-1}{2}(M_{sx} - 2M_x) - \frac{T_y}{c_y}\frac{k-1}{2}(M_{sy} - 2M_y)\right) \tag{4.34}$$

Thus the static temperatures upstream and downstream are affected by the shock wave. This result is intuitive as the shock wave is contributing to the internal energy of the fluid as it passes.

A normal shock is actually a special case of an oblique shock where the deflection angle is 0 (see Figure 4-11). Deflection angles are caused by a sudden change in boundary conditions of the fluid due to a change in geometry. This change in boundary conditions transforms the entire flow field, and is an integral component of both ramjet engines and Ramgen compressor technology.

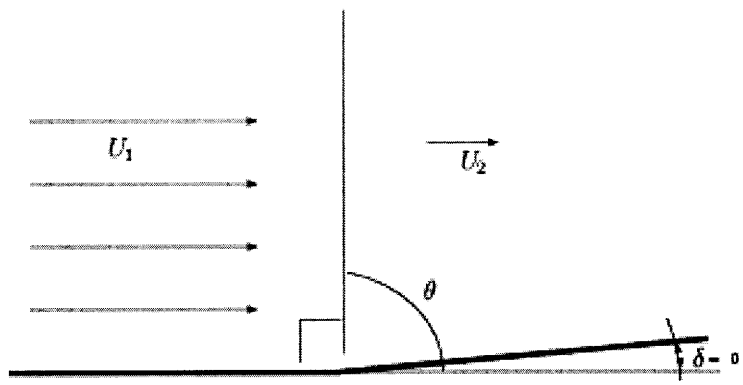

Figure 4-11: Normal shock presented as a special case of oblique shock with deflection angle $\delta = 0$ [28]

Positive deflection angles have the impact of reducing the speed of fluid flow, whereas negative deflection angles increase the fluid flow speed. The latter case is governed by the Prandtl-Meyer function and is a special case of fluid flow called expansion flow. It will not be explained here as it is not germane to Ramgen technology, which only experiences positive deflection angles.

Generally after a shock, the flow is always subsonic. However, the direction of flow itself can be separated from the magnitude and broken down into two main components – a normal component and a tangent component. The normal component is normal to a specific compression line that defines the oblique shock (see Figure 4-12), and is the only component to change magnitude during a shock. The tangent component is parallel to the compression line and is unaffected by the shock.

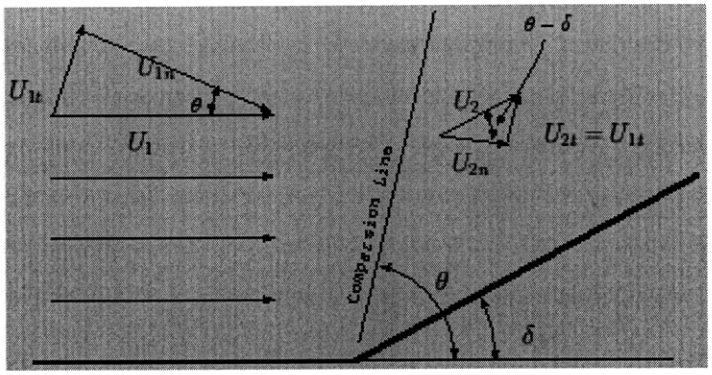

Figure 4-12: Components of oblique shock before and after the shock [28]

The equations for mass, momentum and energy are similar to those of normal shock described earlier except that instead of the total velocity term U, only its normal component is relevant. For example the momentum balance (equation (4.18)) now reads

$$P_x + \rho_x U_{xn}{}^2 = P_y + \rho_y U_{yn}{}^2 \tag{4.35}$$

Now we can relate the Mach angle θ and deflection angle δ to the normal velocities before and after the shock ('1' and '2' respectively) with the following equations:

$$\tan\theta = \frac{U_{1n}}{U_{1t}} \tag{4.36}$$

and after the shock:

$$\tan(\theta - \delta) = \frac{U_{2n}}{U_{2t}} \tag{4.37}$$

These equations combined with the mass, energy and momentum balances can be solved to produce three different solutions: a weak shock, a strong shock and a physically impossible solution. The weak solution is empirically the most common and is represented by the case where the shock turns to a slight extent:

$$\frac{\tan(\theta)}{\tan(\theta - \delta)} = \frac{U_{1n}}{U_{2n}} \tag{4.38}$$

This type of expression relating velocity to flow geometry can also be expressed in terms of Mach number as such:

$$\sin(\theta) = \frac{M_{1n}}{M_1} \tag{4.39}$$

and correspondingly,

$$\sin(\theta - \delta) = \frac{M_{2n}}{M_2} \tag{4.40}$$

There is no overall energy change across an oblique shock, which implies that the total acoustic velocity also remains unchanged. However, the temperatures across the shock are different, and so the tangential Mach numbers are also different (even though tangential velocity is the same).

An equation needs to be developed that relates both angles together with the overall Mach numbers. Such an equation would be very useful for design purposes since the compression line is a theoretical construct and can be developed using equations such as (4.40) to be

$$\tan\delta = 2\cot\theta\left[\frac{M_1^2\sin^2\theta - 1}{M_1^2(k+\cos 2\theta)+2}\right] \tag{4.41}$$

Now to find how properties change over an oblique shock wave, we can simply replace M_1 in the normal shock equations with $M_1 \sin\theta$ such as here for equation (4.42)

$$\frac{P_2}{P_1} = \frac{2k}{k+1}M_1^2\sin^2\theta - \frac{k-1}{k+1} \tag{4.42}$$

Similarly the density, downstream Mach number and temperatures can be expressed for oblique shock waves:

$$\frac{T_2}{T_1} = \frac{2k}{(k+1)^2}M_1\sin^2\theta - \frac{k-1}{(k+1)^2 M_1}[(k-1)M_1^2 + 2] \tag{4.43}$$

$$\frac{\rho_2}{\rho_1} = \frac{(k+1)M_1^2\sin^2\theta}{(k-1)M_1^2\sin^2\theta + 2} \tag{4.44}$$

$$M_2^2 \sin^2(\theta - \delta) = \frac{[(k-1)M_1^2 \sin^2\theta + 2]}{2kM_1^2 \sin^2\theta + 2 - (k-1)} \tag{4.45}$$

It is seen that all these ratios have a strong dependence on upstream Mach number M_1. This is significant for the Ramgen technology, where the upstream Mach number may be modified to produce different temperature and pressure ratios. Further details will be presented in the Ramgen Design section.

Another important equation for relating the normal component of flow velocities before and after the shock is the Prandtl relation:

$$U_{n1}U_{n2} = c^2 - \frac{k-1}{k+1}U_t^2 \tag{4.46}$$

Some typical values for upstream and downstream Mach numbers for different deflection and shock angles are presented in Table 4-1. Many different sets of values are depicted in graphical form in Figure 4-13.

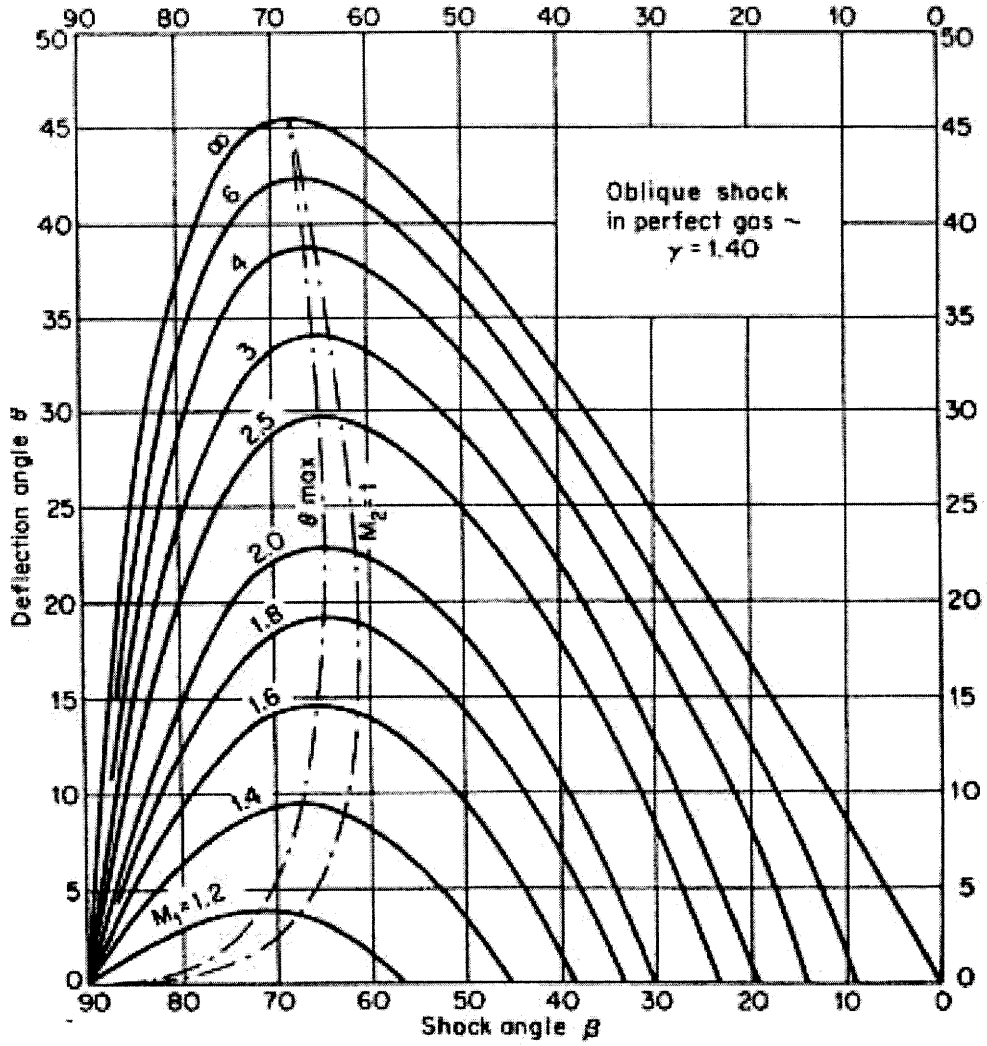

Figure 4-13: How deflection angle and shock angle are related to solutions of oblique shocks for different upstream Mach numbers [29]

Table 4-1: Typical values for shock geometry and corresponding Mach numbers [28]

M_1	M_2	Max Deflection angle δ (degrees)	Max Shock angle θ (degrees)
2	0.925	22.97	64.64
3	0.969	38.092	65.231
5	0.982	41.117	66.567
10	0.996	44.429	67.44

Another type of shock that is important for the Ramgen Power Systems design is called a reflected shock, where a compressible flow over a wedge encounters an inclined wall. Figure 4-14 depicts the case of a reflected shock. As the flow changes direction rapidly from zone 1 to zone 2, a reflected shock wave is formed. In fact, reflected shock waves are not different from oblique shock waves but are a way of expressing the case where the flow is inclined but the wall is not. Across the shockwaves, the Mach number of the flow and various other properties change abruptly, as discussed previously.

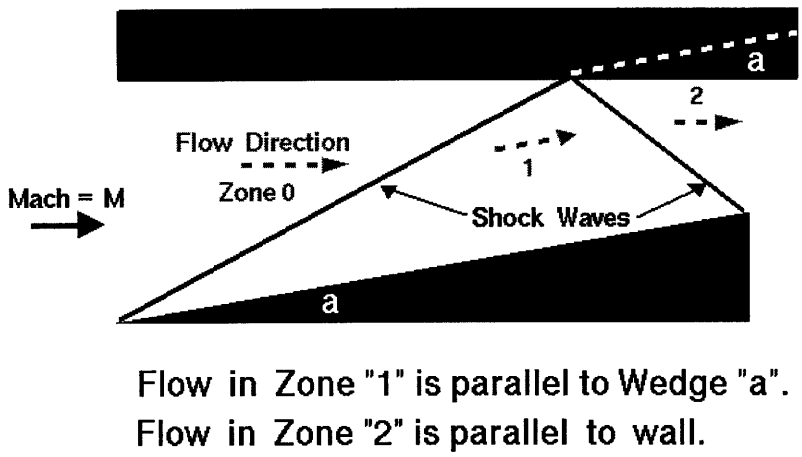

Figure 4-14: Reflected shock waves [30]

4.3 Ramgen background

Found in 1992, Ramgen Power Systems is a research & development company that attempts to leverage supersonic flight technology to build gas compressors of high efficiency and low cost in 'non-flight applications'.

Ramgen specifically is projecting that it will be able to produce a compressor with a 10:1 pressure ratio per stage, with a 100:1 pressure ratio overall. This high pressure ratio implies a more efficient compression, leading to predicted reductions of capital cost by 65% and reductions of operating cost by 25%. For a 400 MW plant, that translates to savings of about $27 million per annum. Also a 72% heat recovery rate is predicted. See Table 4-2 for further specifications reported by Ramgen for their technology.

These savings could significantly lower the barriers to building economically feasible carbon capture-enabled power plants, from coal or other polluting fuels. Hence,

understanding shock compression technology is critical to choosing the best type of compressor for a capture-enabled plant.

Table 4-2: Rampressor shock compressor specifications [7, 31]

Characteristics	Specifications
Technology	Shock Wave
Size (ft)	6' x 12' x 18'
Compression Ratio per Stage	10:1
Estimated Physical Volume (ft^3)	560
Estimated Weight	70570
Mass flow capacity (lbm/hr)	150000
Inlet volume flow capacity (cfm)	21411
No. compression stages	2
No. intercoolers	1
Casings	1
kW	7333
Input HP	9830
Bhp/100	45.9
Isothermal Efficiency	66%
Approx Discharge Temp per stage/casing (F)	470
Max Thermal Recovery Temp (F)	250
% Recoverable	72 %
Cost per Compression Ratio	$425/hp
Capital Cost	$4.3 MM
Installation Cost	$1.1 MM
Total Cost	$5.4 MM

In order to accurately compare shock compression technology to other forms of technology, a model could be designed that accounts for, among other metrics, the possible heat integration that is possible using this technology versus the others. This is directly related to the operating energy costs of the unit and hence the economic feasibility of the plant itself. Another crucial parameter is the power required to run the compressor and any other day-to-day cost that impact the overall operating energy costs. Hence building a reliable model of this new form of technology and integrating into a wider power plant model is important for evaluating this cutting-edge technology.

4.4 Ramgen Design

Ramgen shock compressor technology is highly derivative of existing ramjet engine technology.

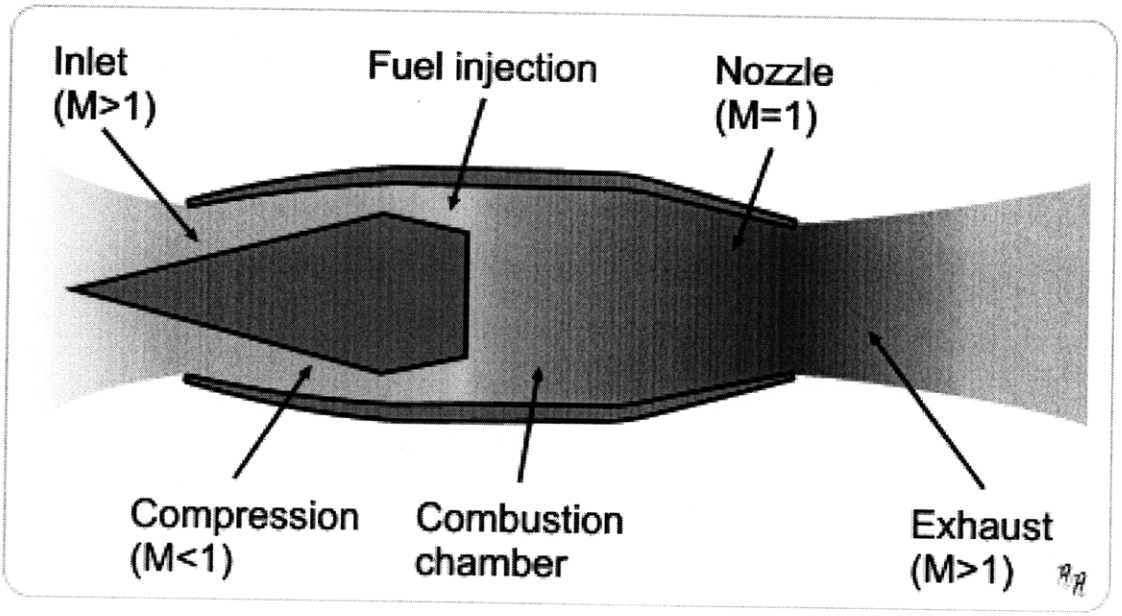

Figure 4-15: Depiction of ramjet engine

Supersonic jet technology such as the type used in a ramjet is similar to that of subsonic jets, except there are no moving parts and hence no turbines in a supersonic system. In fact, the turbines are the limiting factor for the speed of the jet, since the temperature gain with a turbine engine at a Mach 3 would result in a combustion chamber temperature above the melting point of the construction material [27]. The air flows into the engine at supersonic velocities and forced around a fixed object to pressurize or 'ram' the stream in the tight volume (the channels between this fixed object and the engine wall). This creates shockwaves by slowing the waves of air to speeds below the sonic barrier almost immediately. This high pressure gas is then ignited using heat from the combustion of a fuel, and expelled at very high momentum, generating a significant forward thrust to the aircraft.

The process in a ramjet can also be described in terms of a thermodynamic cycle called the Brayton cycle. Using the notation in Figure 4-16, the inlet corresponds to the free stream of air entering the engine at high velocity at point 0. It is compressed to point 2 by the slowing of the stream through a diffuser, which works to convert the high velocity of the gas stream to static pressure. This compression is isentropic in the ideal scenario, corresponding to a vertical line on the T-s diagram, but in reality is not because of the highly entropic shock waves that are formed, as discussed in the previous section. The temperature also increases during this process, as can be seen in the diagram. In reality, the presence of normal shock in the diffuser limits the maximum pressure that can be reached in the subsonic section of the tube.

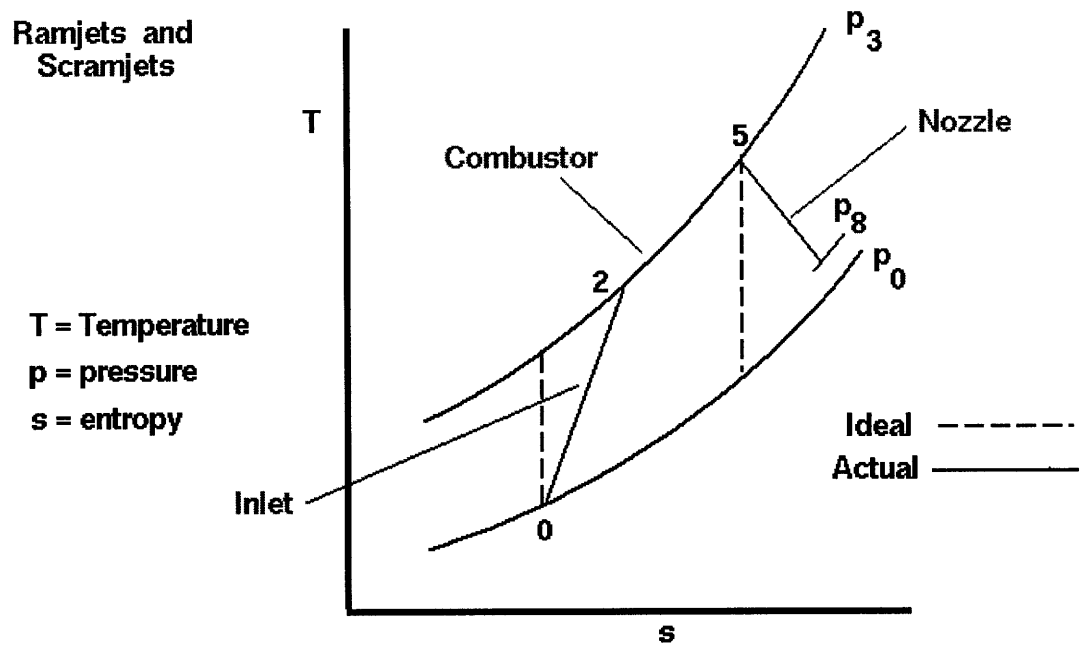

Figure 4-16: Temperature-entropy diagram of a ramjet Brayton Cycle [30]

The stream is then mixed with fuel and burned at constant pressure from points 2 to 5. The efficiency of the combustion and the temperature increase seen depends mainly on the fuel-to-air ratio and the type of fuel employed. This process adds a significant amount of energy to the gas mixture, which is often kept behind a barrier to improve mixing of fuel gases and air. This hot stream is then forced through a nozzle at high momentum to provide thrust as seen on the diagram from points 5 to 8. The area under this curve represents the amount of useful work that is available to accelerate the engine forwards. Ideally, point 8 would be on the same pressure curve as the free stream inlet at point 0; however the converging-diverging nozzle design allows some losses of energy in friction and drag.

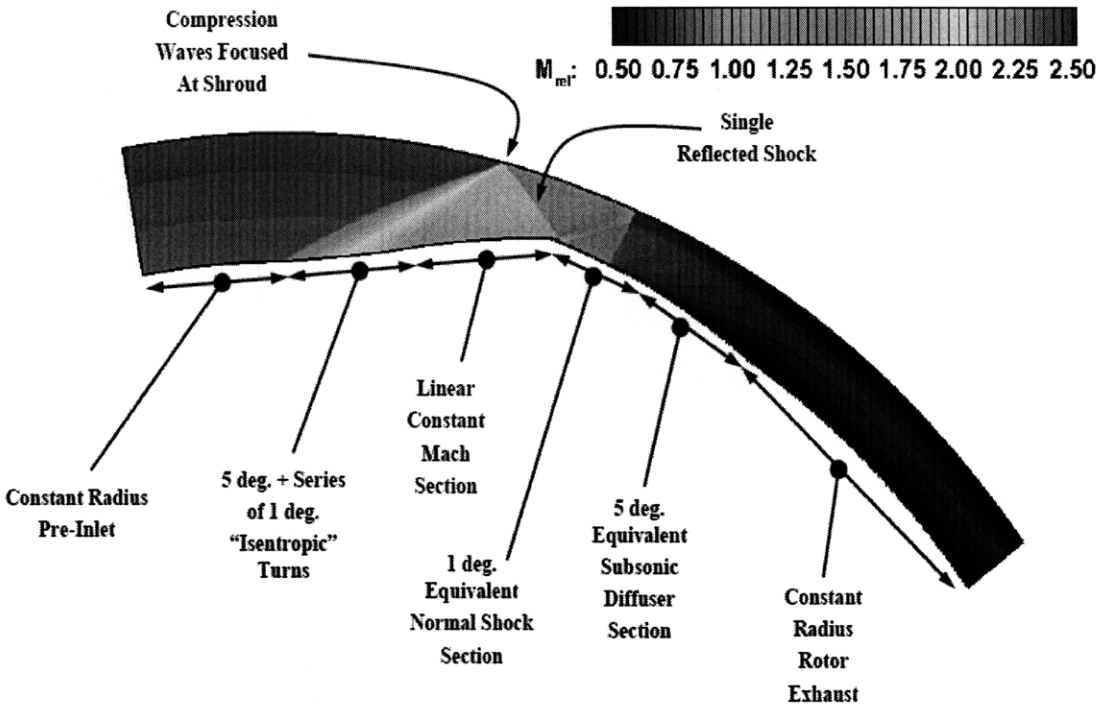

Figure 4-17: The aerodynamic design of a Ramjet/Ramgen compressor inlet and diffuser, obtained from a Ramgen presentation

To analyze exactly how a ramjet works using compressible flow theory, it is useful to examine Figure 4-17. This figure represents a computational fluid dynamics model of how the Mach number of the fluid undergoes significant reduction when the angle of the walls is increased. This change is due to the velocity of the gas stream being converted instead into static pressure as the gas molecules in the incoming stream are compressed into a smaller volume.

This figure is also remarkable for clearly showing the shock waves that arise in the process. It can be seen that the deflection angle is gradually change from 0 to 1 degree small turns, to a 5 degree turns, a very sharp turn and then back to 5 degree turns, 1 degree small turns and then finally constant walls . The deflection in this case is not only due to changes in the lower wall, but also the upper shroud. The oblique shock waves are clearly defined in this figure as well. It is critical to understand where the compression lines are for practical design purposes. There have been cases in the past when designing jets where the oblique shock waves have burned holes in

the jet's body because the shock waves trajectory was not accounted for in the design of the aircraft.

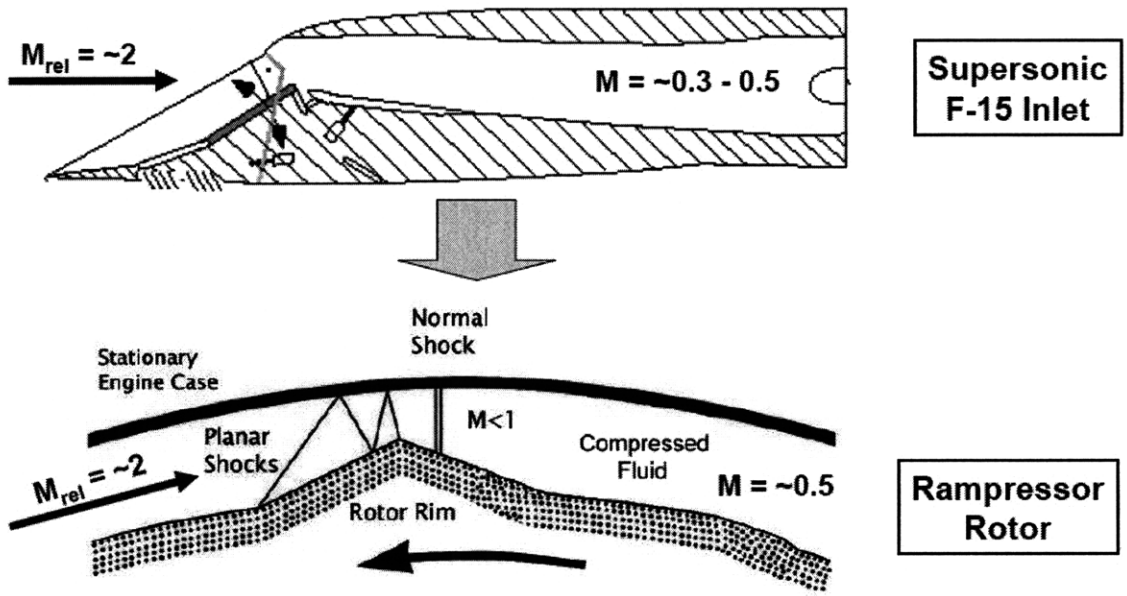

Figure 4-18: Similarity of Ramgen to Ramjet technology

The Ramgen compressor ('Rampressor') uses a similar concept, designing a rotating disk that mimics the effect of the supersonic aircraft intake in compressing the inlet air at high speeds. However, in this case it is the disk moving at a high velocity rather than an aircraft. The rotating disk spinning at supersonic velocities has three raised sections that reproduce the effect of the supersonic ramjet inlet to compress the incoming gas between the driven rotor and shroud wall.

The rotor is operated so that the gas flow speed (a combination of rotor tip speed and gas velocity) is at supersonic levels. The inlet helps to stabilize the oblique/normal shocks in the gas flow path that exists between the stationary external housing of the compressor and the rim of the rotor.

In addition, a pre-swirl compressor wheel is used before the supersonic compression ramp to improve efficiency. This wheel boosts efficiency by increasing the pressure of the incoming gas which is often at ambient pressure. It also helps to increase

the apparent Mach number of the inlet gas by swirling the gas in the direction opposite to rotor rotation, thereby increasing the relative speed of the rotor to the gas. This gain in Mach number before the gas is ingested in the supersonic ramp helps to improve compression ratio.

A gas bypass valve is also used to assist in cases where gas flow needs to be turned down while still maintaining the same high efficiency and compression ratio. This is especially necessary if a constant speed drive motor is used, and helps maintain low output power loads.

The Rampressor claims to have structural and functional innovations that have been critical in attaining the high levels of efficiency Ramgen has supposedly observed. The design and shape of the rotor is meant to minimize aerodynamic leading edges that end up causing serious drag losses in many compressors (such as axial and centrifugal). The Rampressor has five or less aerodynamic leading edges, which reduces viscous drag losses. Ramgen claims this gives them an efficiency advantage of over 10 percentage points in the compression ratio ranges of 10:1 to 30:1 over conventional compression technologies. This is especially true given the high Mach numbers that the Rampressor operates at: from Mach number = 1.5 to Mach number = 4. This is due to rotation rates of the rotor that range generally from 10,000 to 20,000 rpm but can extend as high as 50,000 rpm. The compression provided by the pre-swirl wheels is designed to be 2:1 but is often somewhere around 1.3:1.

Also the shock geometry (shown in Figure 4-18) has been optimized to reduce parasitic losses in the compression cycle. Since shock waves are a cause of energy loss themselves, this may mean that Ramgen has attempted to reduce the amount of oblique shock waves that are present in the supersonic compression ramp leading to the subsonic diffuser.

Other innovations claimed include a lightweight material with a high tensile strength that is use to build the rotor and housing. The low weight reduces capital cost but the high tensile strength helps the rotor to withstand the strong forces associated with supersonic speeds. There is also a separation of the low pressure gases from the high pressure gas in this design.

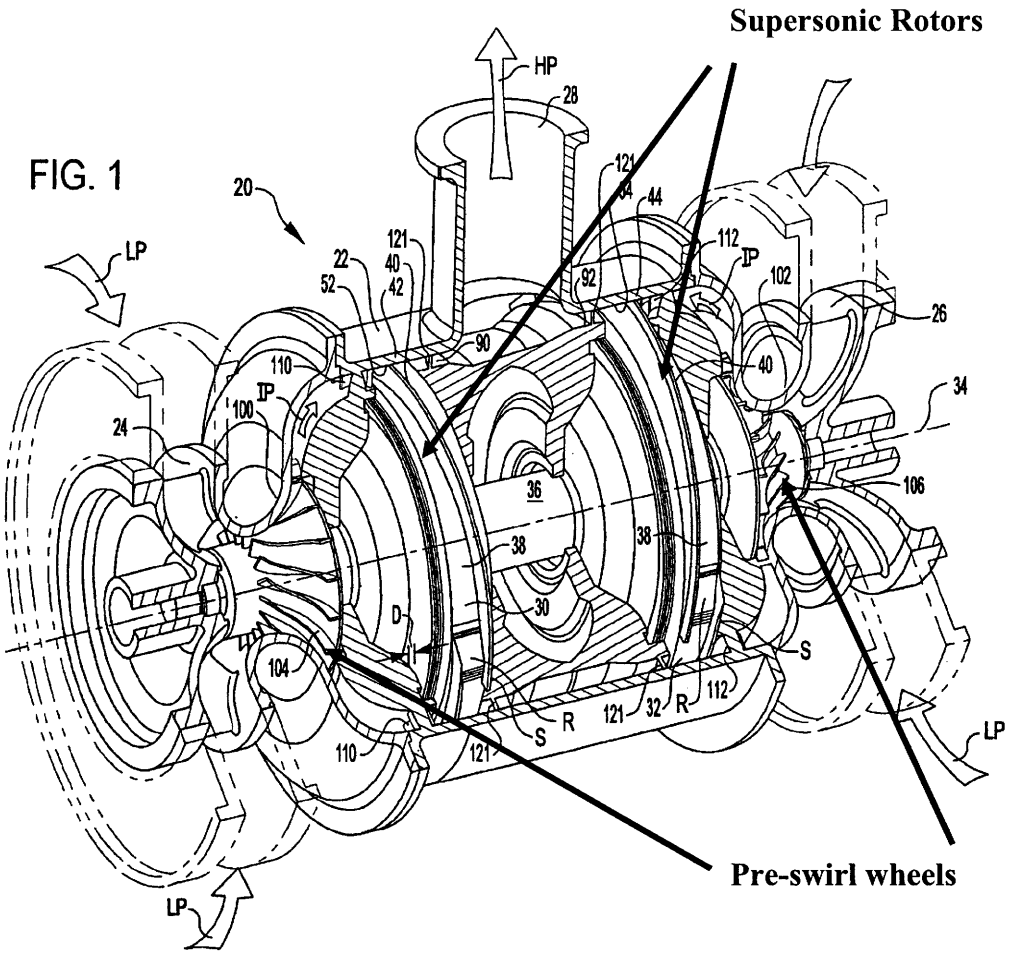

Figure 4-19: Ramgen cut-away drawing of Rampressor showing both low pressure intake and high pressure outlet, as well as pre-swirl and supersonic compression rotors. [32]

Figure 4-19 shows a drawing of the overall system. There are two rotors (labeled) meant for supersonic compression on the same shaft, as well as an integrally mounted, directly driven pair of centrifugal pre-swirl wheels at the inlet (also labeled). Low pressure gas incoming from the intake is compressed by the wheel to an intermediate pressure, and subsequently compressed again by the supersonic rotor to a high pressure. Each rotor has a number of strakes on its outer axial wall and a number of compression ramps as well – generally these are designed to be equal in quantity.

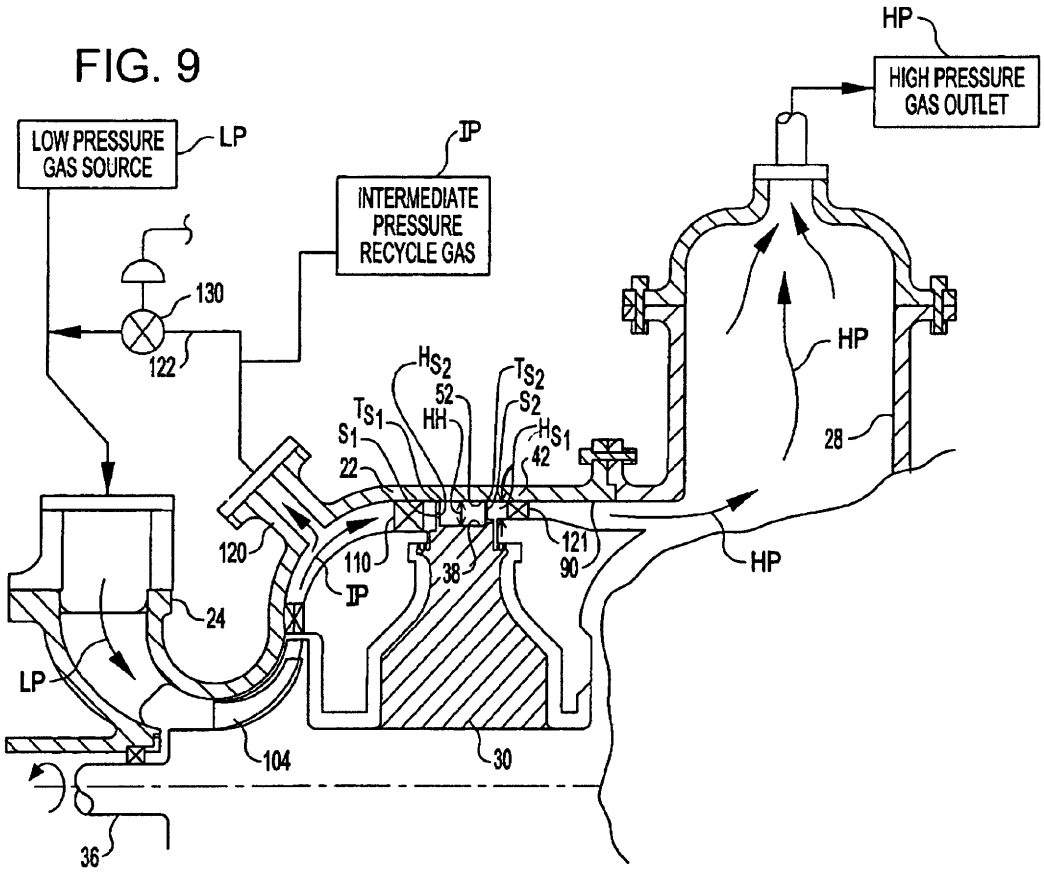

Figure 4-20: Cross-section view of Rampressor casing [32]

Figure 4-20 depicts the bypass line that was discussed previously and also shows a much clearer view of the gas flow path in the Rampressor. The bypass line redirects a portion of the inlet stream (determined by the valve position) back to the inlet and thus helps to maintain optimal power loads even when reduced flows are required from the supersonic compressor.

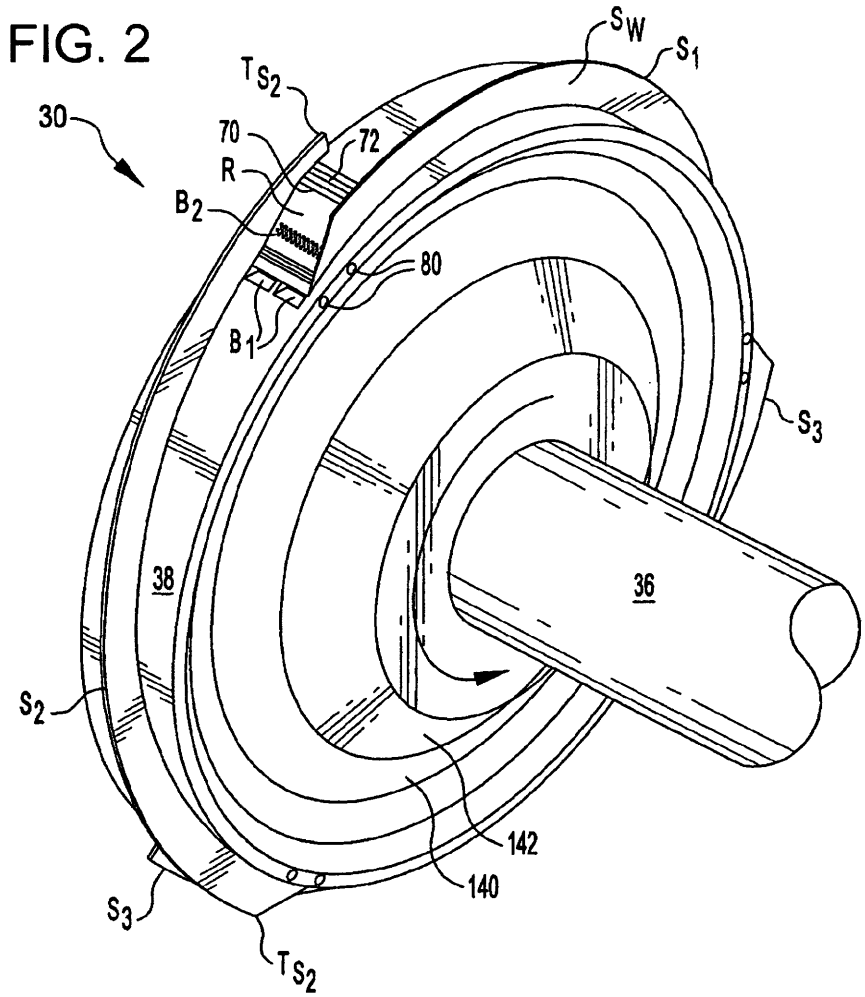

Figure 4-21: Rampressor supersonic compression rotor [32]

Figure 4-21 shows a close-up drawing of the rotor in particular. The compression ramp can clearly be seen (labeled R on the diagram). This incline causes a sharp change in volume for the incoming compressible fluid, thus drastically reducing the speed of the flow and creating shock waves. The energy is not just lost in the shock waves however – it is also converted to static pressure.

The key feature of this diagram is the assortment of strakes, labeled as S in the drawing. The purpose of the strakes is to separate the high pressure gas from the low pressure gas. This is important for obvious reasons but also means that there can be multiple compression ramps on the same rotor. The strakes act fundamentally as a

large screw compressor fan or pump would to help move gases along the radial edge of the rotor with every turn.

The ramps themselves are designed so that they compress the portion of the incoming gas stream that is impinged on by the ramp in the rotation of the rotor about the drive shaft. The gases flow to the rear of the ramp, where they encounter a higher volume diffuser section and expand. This diffuser space finally leads to the outlet.

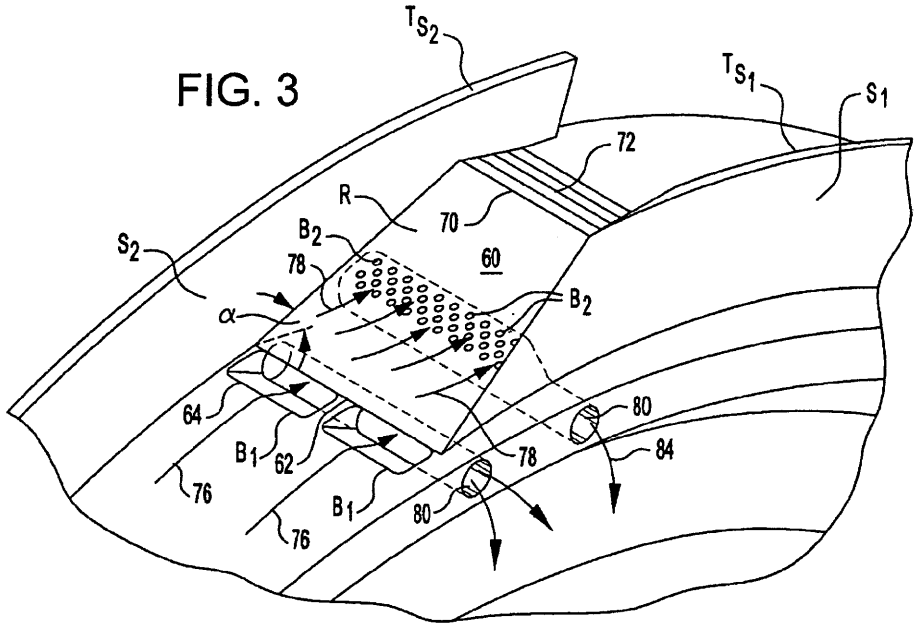

Figure 4-22: Even closer look of the ramp of a Rampressor rotor [32]

Figure 4-22 shows the compressor ramp in more detail. It shows how the strakes are actually somewhat tapered – the leading edge at the top of the strake is about 0.1" in width compared to 0.15" at the bottom of the strake.

The angle α depicted in Figure 4-22 is actually very important to the shock geometry of the compression, as shown in the sample calculations below and in . The angle determines the number of oblique shock waves and hence number of 'zones' (between which Mach number and other properties of the gas change discontinuously). This angle is set by the designers, and can vary from 1 degree to 15 degrees. Its value is dependent on average values of incoming Mach number, temperature and gas density.

Another key feature of the ramp is the array of bleed ports on its face. These bleed ports serve to boost efficiency of the compression by allowing some gas to pass through the ports and emerge from the side, as show by the arrows in Figure 4-22. These bleed ports are meant to remove gas in the boundary layer region.

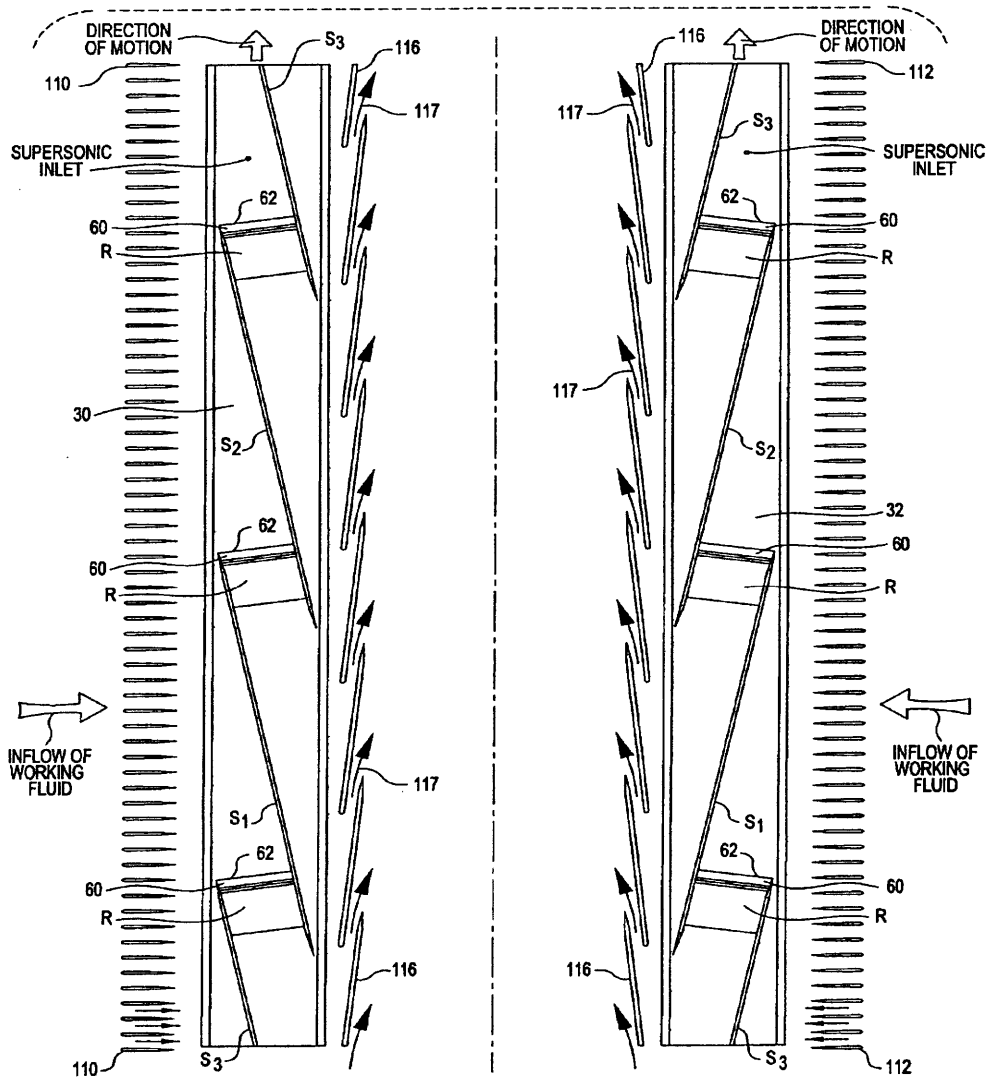

Figure 4-23: Circumferential view of shock compression rotor without inlet pre-swirl wheel [32]

Figure 4-23 shows a circumferential view of the supersonic rotor in the case where no pre-swirl centrifugal wheels are present, with the flow path of the gas clearly marked. The straight lines marked 110 are actually inlet guide vanes (IGV) that help

to straighten the flow before the supersonic rotor acts to compress it. In actuality though, the pre-swirl centrifugal wheels are fairly useful as even a small pressure gain from atmospheric conditions can be multiplied into a much higher pressures using the supersonic rotor. Finally, there are many radial diffuser blades (marked 117) that help to disperse the high pressure gas downstream of the ramp to the outlet, where it can be ejected.

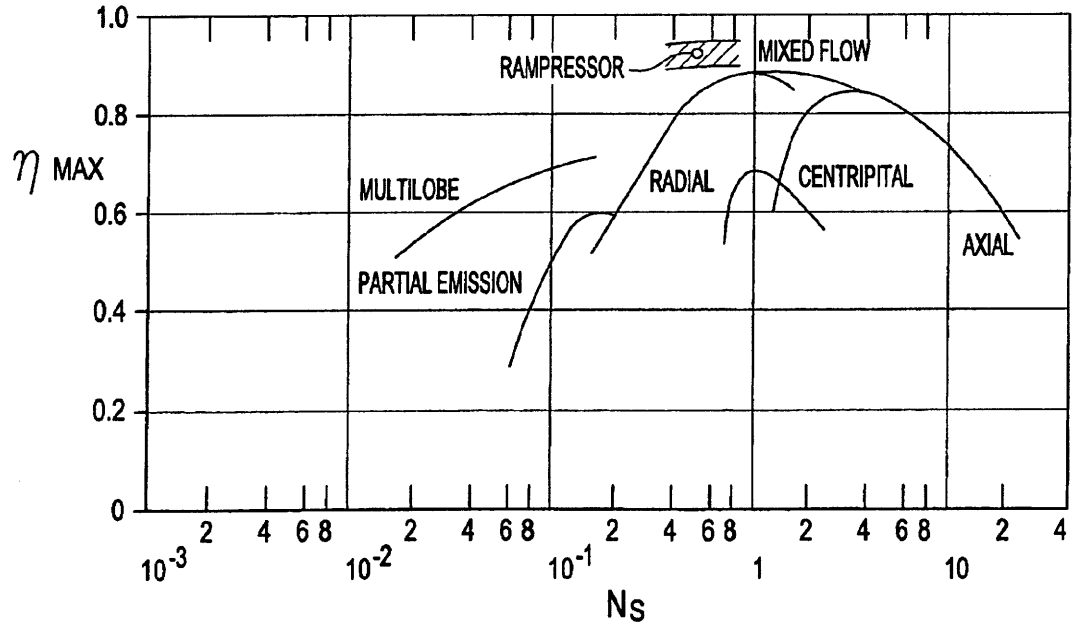

Figure 4-24: Comparison of Rampressor efficiency against other forms of compression [32]

4.5 Basic Simulation of Rampressor

In order to fully understand the Ramgen design, it is vital that some example calculations be carried out to understand on a basic level the ranges of temperatures and pressures that exist within the compressor itself. The attached Appendix consists of a set of rudimentary drawings (or 'frames') that together depict in chronological order the journey of a hypothetical gas molecule that enters the Rampressor, and the presumed properties of the gas at each point. This exercise will help in validating the

claims from Ramgen and also provide an improved understanding of the physics of the gas inside the Rampressor.

The tools used for these calculations predominantly consist of software developed by NASA on its website. These Java-based applets calculate property ratios based on oblique, reflected and normal shock equations that are the same as the ones discussed in Section 4.1 and 4.2. There is scope for specifying three inputs: upstream Mach number, deflection angle and k value. The outputs are all the property ratios (temperature, density and pressure) and in the reflected shock case with multiple shock zones of properties, also a ratio of each of the properties in each zone to the original upstream value.

But in order to build any sort of simulation of the Rampressor, there must be reliable data about the Rampressor itself. Some basics of the Ramgen process are known, such as the inlet Mach number of about 2.5 as shown in Figure 4-17. Using this value, and the value of the deflection angle (also displayed on the computational fluid dynamics model) it is possible to calculate all the property ratios and downstream Mach number for the fluid. Other information about the structure of the Rampressor itself was derived from drawings and information in the Ramgen patent that discusses the invention.

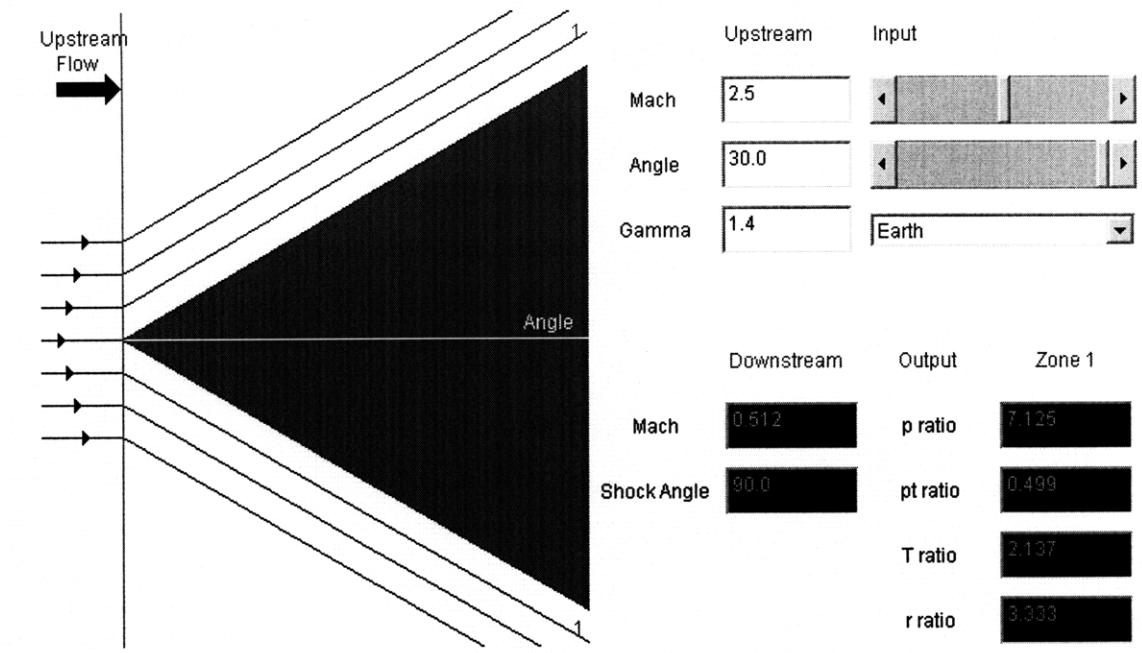

Figure 4-25: Calculation of Downstream conditions and property ratios for upstream properties of M_1=2.5 and δ = 30 degrees in the case of compressible flow over a wedge [30]

4.5.1 Sample Calculations

First, we consider a generic case where oblique shock is present: supersonic flow over a wedge. This case is instructive as it helps us understand the impact a deflection can have on a compressible fluid's Mach number and other properties. The deflection angle was altered so that the downstream Mach number is found to be about 0.5 – roughly the same value as found in downstream in the Ramgen compressor as seen in Figure 4-25.

The results of this trial are that the deflection angle was found to be about 30 degrees to attain a downstream Mach number of about 0.5, as long as the k value (gamma in the applet) remains at 1.4. The corresponding static pressure ratio is about 7.1:1 , whereas the temperature ration is 2.1:1. The total pressure ratio reflects the energy losses and is 0.5:1. The density of the incoming fluid actually increases threefold

as the molecules move closer to the wall of the wedge because of the no-slip boundary condition.

This sample calculation demonstrates that is possible to attain very high static pressure ratios in the case where shock waves are observed in supersonic fluid flow, even though there is a significant energy loss to the shock waves themselves. This is because the kinetic energy of the fluid is being converted to pressure energy.

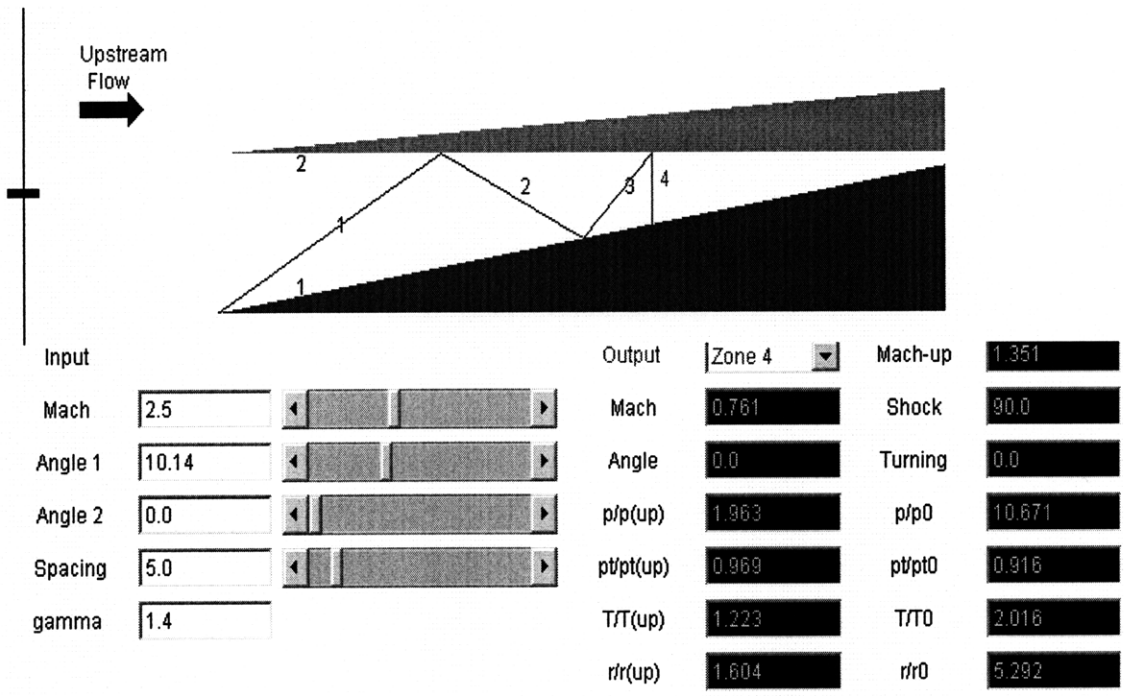

Figure 4-26: Calculation of Downstream conditions and property ratios for upstream properties of M_1=2.5 and δ = 30 degrees in the case of reflected shock [30]

4.5.2 Rampressor case

A more representative case of the Rampressor is the one in which two or more shocks are present, similar to that of Figure 4-17. In this case, both oblique and reflective shocks are present as the compressible fluids flow is deflected twice, once quite sharply. Figure 4-26 depicts this situation. The blue lines represent oblique and reflec-

tive shocks whereas the magenta line reflects a terminal normal shock (also seen in the Ramgen fluid dynamics modeling in Figure 4-17). Each shock line represents a boundary between distinct zones that have characteristic Mach number, temperature, pressure and density properties that can be calculated knowing the upstream Mach number and angle of the deflection.

In this case, similar to that of the previous example, the upstream Mach number was chosen to be 2.5 and the angle was modified to give a subsonic Mach number in the terminal zone: zone 4. The number of shocks change significantly depending on the angle chosen for Angle 1. On the other hand, Angle 2 was chosen to mimic the effect of the shroud (outer) wall of the Ramgen/ramjet intake.

The results in this case were even more representative of the ratios that could be possible in a shock compression system. Although the downstream Mach number was somewhat high at 0.761, the predicted overall pressure ratio (pressure of Zone 4 relative to free stream pressure) was over 10:1 – close to what Ramgen has claimed it can achieve in its Rampressor unit. There is one ratio that is similar to the previous case - an increase in temperature by twofold. However, the density is seen to increase by over 5 times, likely because of the highly confined space the flow is entering. Another astonishing finding from this calculation is a decrease in stagnant (total) pressure by only 9%, compared to over 50% in the last case. This is unexpected, as the addition of the second wall might be expected to significantly reduce the total energy of the flow because of friction against the walls. One explanation for this might be the fact that the previous applet considered a splitting of the flow, and since total pressure might be considered an extensive property, the previous applet may have only considered one of the two split flows.

4.5.3 Frame-by-Frame Analysis

Consider the set of frames in Appendix A. These frames represent the different sections of the Rampressor, with a focus on the sections where gas is traveling. Most of

the frames also have a properties box, which describes the approximate temperature, pressure and Mach number of the gas when it is at the particular section described in the frame. These values help to understand the changes that the gas undergoes inside the Rampressor, and how the gas gets to its final state. Thus, instead of treating the Rampressor simply as a black box, this frame-by-frame analysis tries to account for the presence of the sections mentioned in the patent drawings and their respective effect on gas properties.

In performing the calculations that led to these values, a number of assumptions had to be made. First was that the gas was ideal throughout the process (and thus did not liquefy). It was also assumed that the gas stream of 150,000 lb/hr was entering the Rampressor at approximately 80 F and 22 psia, approximately the conditions an actual low pressure CO_2 stream from the capture-section of a power plant might enter the compression section at. The second was that the pre-swirl wheel had a pressure ratio of about 1.5:1, as mentioned in the patent. The third assumption was that the geometry of the supersonic ramp on the Rampressor rotor was similar to that of Figure 4-17, and that the Mach number profiles and zones from that figure were accurate. It was assumed specifically that there were two jumps of 5 degrees leading to the constant radius diffuser section, as well as around ten 1-degree jumps to create weak oblique shocks and slow the gas down to create static pressure. The k value was assumed to be 1.4.

The calculations at the pre-swirl wheel were conducted assuming a centrifugal compressor, and thus calculations were carried out in a similar fashion to sample calculations in Chapter 3. All supersonic rotor calculations were performed with the aid of the NASA applet. Some more detailed calculations are shown in Appendix A.

4.6 Ramgen Progress

Ramgen makes these claims assuming that state of the art compressor technologies have a performance as specified in Table 4-3.

Table 4-3: Ramgen Performance Claims [31]

Performance Metric	Compression Ratio per stage	Adiabatic Efficiency range
Centrifugal Compressor	1.8-2.8	82-85%
Axial Compressor	1.2-1.4	82-90%
Shock compressor	2.0-15.0	85-90%

The CO_2 compressor has been in development since 1998, when Ramgen received its first funding of note. It has been subject to two major testing initiatives, the RAM 1 and RAM 2, undergoing testing with non-rotating inlets and rotating inlets and varying Mach numbers.

The RAM 1 proof-of-concept test took place over 12 months at a Boeing testing facility. Its aim was to confirm that it was possible to translate the supersonic compression technology of jets to a stationary air application and that a computational fluid dynamic (CFD) model would be able to accurately predict the results of this test. The 11-inch rotor was designed specifically for a pressure ratio of 2.5:1, a tip speed of 1250 ft/sec and a rotation speed of 23,000 rpm. The test was performed simply on air.

The test was deemed successful, with two other notable findings. One was that the Rampressor was self-aspirating; it did not need an impeller or blower to feed the air in at a high velocity. This would reduce the capital cost required for full scale process integration. Also it was found that the common problem of 'surge' was limited in the Rampressor, and easily corrected due to the ability of the turbomachine design to cope with the stresses imposed by a sudden reversal of flow.

The efficiency of the Rampressor was found to be only around 83%, but certain variables were identified to optimize efficiency. These include optimizing the tip speed, rotor geometry, gap between tip and case, among others.

The next test of the Rampressor, called the Ram 2, was meant to test the potential of the technology to scale to meet production demands in a commercial plant. This

meant attempting much higher pressure ratio (predicted 8:1 in air) and rotation speed (45,000 rpm).

The results demonstrated that high pressure ratios could indeed be achieved; 7.8:1 was proven in the demonstration. A relative Mach number of 2.7 was obtained, slightly higher than in RAM 1.

These results can supposedly be extrapolated to use CO_2 instead of air. A demonstration program is being launched by Ramgen to design and test a CO2 compressor for a suction pressure of 220 psia and discharge pressure of 2200 psia, implying the stream would be in a supercritical state since the temperature would also be high. The rotor size will be around 10" and variable speeds will be possible. However, there are still several steps that need to be taken to achieve a better efficiency.

Chapter 5

Energy Analysis

After a basic understanding has been formed of the basic physics of each of the compression technologies, it is important that a careful energy analysis be conducted to understand the potential energy savings associated with each technology. Ramgen's claim of 72% recoverable thermal energy is at the crux of its value proposition of being more economical a compressor than its competitors. Basic thermodynamic analyses can shed more light onto this matter, and a comparison between the different compression technologies in terms of how much energy they require to operate will be instructive when power plant managers make the decision about which technology to purchase. This chapter will attempt to quantify these savings.

5.1 Ideal Cases

There are two ways we will use to calculate parameters related to available heat and energy in a shock compression system. First we will try to use manual calculations similar to those explained in Chapter 3 for other technologies. This is mostly to understand how the calculations are performed. The equations used in these calculations are not specific to shock-compression, but will instead model the effect of having a different pressure ratio for a compressor on the energy balance of the system. Next we will try to model the cases on Aspen-Plus to determine more accurate results.

5.1.1 Calculations

We will first begin with an overall energy balance of three different cases that model carbon dioxide compression in a capture-enabled power plant. These consist of a base case with no intercooling, a case with one intercooler compression technology (modeling the Ramgen shock compression case) and a case with five stages of compression (modeling a centrifugal compressor). Refer to Figure 5-1 for a basic schematic of the system.

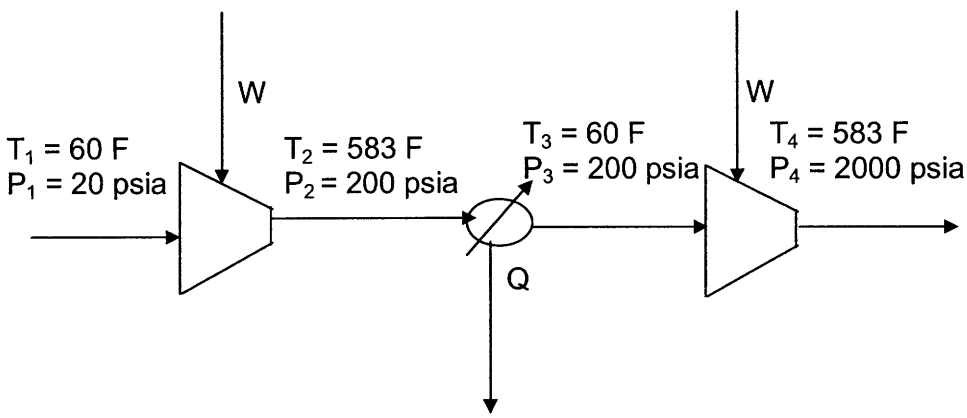

Figure 5-1: Schematic of Rampressor shock compression system, used for energy balance purposes

The assumptions are below. These were formulated to facilitate comparison with the laims made by Ramgen, presented in Chapter 4.

- Incoming gas is pure carbon dioxide at a molecular weight of 44 g/mol
- Incoming gas is at 20 psia and T = 80 F
- Compression is adiabatic and reversible
- Compressor used is Rampressor, with a pressure ratio of 10:1

- Pressure of gas leaving last compressor is 2200 psia
- Ratio of specific heats or k = 1.4
- Weight flow = 150,000 lb/hr
- There is no pressure loss associated with cooling
- Efficiency is 80%

Thus we can say

$R = 1545/44 = 35.1$ ft-lb/lb °R

$T_1 = 80$ °F +460 °R = 540 °R

$(k-1)/k = 0.286$

Base Case– No intercooling (Q=0)

We can basically consider the system as closed, and one giant compressor at a pressure ratio of 100:1 assuming there are no major losses between compressors.

Final temperature as given by equation (3.18)

$T_2 = 540\ (100^{0.286}) - 460 = 1555.55$ °F

From equation (3.20)

$H_a = 1 \times 35.1 \times 540 * (100^{0.286} - 1) / 0.286$

$= 181{,}090$ ft-lb /lb °R

From equation (3.23)

$W_a = 150000 * H_a / 33000 / 0.8 / 60 = 17148.75$ hp

Case (1) – One intercooler, running cooling water, modeling two-stage Ramgen shock compressor train

Assumptions for intercooler:

Incoming conditions (temperature and pressure) of the second compressor are the same as the first compressor (ie perfect cooling)

The compression ratio per stage is calculated as $(P_{final}/P_{inlet})^{1/n}$ where n is the number of stages.

One intercooler implies two stages, so the compression ratio per stage is given by

$r_p = 100^{1/2} = 10$

Final temperature as given by equation (3.18)

$T_2 = 540\ (10^{0.286})\ -460 = 583.26\ °F$

From equation (3.20)

$H_a = 1 \times 35.1 \times 540 * (10^{0.286} - 1) / 0.286$

$= 61764.08$ ft-lb /lb °R

From equation (3.23)

$W_a = 150000 * H_a / 33000 * 2 / 0.8 / 60 = 11697.73$ hp

This amounts to **68%** of the base case power requirement

Clearly an intercooler reduces the overall power load on the system. However this is assuming a perfect intercooler. In a real power plant, the heat transfer would likely be less than perfectly efficient and thus the inlet conditions for the second compressor would not match that of the first compressor. Later, we will attempt to analyze the effect of this case on the energy balance of the system.

Case (2) – Four intercoolers, running cooling water, modeling five-stage centrifugal compressor train

Four intercoolers, or five stages, implies the compression ratio per stage is given by

$r_p = 100^{1/5} = 2.5$

Final temperature after each compression stage as given by equation (3.18)

$T_2 = 540\ (2.5^{0.286})\ -460 = 241.78\ °F$

From equation (3.20)

$H_a = 1 \times 35.1 \times 540 * (2.5^{0.286} - 1) / 0.286$

$= 19855.54$ ft-lb /lb °R

From equation (3.23)

$W_a = 150000 * H_a / 33000 * 5 / 0.8 / 60 = 9401.3$ hp

This amounts to **54.8%** of the base case power requirement

As an aside, we should also examine the isothermal case, which represents an infinite number of stages

From equation (3.23)

$W_a = 150000 * 35.1 * 540 * \ln(100) / 33000 / 60 = 6612.5$ hp

This amounts to **38.6%** of the base case power requirement, and represents the theoretical power limit of compression. This means it is actually a lower bound in terms of the minimum possible work required to compress 150,000 lb/hr of carbon dioxide incoming at atmospheric conditions to a pressure of about 2200 psia.

The high compression ratio required in carbon dioxide compression means that intercoolers seem to have a relatively high impact in terms of reducing the power consumption of the compressors. This conclusion can be drawn from the fact that in the calculations performed in Chapter 3, the theoretical power limit (isothermal case) was much higher relative to the base case at about 70%. Here it is 40%.

However, in a real power plant there are several important inefficiencies that must be accounted for. The next few sections will try to improve upon these calculations in an attempt to find a more accurate representation of the actual behavior of the system

5.1.2 Aspen Model

An Aspen Model of the Rampressor process can also be constructed (see Figure 5-2). This model will help in future sections where heat integration into the rest of the capture-enabled power plant will be required. The figure shows the two stages of the

Rampressor and the corresponding intercoolers. Also labeled are the temperatures and pressures of all the streams.

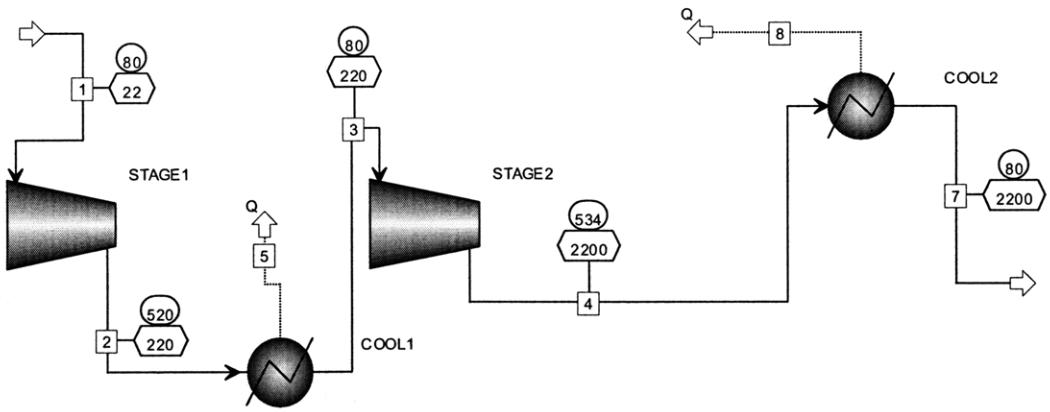

Figure 5-2: Aspen model of Rampressor arrangement

The model employs a Peng-Robinson- Boston Mathias property method with a pure CO_2 stream at 150,000 lbm/hr

The conclusions from the model are that the horsepower required for each compressor is about 5847 hp and the outlet temperature is about 520 F, similar to that as predicted in the manual calculations above (approximately 580 F). Heat available from the coolers is about 15 MMBtu/hr each.

5.2 Heat Integration

It is expected that hot streams of CO_2 will be available to route to other parts of the capture-enabled power plant so that the available heat can be efficiently leveraged. It is worth understanding how much heat can be recovered as well as what various arrangements are possible, in terms of location of heat sink and configuration of plant. This is because all heat that is recovered reduces operating cost of running the plant. In this section, we will attempt to quantify the recoverable heat using Aspen models

of the two major configurations of capture-enabled plants (as discussed in Chapter 2): post-combustion and pre-combustion plants (IGCC).

It should be noted however that there is no available data as to how the Rampressor operates, and without any performance curves it is difficult to determine power requirements for a two-stage 100:1 Ramgen compression train. However, Ramgen has stated that its power requirements are equivalent to that of conventional compressors, and taking that as the best case, we can model a Rampressor on Aspen in a similar fashion to that of a conventional compressor.

5.2.1 Pre-combustion IGCC plant

Heat integration in a pre-combustion IGCC power-plant is quite possible, since the capture process often uses a physical solvent like Selexol which needs to be regenerated. See Figure 5-3 at the end of this section for a representation of the 'Selexol' process, where carbon dioxide is captured from the flue gas by contacting it with Selexol. Sulfur is also removed and sent to a Claus unit for processing, and hydrogen is recovered to produce electricity.

The process in the figure was modified to produce another Selexol process model in Aspen Plus was derived from work done in the MIT Energy Initiative in the BP Conversion project. This model was not designed specifically to account for a shock compression system, but was used as input for calculations presented here. [33]

The main heat sink in this process is the heat required for the reboiler in the Stripper column. This column helps separate hydrogen sulfide (H_2S) and CO_2 from the Selexol stream and regenerate lean Selexol that can be sent back to the absorption columns. Other than that, the main heat sinks in the process are the pumps - energy is required to drive the pumps and compressors that are omnipresent in the system.

The basic process for heat integration will be as follows: hot CO_2 from the Rampressor (both after second stage and first stage) will be transported to the reboiler, where the streams will be contacted with the bottoms liquid in a heat exchanger. This will cool the CO_2 streams to about 306 F. The remaining heat can be used to heat boiler feedwater to about 266 F in a counter-current heat exchanger. This would bring

the temperature of the CO_2 streams down to about 120 F. The remaining cooling must be performed by cooling water. The final temperature was chosen to be 110 F to maintain carbon dioxide above its critical point, which is about 88 F for pure carbon dioxide.

However, because the main advantage of the Rampressor over conventional compressors is the process by which heat is exchanged with the reboiler, only this section of cooling will be examined in this model in order to quantify the energy savings.

It is thus important to model the Stripper column rigorously to determine whether the heat available from the Rampressor would be of use for the reboiler. Running an Aspen simulation on the Stripper shows the following results:

Reboiler/ bottom-stage performance for Stripper, Pre-Combustion

Temperature: 266 F

Net Heat Duty: 166 MMBtu/ hr

Bottoms rate: 3543852 lbm/hr

The temperature and net heat duty are especially important values in the configuration of the CO_2 compression process so that it integrates well with the carbon capture equipment. This is because the hot CO_2 streams emerging from each stage of the Ramgen compressor will be able to supply heat to the reboiler to offset some of the energy penalty in heating the bottoms streams. The temperature the hot stream of CO_2 can be cooled down to is necessarily higher than the temperature of the bottoms stream by a certain buffer to maintain low cost for the heat exchanger. In our Aspen Plus model of the Rampressor integrated with the Selexol process, we chose a differential of 40 F, which should be sufficient to provide efficient cooling.

Another question to be answered is how much of the net heat duty required in the bottoms can be provided by exchanging with the hot CO_2 streams? The more heat that can be offset, the lower the operating costs of the entire process.

But it is not only the reboiler that is important for integration – the CO_2 streams going from the Selexol process into the Rampressor must also be accounted for in our

Aspen compression process model. There are two streams emerging from the Selexol process that are meant for CO_2 sequestration – a low pressure (LP) stream and a medium pressure (MP) stream. The low pressure CO_2 stream has a far higher mass flow rate, but has only trace amounts of substances other than carbon dioxide. The medium pressure CO_2 stream on the other hand, has a significant mole fraction of hydrogen. This may be significant when the thermodynamic properties of the compressed stream is analysed to understand whether or not any liquid is formed within the Rampressor. These streams have H_2O in them, but that component would typically be separated out before the compression section, leaving a dehydrated stream that cannot form liquid water in the compressor.

The relative pressure values of the MP and LP stream are especially important, as the pressure ratio from MP:LP may well determine the quantity and type of compressors needed. In this case, the LP stream is at a pressure of about 22 psia whereas the MP stream is at a pressure of about 160 psia, a ratio of almost 8:1. The Rampressor pressure ratio is 10:1, whereas conventional compressors such as centrifugal or axial have a maximum pressure ratio of about 3:1. The options for compressing the low pressure stream to the medium pressure are 2 conventional centrifugal compressors or simply one Rampressor. Because the capital cost of the Rampressor is purported to be significantly less than the centrifugal compressors, the Rampressor may be the best unit for this purpose.

An Aspen model was created with this configuration, for the purpose of understanding how much heat can be recovered from the Ramgen compressor process as well as setting up a basis for integration with the CO_2 streams captured in the Selexol process. See Figure 5-4 at the end of this section.

Two metrics are important to calculate – heat recovery and power recovery. The first is a metric used by Ramgen for comparison purposes, and constitutes the amount of heat in a compressed stream that can be recovered in useful heat as a proportion of the total amount of heat in the stream (given a minimum temperature of 110 F). The second is power recovery, which requires finding how much power can be

generated from the recovered heat from the hot CO_2 stream as a proportion of the power required to drive the compressor

Results

It was found that the heat that can potentially be supplied to the reboiler is 38.6 MMBtu/hr after the first stage and about 88.65 MM Btu/hr after the second stage, for a total of 127.25 MMBtu/hr. This accounts for a significant portion of the heat duty of the reboiler which is about 166 MMBtu/hr. (about 82.5%). The horsepower required to power the two Rampressors was 32419 hp for the first stage and 43025 hp for the second stage.

Heat recovery is found to be 49% for the first stage and 47% for the second stage. 127.25 MMBtu/hr in recovered heat will be used to create low pressure steam at 0.45 bar. This steam can be used to drive a turbine to produce 4.44 MW of power or 5963 hp, which represents a power recovery of 7.9%.

5.2.2 Post-combustion

The main heat sink in a post-combustion unit is the heat required to regenerate the amine solvent in a stripper column, similar to that in pre-combustion. However, there is a marked difference in properties:

Reboiler/ bottom-stage performance for Stripper, Post-Combustion [33]

Temperature: 254 F

Heat Duty: 440 MMBtu/ hr

Bottoms rate: 3774026 lbm/hr

Much of what applies to the pre-combustion case also applies to the post-combustion case. The main differences are simply in the composition and properties of the feed CO_2 stream to the Rampressor as well as the fact that there is only one feed stream in the post-combustion case instead of two. This will not materially change the modeling process significantly. Thus, much of the process in the previous section can be emulated for this section.

Results

It was found that the heat that can potentially be supplied to the reboiler is 15.6 MMBtu/hr after the first stage and about 18.3 MM Btu/hr after the second stage, for a total of 33.9 MMBtu/hr. This accounts for a much slimmer portion of the heat duty of the reboiler which is about 440 MMBtu/hr. (about 7.7%). The horsepower required to power the two Rampressors was 9767.65 hp for the first stage and 9318 hp for the second stage.

The heat recovery was calculated similar to the previous case. Heat recovery is found to be 61.94% for the first stage and 46.3% for the second stage. 33.9 MMBtu/hr in recovered heat will be used to create low pressure steam at 0.45 bar. This steam can be used to drive a turbine to produce 1.2 MW of power or 1611 hp, which represents a power recovery of 8.44%.

Table 5-1 – Summary of results from heat integration calculations broken down per stage

	Pre-combustion Stage 1	Pre-combustion Stage 2	Post-combustion Stage 1	Post-Combustion Stage 2
Mass flow (lb/hr)	974186	1060000	237505	237505
Power requirement (hp)	32419	43025	9767.65	9318
Heat recovered as low pressure steam (MM Btu/hr)	38.6	88.65	15.6	18.3
Cooling duty (MM Btu/hr)	40.47	99.95	9.98	21.2
Exit temperature (F)	459	580	564	572
Heat recovery (%)	49	47	61.94	46.3

Comparison to Selexol model

The amount of heat that can be recovered from the Rampressor process for the Selexol process is far higher than the amount of heat that can be recovered for the post-combustion process. This is because the mass flow rate of the feed CO_2 steam in the post-combustion case is about 237000 lb/hr whereas the mass flow rate of the feed CO_2 stream in the Selexol stream is much higher at 1062000 lb/hr. This might also help explain the much higher work requirements for the Rampressor units in the Selexol case. However the overall heat recovery is higher for the post-combustion case than the Selexol case.

5.2.3 Conventional compressors

It is also useful to model a conventional compressor under similar conditions to both of the cases above. A six stage centrifugal compressor is selected in conditions similar that what would be observed in a pre-combustion IGCC plant or a post-combustion power plant. Five intercoolers are also present. In the post-combustion case, water is removed before the stream is compressed to prevent formation of liquid inside the compressor.

An Aspen Plus model of this case is presented in Figure 5-5 and Figure 5-6 at the end of this section. The very same feed streams were used as for the Rampressor cases above.

Results

Since there is no power to be recovered for conventional compressors, the most important results are the power requirements and cooling duties. The power requirement for a conventional 6-stage compressor in a **pre**-combustion power plant is 64,314 hp and the cooling duty is 255 MM Btu / hr.

The power requirement for a conventional 6-stage compressor in a **post**-combustion power plant is 16,576 hp and the cooling duty is 255 MM Btu / hr.

5.2.4 Comparison of all results

Table 5-2 – Comparison of heat integration results

	Pre-combustion Rampressor	Pre-combustion Conventional	Post-combustion Rampressor	Post-combustion Conventional
No. Stages	2	6	2	6
Mass Flow (lb/hr)	1,060,000	1,060,000	237,505	237,505
Power requirement (hp)	75,532	64314	19,085	16,576
Heat recovered (MM Btu /hr)	127.25	0	33.9	0
Cooling Duty (MM Btu/hr)	140.42	255	31.18	61.9
Power recovery (%)	7.9	0	8.4	0

We find that the conventional compressors have a lower power requirement than the Rampressors in both types of plant configurations. This is to be expected, as more power is required for the higher compression ratio that is the defining characteristic of the Rampressor system (assuming they are equally efficient). Conventional compressors clearly have a higher cooling duty, however. This is because they cannot use the heat in the compressed CO_2 streams in any useful way, and therefore must instead use cooling water or some other form of energy to cool the streams.

Power recovery is also nil for both conventional compressors, due to the fact that there is no way to recover the heat from the compressed streams; these are simply not hot enough.

To compare the results for the two configurations, we find that the power requirement and cooling duty are higher for the pre-combustion case than the post-combustion plant. This is likely because of the much higher mass flow in our pre-combustion Selexol model. Power recoveries are almost equal, however.

Caveats with this analysis include the fact that efficiencies for the Rampressor and conventional compressor were assumed to be roughly the same, which may not be the case. However, the Rampressor has not been proven at scale just yet.

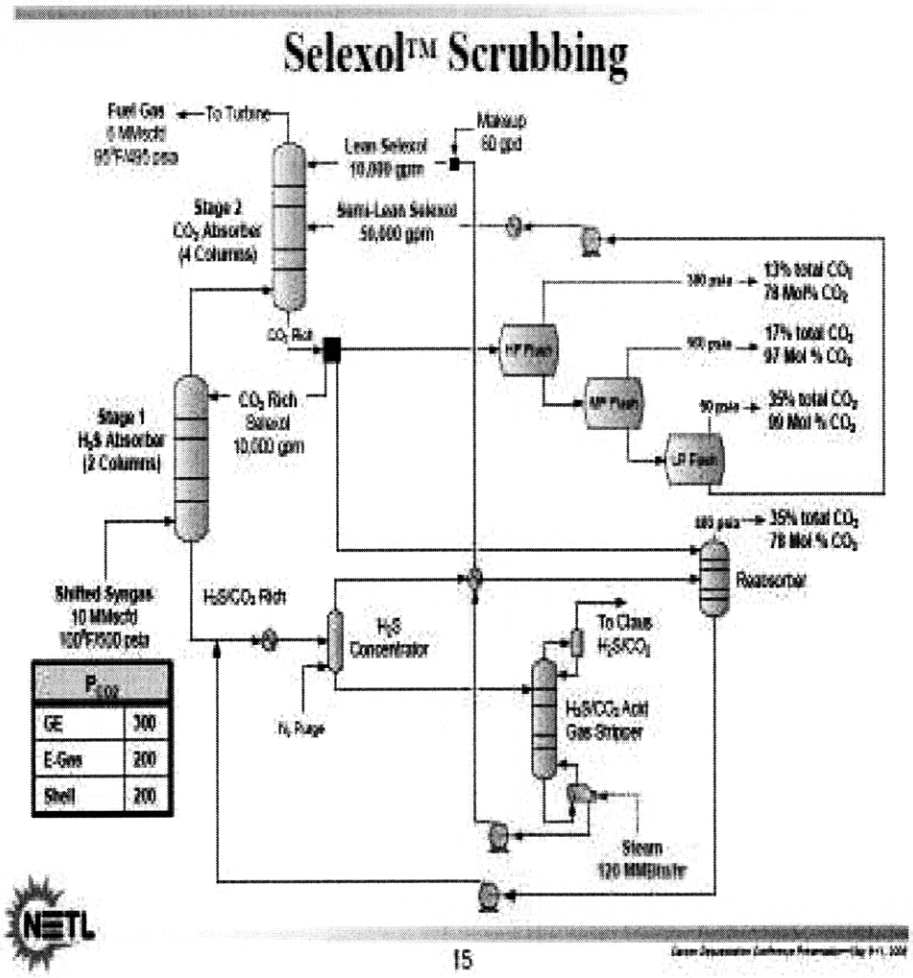

Figure 5-3: A model that was used as a basis for calculating exit CO_2 conditions. This NETL model was modified in the MIT report. [34]

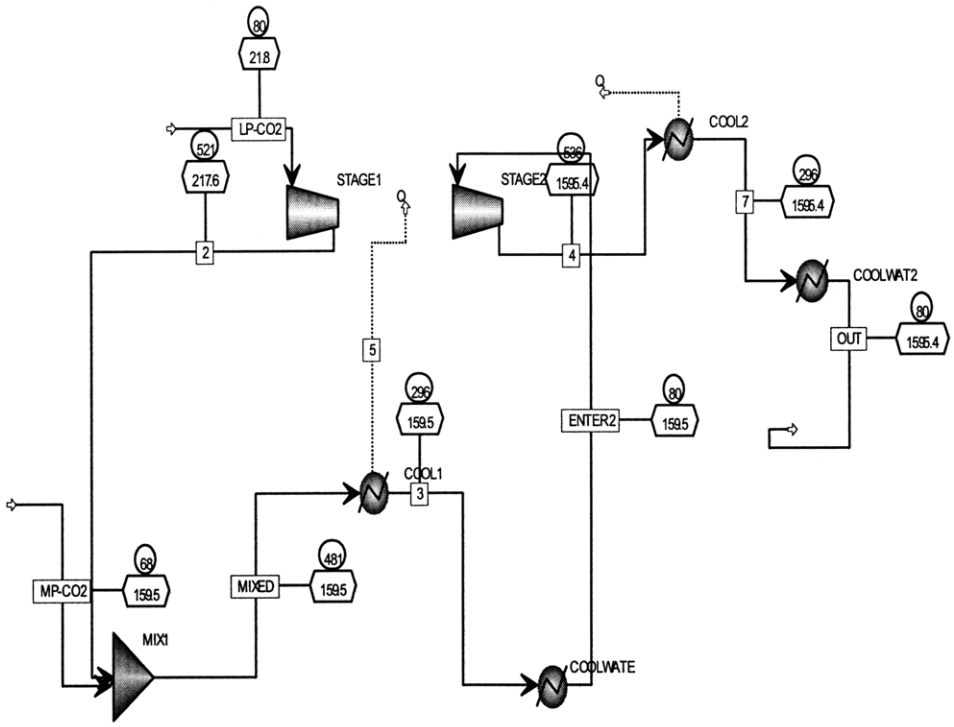

Figure 5-4: Ramgen process model integrated with pre-combustion carbon capture (Selexol process)

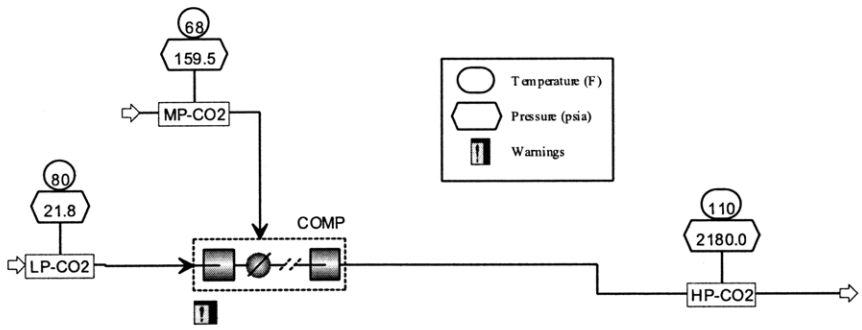

Figure 5-5 - Conventional multi-stage compressor model in Aspen Plus for the pre-combustion case

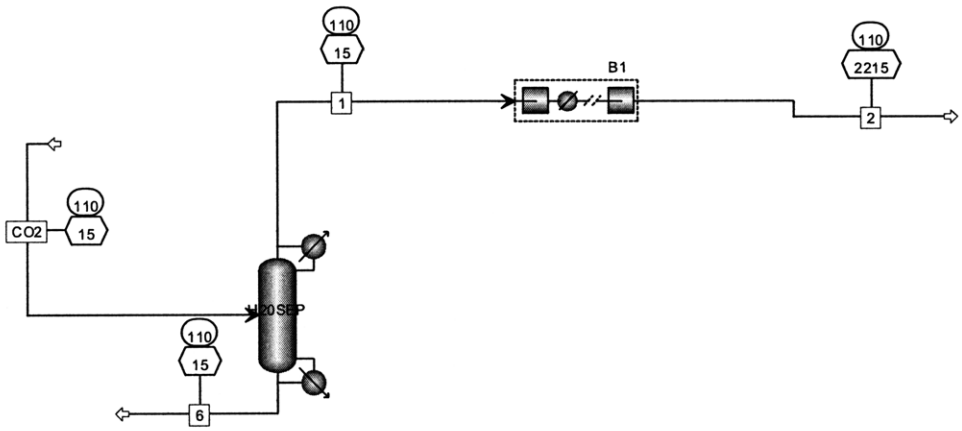

Figure 5-6 - Conventional multi-stage compressor model in Aspen Plus for the post-combustion case. The feed stream is dehydrated beforehand

Chapter 6

Economic Analysis

The purpose of this thesis was to evaluate compression technologies used in carbon capture and sequestration applications. In order to complete this, it is necessary to discuss their benefits and drawbacks in economic terms as well as technical. The following chapter will present an overview of the economics involved in choosing between various compression technologies.

6.1 Review of CCS Economics

Before examining the specific economics of compression within a power plant, it is necessary to understand the overall economics of the power plant itself and compare the case used in this study with the cases used by other sources.

The following section will describe the broader economic picture of both capture-enabled power plants and power plants without capture in order to gain an understanding of what constitutes a baseline power plant. Many of these numbers are derived from the NETL Cost and Performance Baseline report.

The fundamental operating economics of a power plant rely on key metrics, such as capture rate, gross power, auxiliary power requirement, efficiency and heat rate. These terms are defined below:

Capture rate: The percent of emitted carbon dioxide that is captured by a process in the power plant (such as with a Selexol or amine-based solvent)

Auxiliary power: Power needed to support the basic power needs of the plant. Examples of power sinks in the plant are carbon dioxide compressors, carbon capture operations, air separation unit and base power load (running pumps, etc)

Gross power: Total amount of power produced by the plant. Total power less auxiliary power is the net power produced.

Efficiency (HHV): The proportion of input energy that is converted by the power plant to electrical energy. This is generally thermal efficiency for a power plant purposes calculated on a Higher Heating Value (HHV), where the reference cooling temperature is taken to be 25 C instead of 150 C in the case of Lower Heating Value (LHV) [35]

Heat rate (Btu/ kWh): The amount of heat released through combustion of a fuel compared to the amount of electricity produced

A measure commonly used to account for electricity generation economics is the levelized cost of electricity (COE), which is the constant dollar electricity price over the life of a plant to pay for all operating expenses, debt payments as well as dividends to investors. COE is made up of capital cost, operating and maintenance costs and fuel costs. It has been found to be around 4-5 cents per kilowatt-hour for PC plants without capture, 6-9 cents per kilowatt-hour for PC plants wit capture. For IGCC plants, the range for plants with capture is about 5-7 [9]. Capital cost of the equipment particularly plays a major role in determining the long-term viability of a power plant. Furthermore, there is potentially a cost associated with emissions of harmful gases, depending on the state of environmental regulation.

Various configurations of power plants are possible, such as pulverized coal (PC), natural gas combined cycle (NGCC) and integrated gasification combined cycle (IGCC). For this section the focus will be on the ones most relevant to the thesis topic and the configurations examined in previous chapters. These include a pre-

combustion Selexol carbon-capture IGCC power plant (using a GE gasifier), a post-combustion PC plant with an amine-based solvent for carbon capture and for comparison purposes, a GE IGCC plant and a PC plant with no carbon capture. These all have varying gross power outputs and thus are difficult to compare, but are still useful in understanding how the economics of each individual plant look like.

Table 6-1: Overall operating economics for various plant configurations [7]

	IGCC No capture	**IGCC w/ Capture**	**PC No capture**	**PC w/ Capture**
Gross Power Output (kW)	770,350	744,960	583,315	679,923
Auxiliary Power Requirement (kW)	130,100	189,250	32,870	130,123
Net Power Output (kW)	640,250	555,675	550,445	549,613
Coal flow rate (lb/hr)	480,634	500,379	437,699	646,589
HHV thermal input (kW)	1,674,044	1,710,379	1,496,479	2,210,668
Net HHV plant efficiency (%)	38.2	32.5	36.8	24.9
Net plant HHV heat rate (BTU/kW-h)	8,922	10,505	9,276	13,724
Raw water usage (GPM)	4,003	4,579	6,212	14,098
Total plant cost	1,160,139	1,328,209	852,612	1,591,277

($x1000)				
Total plant cost ($/ kW)	1,813	1,813	1,549	2,895
CO_2 emissions (lb /hr)	1,123,781	2,390	1,038,110	152,975

A few trends can be noted from Table 6-1, accounting for the difference in gross power output. The first is that plant efficiency is higher for IGCC plants than PC plants, and that plants with carbon capture have a lower efficiency than plants without capture. This is partly due to the higher auxiliary power requirements for carbon capture and compression in a capture-enabled power plant. In general, PC plants also require much more water. Auxiliary power requirements are highest in IGCC plants. Total plant cost is highest for PC plants with carbon capture equipment, and lowest for PC plants that do not require carbon capture. IGCC power plant costs are somewhere in between. Carbon dioxide emissions are roughly equal for IGCC and PC plants with no carbon capture, but IGCC with carbon capture reduces emissions by a much more significant amount (capture rates are different in the NETL numbers).

It is useful to perform some basic calculations to understand how some of these numbers were derived, with a focus on finding the amount of carbon captured in a 550 MW power plant. Assuming bituminous coal (being used in this study) has a chemical formula of $CH_{.793}N_{.015}O_{.078}$ [36] and that all the carbon is converted to carbon dioxide on a molar basis (ie complete combustion), we can use the power rating of the plant (550 MW) to calculate the input coal flow rate and then find the output CO_2 flow rate.

Assumed inputs:

Power input: 556 MW for IGCC w/o capture and 550 for PC w/o capture

Thermal efficiency: 38.2% for IGCC without capture and 36.2% for PC without capture

Molecular weight of bituminous coal [36]14.27 g/mol

Molecular weight of carbon dioxide: 44 g/mol.

High heating value of bituminous coal: 8.47 kW -h / kg

Capture rate = 90%

To find the input power for a power plant, we can use the formula:

Input power * thermal efficiency = Power generated

We can then find the input coal flowrate using the equation:

Coal flowrate = Input power/ HHV_{coal}

We can use the following formula to find a rough estimate of the carbon dioxide being produced in the process:

Carbon dioxide produced (lb/hr) = MW_{CO2} ;/ MW_{coal} * Coal Flowrate (lb/hr)s * capture rate

Using this formula, the following values are found for total CO_2 produced in the process:

Table 6-2: Comparison of hand calculations and NETL report

	IGCC w/o carbon capture	**PC w/o carbon capture**
CO_2 production (lb /hr) – NETL	1,123,781	1,038,110
CO_2 production (lb /hr) – hand calculation	1,048,256	1,006,257

These results show how the predicted CO_2 production is lower than the NETL CO_2 production by less than 100 M lb/hr in both cases. This gap may be due to the fact that we assumed a 90% capture rate, which was not the case for the NETL numbers,

but was applied in our calculations to show how a capture rate can be used in these calculations.

These flow rates of carbon dioxide will be critical when deciding how many compressor trains are needed in parallel to compress a stream of captured carbon dioxide. Further analysis will be conducted in subsequent sections.

6.2 Compressor Economics for Managers

6.2.1 Conventional Compressor

The type of compressor considered to be a representative case of 'existing technology' will be a multi-staged centrifugal compressor, integrally geared. This is the most common type of compressor for these types of applications, mainly because of its advantages in relatively high capacity, high efficiency and low cost. This type of compressor is also the type used in the NETL report.

The most important metrics to a plant engineer when purchasing equipment that meets all the required technical specifications are the capital cost of the equipment and the operating cost in both energy and materials. Thus, the first step in understanding centrifugal compressor economics is finding typical capital and operating costs (on a yearly basis).

The capital cost from the NETL report is said to be $17.7 million for the equipment needed for 5 compressor trains (4 stages and 1 spare). The average cost per centrifugal compressor train is therefore $3.54 million. Each compressor train consists of 6 individual stages with 5 intercoolers. There is also a gas drying unit before the compressor train to remove the water. The installation cost is $10.65 million based on labor needed to transport and set up the equipment on site.

Other sources should be consulted to verify this capital cost. Another report suggests the price is around $20 million for a compressor to pressurize 750,000 lbs/hr to 1300 psia [37]. The differences in design conditions make a comparison between different conventional technologies' capital cost somewhat difficult.

The operating costs can be calculated by assessing the value of the input power to the compressor, in addition to the energy required to cool the hot streams in between each stage. Calculations performed in chapter 5 have produced the results needed for quantifying the operating cost of the compressor train. The economics are presented in section 6.2.3

6.2.2 Rampressor

The new technology being evaluated in this thesis is the Rampressor, a compressor that uses shock-waves to pressurize relatively heavy gases. The physics and design behind this technology is described in Chapter 4. It is meant to be used in power plants in two stages, with a special intercooler in between the stages and a cooler after the stages as well. The difference between the coolers in a two-stage Rampressor system and a conventional compressor system is that because the temperature of the compressed gas stream exiting each Rampressor stage is much higher than the temperature exiting each conventional compressor stage, this extra heat can be removed in a heat exchanger, and an intermediate fluid can be transported to other areas of the plant where there are heat sinks and used in heat exchangers to supply heat.

The advantage of these hotter-than-usual compressed streams from the Rampressor is that some heat can be recovered to reduce the steam requirements in the plant. This can reduce the operating cost of the plant. But as Table 5-2 shows, there is already a greater power requirement to running the Rampressor due to the high compression ratios, which may mean that energy savings are nullified.

The capital cost of the Rampressor is also a key factor in making a decision whether to purchase the compressor or not. The firm thinks it can sell the compressor

for about $4.3 MM, with an extra $1.1 MM for installation. This is for a compressor train with a capacity of 150,000 lb/hr. [31]

6.2.3 Economic Comparison

It is now possible to compare the economics of the breakthrough and traditional technologies, with a focus on capital cost and operating costs. Other factors such as technical and administrative risk, will be accounted for afterwards.

To perform these calculations, we need to assume a price of electricity. Using the Energy Information Administration database, we find the average price of electricity for the United States in 2008 was 9.67 cents per kilowatt-hour or $96.7 per megawatt-hour [38]. This is different from the COE explained in earlier sections since this is the price electricity is sold for by the utilities, and is a market value for electricity. This was used in the comparison in Table 6-3 and was assumed to be 6.5 cents per kilowatt-hour for all configurations for simplicity purposes. [9]

Table 6-3 - Comparison of economics between the Rampressor and conventional compressor in both pre-combustion and post-combustion economics

	Pre-combustion Rampressor	Pre-combustion Conventional	Post-combustion Rampressor	Post-combustion Conventional
No. Stages	2	6	2	6
Mass Flow of plant (lb/hr)	1,060,000	1,060,000	237,505	237,505
Capacity of compressor train (lb/hr)	150,000	270,000	150,000	270,000
Number of compressor trains required	8	4	2	1
Total equipment capital cost ($ x 1,000,000)	34	14	8	3.54
Power requirement (hp)	75,532	64314	19,085	16,576
Normalized power requirement (hp/ (1000 lb-hr))	71	61	81	70
Cost of power ($/hr)	3662	3118	925	802
Heat recovered (MM Btu /hr)	127	0	34	0
Value of heat recovered ($/hr)	289	0	77	0
Cooling Duty (MM Btu/hr)	140	255	31	62

Cost of Cooling Duty ($/hr)	318	578	71	140
Total Operating Cost ($/hr)	3692	3697	919	942

We find that the operating costs for conventional compressors are virtually identical to that of the Rampressor, even given the benefits of heat recovery. This is because the power requirement for the conventional compressor is much lower. The cost of both types of compressors over time is presented in Figure 6-1, assuming all other variables such as fuel costs are kept constant.

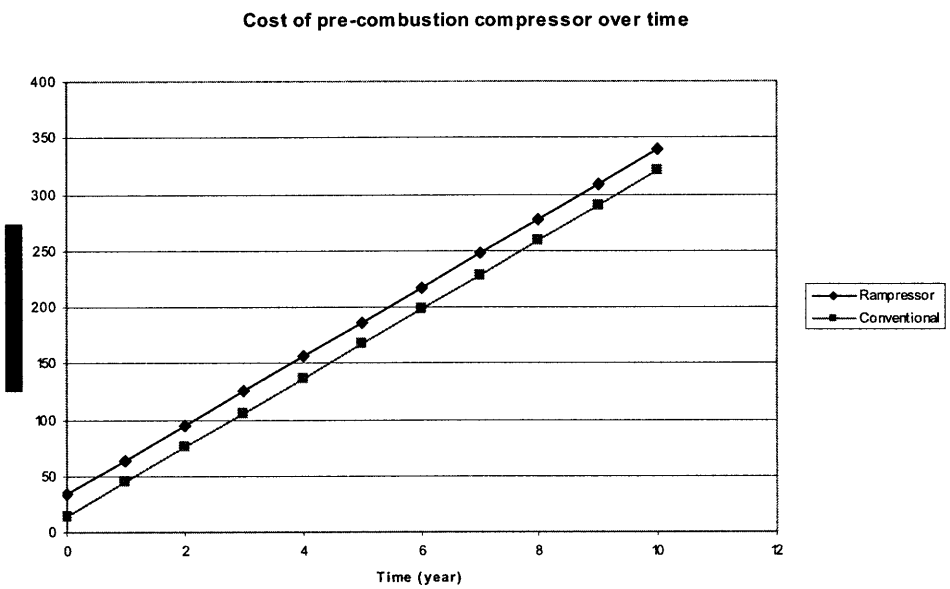

Figure 6-1: Cost of both a Rampressor and Conventional compressor over time to a pre-combustion plant, based on capital and operating costs alone.

Figure 6-1 shows how the operating costs become much more important than the capital cost after just over a year of operation. This means that for a plant manager, reduc-

ing the energy load of the compressor is actually much more important than the up front capital cost.

However since there is no benefit for the Rampressor in operating cost, this will not affect the decision of a plant manager. Our calculations show that since the capacity of the Rampressor is lower than that of conventional compressors, more Rampressor compressor trains are required, increasing the capital cost even higher than the conventional compressor.

6.2.4 Caveats in analysis

There are several aspects to this analysis that have not been included in this study. Maintenance costs may be the most significant of these. Without any data from a Rampressor operating at commercial scale for a reasonable duration of time, it is difficult to assess what might go wrong and what maintenance would be associated with the new shock compressor.

Reliability is another factor. Will the performance of the Rampressor be consistent under various conditions such as ambient conditions, changes in purity of stream, plant shutdowns and so forth? More data is needed before this question can be satisfactorily answered.

Another risk for a manager would be the risk that rapid development of the Rampressor may render any purchased product obsolete very quickly. This is a risk with purchasing any new technology, but must still be accounted for, especially since plant lifetimes tend to extend for several decades, whereas development cycles may only last two or three years, depending on financing.

Finally, safety may be a concern for a new technology without much prior validation. The supersonic speeds of the rotor combined with the extra hot compressed discharge CO_2 streams may be the prime threats.

Chapter 7

Conclusions & Recommendations

The objective of this study was to evaluate a shock compression technology in the context of the technological developments in capture-enabled power plants and conventional CO_2 compressors. The previous chapters have performed this evaluation with careful consideration to both technical (Chapter 5) and economic (Chapter 6) factors thought to be crucial to the success of this technology. Chapter 2 provided a technical context for the power plant configurations in which a CO_2 compressor would operate in, while Chapters 3 and 4 explained existing and shock-compression technologies for CO_2 pressurization respectively.

It is clear that novel compression technologies tend to have very long development timelines, as can be seen from the historical study of centrifugal and axial compressors. In most cases, the compressor development is not completed until there is an urgent need for the technology (like the airplane for axial compressors, or the air-conditioner for centrifugal). The pressing demand often engenders increased engineering focus and better financing, a potent combination for innovation and commercialization. The Rampressor technology may be timely in that it may also be addressing a pressing need with its application in so-called 'clean coal' power plants, a technology supported by policy makers in many developed countries, especially the United

States. However, there has not been any major legislation passed as yet that would make carbon capture a necessity. Without stringent legislation in the form of a carbon tax or cap-and-trade system, the outlook for increased financing and engineering focus for the Rampressor technology development remains dim. As development only begun relatively recently for this specific application, this may mean there is a chance the technology may not ever find any real use.

A basic examination of the physics of shock compression confirms that the Rampressor is a technically feasible device and that the claimed compression ratio and temperature gain for a compressed CO_2 stream are not unreasonable. The previous application of supersonic ramps in aircraft is a strong validation point as well. Basic simulations performed in Chapter 4 roughly corroborate the claims of Ramgen in performance terms.

However, the benefits of the Rampressor in terms of power recovery are less clear. Useful work is being put into the compressor but only heat is being extracted, meaning that there will always be the significant energy loss associated with converting heat back to work. Calculations performed in Chapter 5 find that conventional compressors have a lower power requirement but a higher net cooling duty than the Rampressors in both types of plant configurations studied (pre-combustion and post-combustion coal-fired power plants). In comparison of the results for the two configurations, we find that the power requirement and cooling duty are higher for the pre-combustion case than the post-combustion plant. This is likely because of the much higher mass flow in our pre-combustion Selexol model. Power recoveries are almost equal, however. A summary table to compare all four cases is reproduced in

Table 7-1.

Table 7-1– Comparison of heat integration results

	Pre-combustion Rampressor	Pre-combustion Conventional	Post-combustion Rampressor	Post-combustion Conventional
No. Stages	2	6	2	6
Mass Flow (lb/hr)	1,060,000	1,060,000	237,505	237,505
Power requirement (hp)	75,532	64,314	19,085	16,576
Heat recovered (MM Btu /hr)	127.25	0	33.9	0
Cooling Duty (MM Btu/hr)	140.42	255	31.18	61.9
Power recovery (%)	7.9	0	8.4	0

Finally an economic analysis was conducted in Chapter 6 to determine whether the potential for heat integration with the rest of the power plant would make the Rampressor an attractive option for purchasing engineers. A summary is presented in Table 6-3 and reproduced in Table 7-2 below. It was found that the operating costs of the Rampressor are not significantly lower than that of conventional compressors for any type of plant configuration, and given its relatively low capacity, its capital cost may even be higher. It was also found that operating cost is more important than capital cost as criteria for choosing a compressor, as operating cost exceeds capital cost after just two years of operation.

Thus as it stands plant managers or engineers deciding which technology to purchase for a commercial-scale pre-combustion or post-combustion power plant should choose conventional compressors over shock compressors from Ramgen, given the inherent risk in picking a new, unproven technology. These risks include unknown maintenance costs, unforeseen safety issues and potential that the machinery does not

perform as claimed. But the decision-making process may be drastically altered if the input power required to drive the Rampressor can be reduced substantially – perhaps by a more efficient design of the supersonic rotor and shock geometry. Currently however, the power recovery from heat integration is simply too low in any power plant configuration to justify the risk and capital cost.

There are several caveats to this analysis. Several assumptions were made with these calculations, including a key assumption that efficiencies of the Rampressor and conventional compressor are roughly equal. Also multiple factors were not included in this study, such as maintenance costs, time-variant factors such as development cycles and macroeconomic variables such as inflation. These should be included in future studies of this technology.

Table 7-2 – Comparison of economics between the Rampressor and conventional compressor in both pre-combustion and post-combustion economics

	Pre-combustion Rampressor	Pre-combustion Conventional	Post-combustion Rampressor	Post-combustion Conventional
No. Stages	2	6	2	6
Mass Flow of plant (lb/hr)	1,060,000	1,060,000	237,505	237,505
Capacity of compressor train (lb/hr)	150,000	270,000	150,000	270,000
Number of compressor trains required	8	4	2	1
Total equipment capital cost ($ x 1,000,000)	34	14	8	3.54
Power requirement (hp)	75,532	64314	19,085	16,576
Normalized power requirement (hp/ (1000 lb-hr))	71	61	81	70
Cost of power ($/hr)	3662	3118	925	802
Heat recovered (MM Btu /hr)	127	0	34	0
Value of heat recovered ($/hr)	289	0	77	0
Cooling Duty (MM Btu/hr)	140	255	31	62

Cost of Cooling Duty ($/hr)	318	578	71	140
Total Operating Cost ($/hr)	3692	3697	919	942

7.1 Future Work

The Rampressor remains a fledgling technology and could be investigated further if new breakthroughs are achieved in reducing power requirements or capital cost. The potential savings from a highly efficient CO_2 compressor would certainly help capture-enabled power systems become a more feasible option for policymakers and private corporations deciding on an energy supply mix.

Future work can thus be conducted on evaluating this technology. In particular, more in-depth analyses may be performed on the fluid dynamics involved in the shock-compression process. Using computational CFD models, it is possible to obtain more accurate results for each of the shock zone properties. These results will allow for a better understanding of what kind of compression ratios and temperature gains are possible. The CFD models can then generate performance curves that can be leveraged in the Aspen Plus model to provide an improved simulation of the Rampressor in the context of plant operation.

It may also be useful to try even more configurations of power plants to see if more of the heat available in the hot compressed CO_2 streams can be utilized. This would increase the power recovery of the Rampressor unit and improve its economic viability. There is especially scope for reconfiguring the Selexol-based carbon capture unit of a pre-combustion power plant. For example, a reabsorber can be added to the process to aid solvent recovery, producing a CO_2 stream at a very high pressure. Also,

the medium pressure stream can be recycled in a similar manner to the high pressure stream from the series of flash drums. This aids hydrogen recovery.

Economic modeling can be improved greatly by the use of more complex forecasts to predict how demand of compressors may change over the next few years, and what kind of uncertainty there is in policy decisions that drive this demand. In addition, with the availability of more data on the breakdown of equipment and materials, it is possible to forecast how the costs for the Rampressor will differ from the projected costs of conventional technologies. Maintenance costs should also be included in the operating costs when a comparison is performed between the technologies. Also as the technologies mature, it is likely that there will be significant positive step-changes in the performance of the Rampressor. It may be possible to model these and their impact on economic feasibility by employing historical analogues for other capital-intensive technologies in a growing market.

Finally, performance data should be collected as the Rampressor goes through further testing in pilot or demonstration phases. This performance data could be fed into the Aspen model or a CFD simulation to help increase their validity and more accurately determine what the actual required input power is for the Rampressor to achieve the desired compression ratio. The data is also a key indicator of the technological development cycle of the Rampressor, and can help with projections of how much time and money are needed to achieve certain efficiency and scale metrics.

Appendix A

Frame-by-Frame Rampressor Analysis

To understand the physics of the Rampressor, it was useful to construct a set of hand-drawn frames to simulate the process of compression. These frames are derived almost exclusively from information in the Ramgen patent and Ramgen presentations.

Each frame has a purple label in the lower left corner containing the step number and a short description. In addition, each frame has an estimate for the current velocity, temperature and pressure for gas at the specified point in a frame (the point is depicted by a hypothetical gas molecule, colored in red). Along with the frames, calculations are presented below where appropriate.

In performing the calculations that led to the values for temperature, pressure and velocity of the gas at various stages in the process, a number of assumptions had to be made. First was that the gas was ideal throughout the process (and thus did not liquefy). Actually, CO_2 normally exits the compressor at a high pressure (from 1600 – 2200), putting it in the supercritical phase. The key implication of the ideal assumption is therefore the fact that heat capacity is assumed to be constant throughout the process, regardless of temperature or pressure. It was also assumed that the gas stream of 150,000 lb/hr was entering the Rampressor at approximately 80 F and 22 psia, approximately the conditions of the actual low pressure CO_2 stream leaving the capture-section of a power plant might. The second was that the pre-swirl wheel had a pres-

sure ratio of about 1.5:1, as mentioned in the patent. The third assumption was that the geometry of the supersonic ramp on the Rampressor rotor was similar to that of Figure 4-17, and that the Mach number of the incoming stream of gas relative to the supersonic rotor is at roughly 2.5 M. It was assumed specifically that there were two jumps of 5 degrees leading to the constant radius diffuser section, as well as around ten 1-degree jumps to create weak oblique shocks and slow the gas down to create static pressure. The specific heat ratio was assumed to be 1.4 (although this tends to change with temperature for any gas).

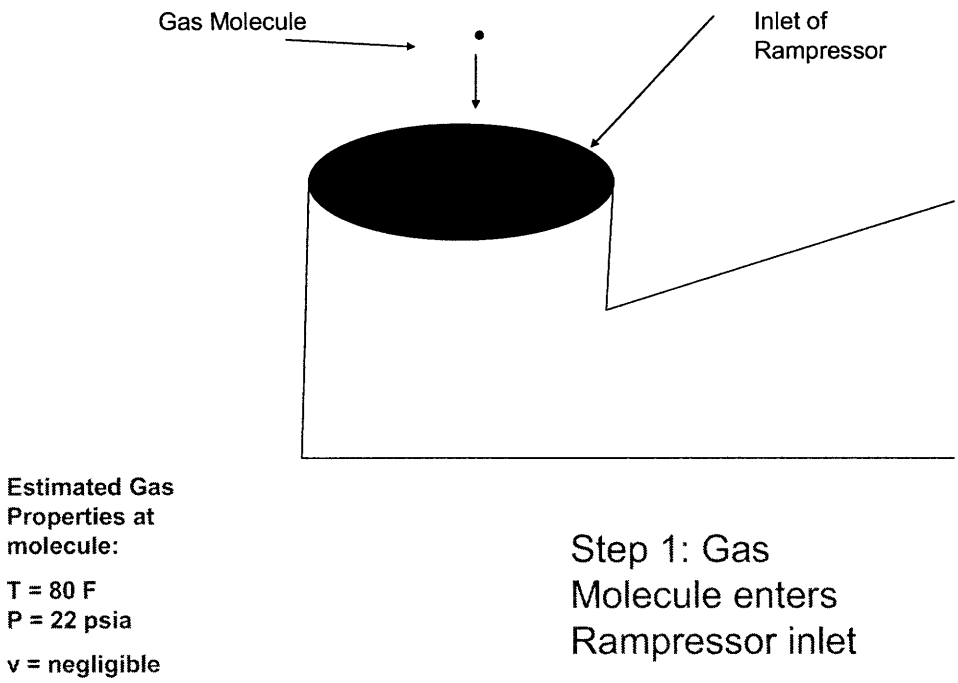

The entering conditions for the Rampressor were derived with the assumption that the entering gas was stagnant, pure CO_2 at room temperature and slightly higher than room pressure. The pressure was chosen with the knowledge that exit pressure for a carbon dioxide compression unit is normally stipulated to be 2200 psia (depending on

how far the CO_2 has to be transported), and that the Rampressor has a 100:1 compression ration in two stages. Therefore, the starting pressure has to be around 22 psia. This starting pressure has also been verified by MIT Aspen models that simulate the CO_2 carbon capture unit operation.

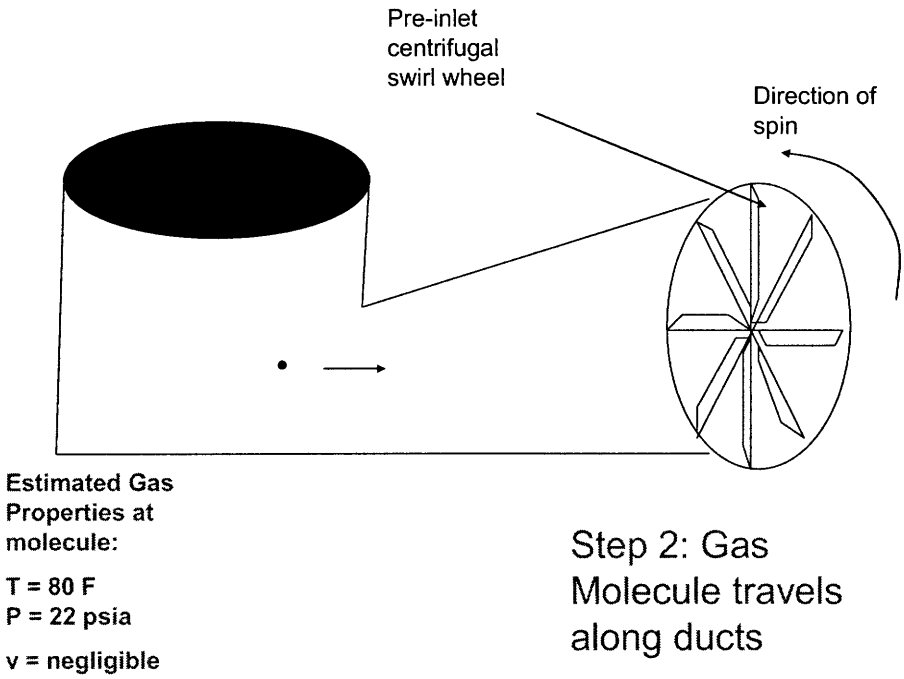

The purpose of the pre-inlet swirl wheel is to provide a boost to the gas that is entering at a negligible velocity. This additional velocity can also be converted to static pressure in a diffuser (seen below).

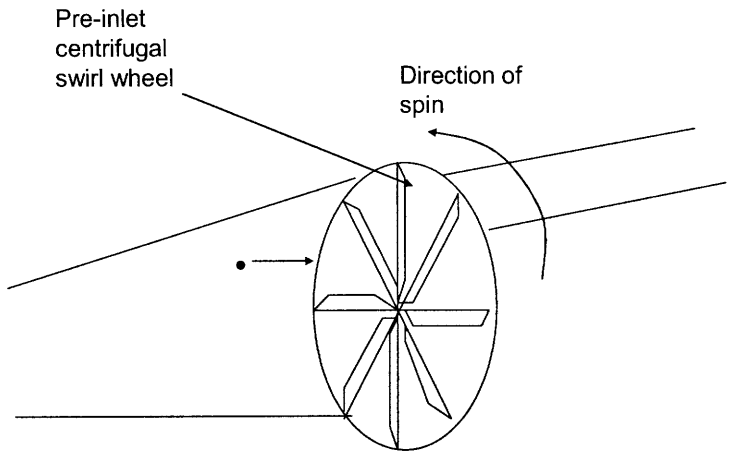

Estimated Gas Properties at molecule:

T = 80 F
P = 22 psia

v = negligible

Step 3: Gas Molecule enters pre-inlet centrifugal swirl wheel

The pre-inlet swirl wheel spins in the opposite direction to the supersonic rotor in order to impart an even greater velocity to the gas molecules relative to the rotor. This increases the potential static pressure ratio.

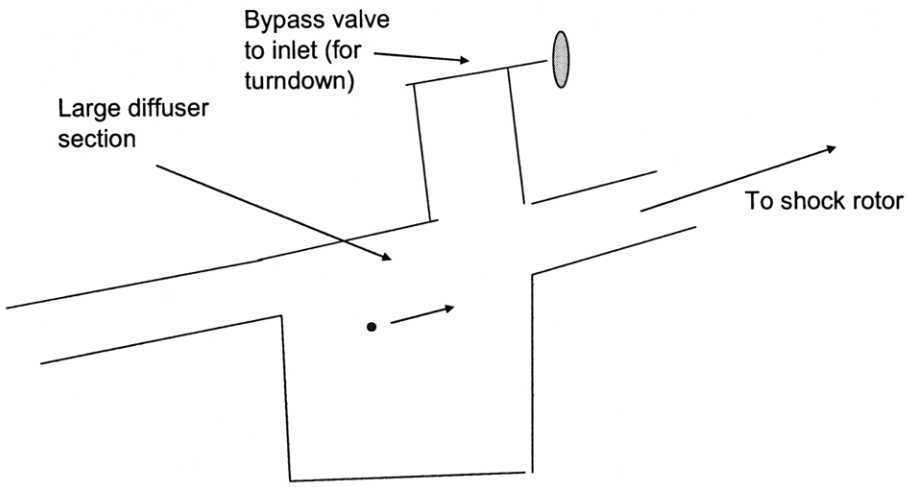

Estimated Gas Properties at molecule:

T = 146 F
P = 33 psia

v = 0.1 M

Step 4: Gas Molecule exits pre-swirl wheel at higher pressure

These calculations were performed assuming an overall pressure ratio of about 1.5:1 for the centrifugal wheel, as stated in the Ramgen patent. This means the final pressure of the gas would be around 22 * 1.5 = 33 psia. The velocity was assumed to have been increased slightly to 0.1 M since all of the kinetic energy could not have been converted to static pressure. Using the equations set forth in Chapter 3, it is also possible to calculate the temperature gain

Gas= Carbon Dioxide (Mol Wt = 44 g/mol)

k = 1.4

Inlet pressure = 22 psia

Outlet Pressure = 33 psia

Inlet Temperature = 80 F

Weight flow = 150000 lb/hr

R = 1545/44 = 35.1 ft-lb/lb °R

$T_1 = 80 + 460 = 540$ °R

$(k-1)/k = 0.286$

Final temperature as given by equation (3.18)

$T_f = 540\ (1.5^{0.286}) - 460 = 146$ °F

.

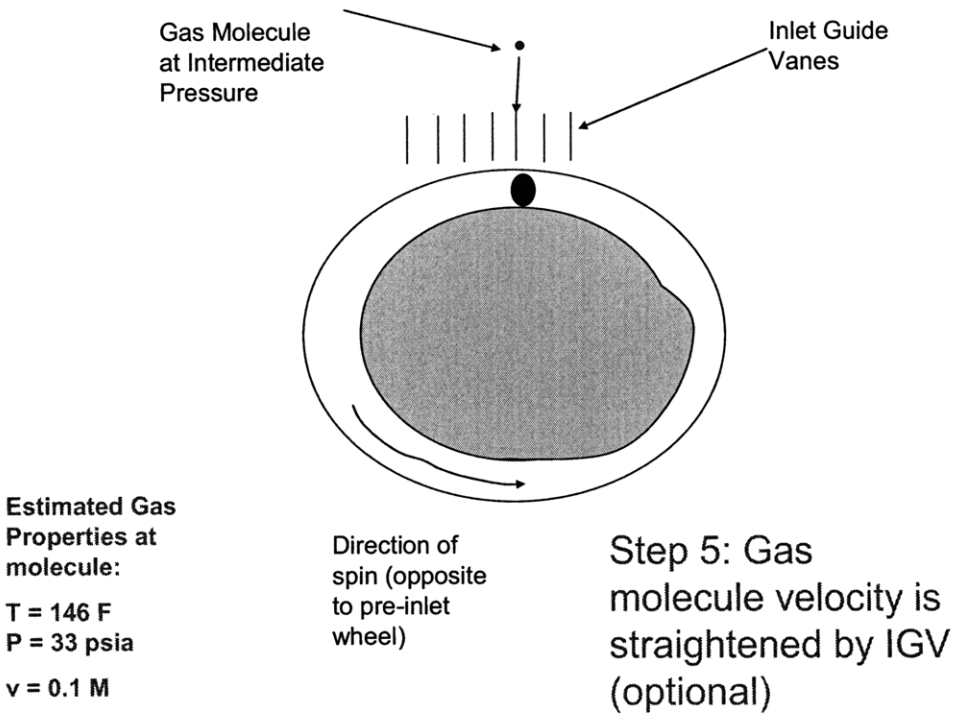

This step may also include flow straighteners to reduce swirl; however these were mentioned as optional in the patent and therefore neglected.

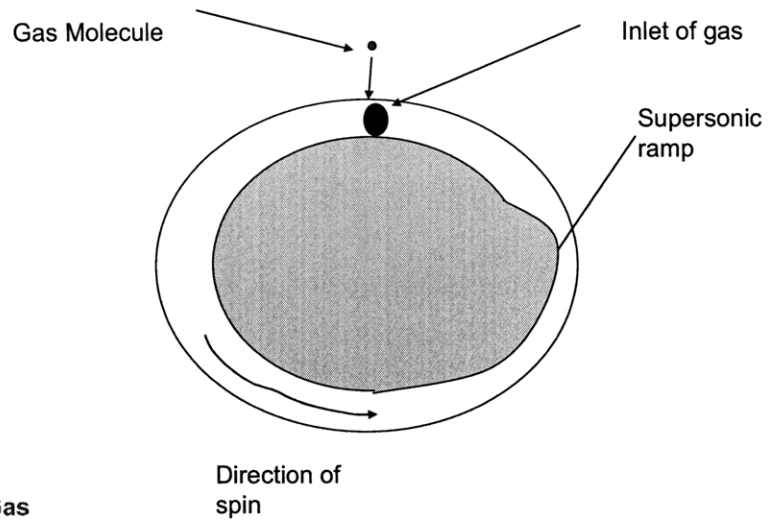

Estimated Gas Properties at molecule:

T = 146 F
P = 33 psia

v = 0.1 M

Step 6: Gas Molecule enters Rampressor axially

Each supersonic rotor also has multiple ramps separated by strakes; however, for demonstration purposes only one is shown here.

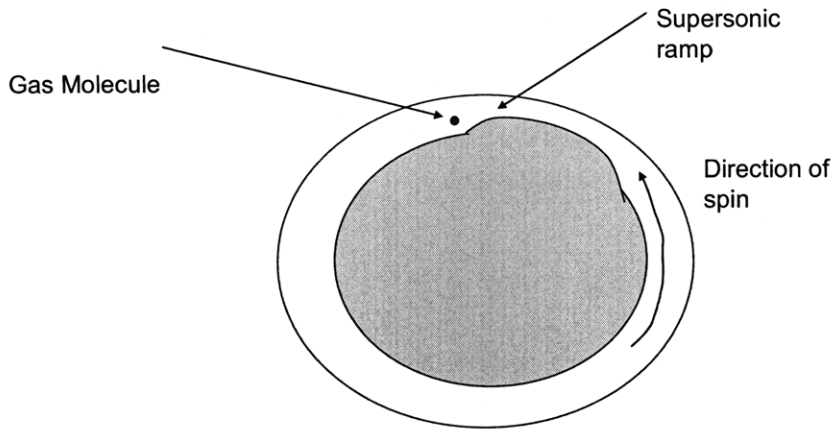

Estimated Gas Properties at molecule:

T = 146 F
P = 33 psia

v = 2.5 M

Step 7: Molecule is carried along by motion of rotor.

The rotor tip moves at supersonic speed, leading to a gas relative velocity of about 2.5 Mach (according to Ramgen tests [31]). Shear effects are neglected by assuming the gas is inviscid and therefore the boundary layer is very small.

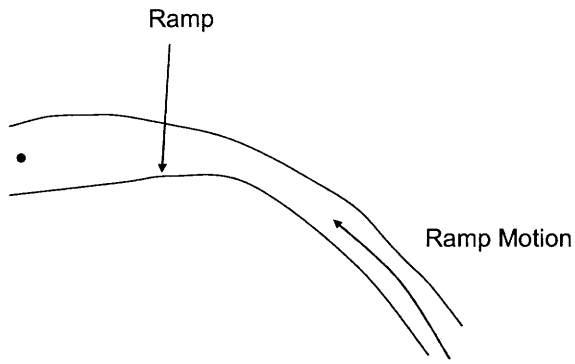

Estimated Gas Properties at molecule:

T = 146 F
P = 33 psia

v = 2.5 M

Step 8: Molecule approaches ramp in constant-radius inlet

This drawing is similar to the CFD model results from Ramgen presented in Chapter 4. That diagram was used as an input to the following calculations, since it contained the basic information required to perform some simple calculations such as incoming Mach number and ramp geometry.

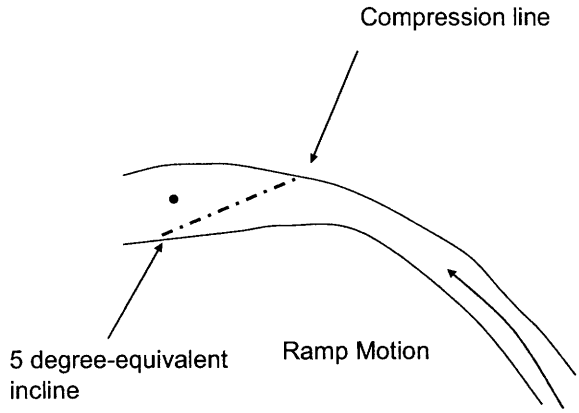

Estimated Gas Properties at molecule:

T = 146 F
P = 33 psia

v = 2.5 M

Step 9: Compression lines form as oblique shock waves are created due to a 5 degree incline in the ramp.

An explanation of oblique shock waves can be found in Chapter 4. A 5 degree-equivalent incline refers to a sudden increase in the angle of the ramp relative to the shroud wall, thus compressing the gas quickly in a short period of time. This sudden change in angle produces an oblique shock wave when the gas stream is entering at supersonic speeds.

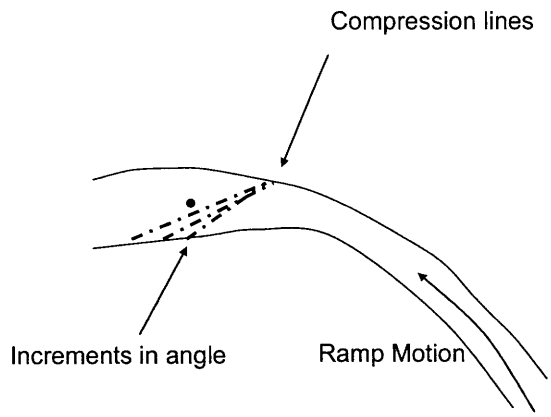

Estimated Gas Properties at molecule:

T = 146 F

P = 33 psia

v = 2.5 M

Step 10: Multiple compression lines occur as a result of 1 degree increments in ramp angle

These results were obtained from NASA applets that are demonstrated in Chapter 4, along with underlying equations. Basically for each increment in angle, there is a separate zone with its own unique properties created (a compression line is the boundary for a sharp discontinuity in properties). The angle and incoming Mach number act as inputs to equations 4.41 to 4.45 to generate a table such as Table 4-2. These equations are what the NASA applets use to perform oblique angle calculations. All equations were verified with ones displayed on the NASA website to ensure they were identical. These equations are displayed below:

$$\tan\delta = 2\cot\theta\left[\frac{M_1^2\sin^2\theta - 1}{M_1^2(k+\cos 2\theta)+2}\right]$$

$$\frac{P_2}{P_1} = \frac{2k}{k+1} M_1^2 \sin^2\theta - \frac{k-1}{k+1}$$

$$\frac{T_2}{T_1} = \frac{2k}{(k+1)^2} M_1 \sin^2\theta - \frac{k-1}{(k+1)^2 M_1}[(k-1)M_1^2 + 2]$$

$$\frac{\rho_2}{\rho_1} = \frac{(k+1)M_1^2 \sin^2\theta}{(k-1)M_1^2 \sin^2\theta + 2}$$

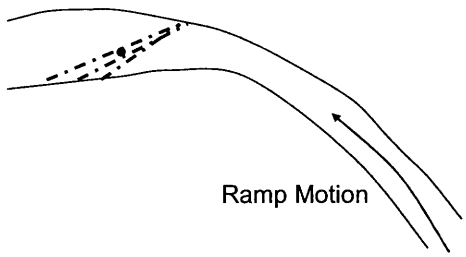

Estimated Gas Properties at molecule:

T = 269 F

P = 45.54 psia

v = 2.3 M

Step 11: As the molecule crosses these lines, its properties change abruptly

The equations displayed for the previous slide are solved together with the incoming Mach number and deflection angle as input for each simulation. The NASA simulation performs these calculations with an applet tool that calculates the pressure, temperature and density ratios for each zone. The downstream Mach number and thus velocity can be expressed with the equation

$$M_2^2 \sin^2(\theta - \delta) = \frac{[(k-1)M_1^2 \sin^2\theta + 2]}{2kM_1^2 \sin^2\theta + 2 - (k-1)}$$

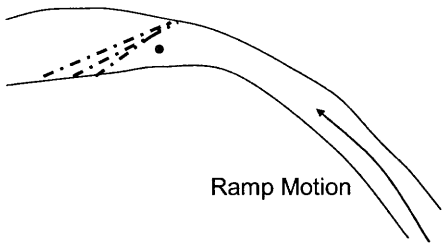

Estimated Gas Properties at molecule:

T = 400 F

P = 80 psia

v = 1.8 M

Step 12: Molecule enters a linear section where it maintains constant properties

By now the temperature and pressure have increased significantly whereas the velocity has declined significantly. In this section, there are no more sudden inclines and thus the properties of the gas remain constant. All in all, it was assumed that there was one major 5 degree-equivalent incline followed by two smaller 1 degree-equivalent inclines.

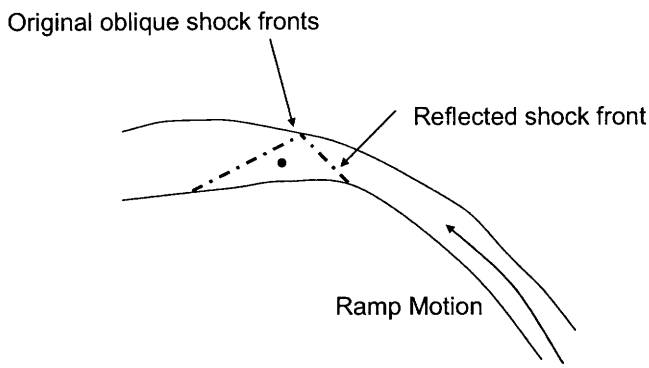

Estimated Gas Properties at molecule:

T = 400 F

P = 80 psia

v = 1.8 M

Step 13: A single reflected compression line is generated from the previous oblique shocks

The physics of reflected shock are explained in Chapter 4. As the oblique shock is reflected, it creates new zones of specific properties. The reflection continues until the Mach number is reduced below 1, and an oblique shock can no longer be supported. Ideally, the geometry of the supersonic ramp would be optimized to reduce the number of shocks, since there is an energy penalty associated with the gas crossing every compression line.

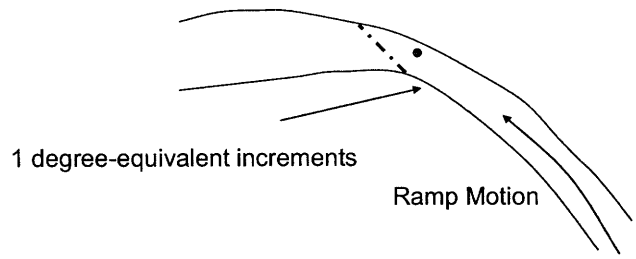

Estimated Gas Properties at molecule:
T = 579 F
P = 172.8 psia
v = 1.3 M

Step 14: Molecule enters a narrow zone at with 1 degree-equivalent increments in angle.

There is a separate NASA applet specially created for reflected shock applications that was applied for these calculations. The equations used are identical to those of oblique shock explained above but account for multiple zones and explain how the temperature and pressure ratios change from zone-to-zone as well as from the upstream conditions. At this point in the compressor, the gas is slowing down considerably and approaching subsonic velocities.

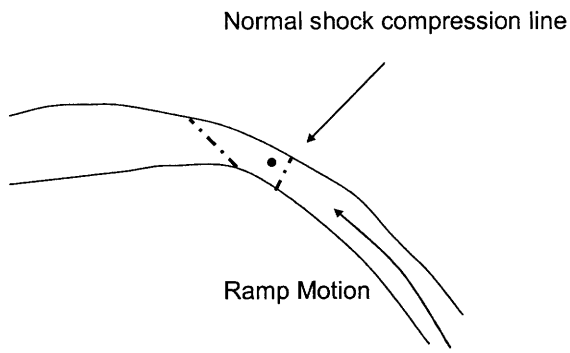

Estimated Gas Properties at molecule:
T = 579 F
P = 172.8 psia
v = 1.3 M

Step 15: Normal shock forms as gas velocity is reduced

Normal shock typically forms as a gas slows down to subsonic velocities. It always forms the final zone in a series of shock zones. In this stage, the gas is crossing its final compression line to enter into the subsonic phase. This is partly due to another series of 1 degree-equivalent inclines.

Although the NASA applet could be used for these calculations, it is useful to reiterate the basic equations. Downstream Mach number is just a function of upstream Mach number and the specific heat capacity ratio

$$M_y^{\,2} = \frac{M_x^{\,2} + \dfrac{2}{k-1}}{-1 + \dfrac{2k}{k-1} M_x^{\,2}}$$

Pressure ratio and temperature ratio for normal shock also have much simpler equations than that of oblique shock

$$\frac{P_y}{P_x} = \frac{2k}{k+1} M_x^{\,2} - \frac{k-1}{k+1}$$

$$\frac{T_y}{T_x} = \frac{1 + \frac{k-1}{2} M_x^{\,2}}{1 + \frac{k-1}{2} M_y^{\,2}}$$

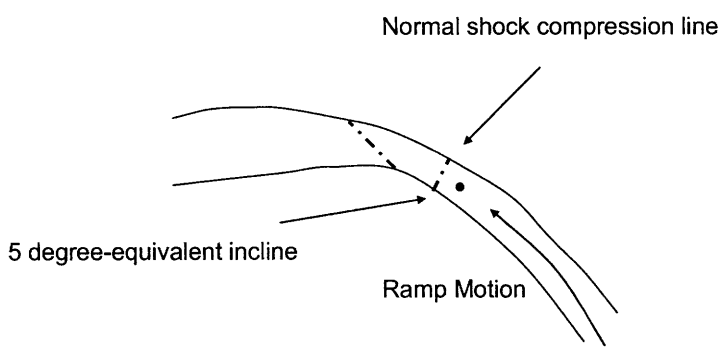

Estimated Molecule Properties:

T = 710 F

P = 258 psia

v = 0.7 M

Step 16: Gas molecule in subsonic diffuser section slows down further, converting velocity energy to static pressure

The incline mentioned on this diagram serves to increase the space between rotor and shroud wall. This space effectively serves as an expander/diffuser, helping to convert the kinetic energy of the gas into static pressure. At this point, the process is very similar to that of a conventional compressor, except the gas starting velocity is much higher and the expander much smaller.

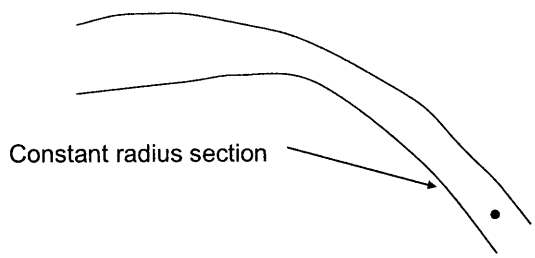

Estimated Molecule Properties:

T = 710 F

P = 258 psia

v = 0.7 M

Step 17: Gas molecule enters a constant radius section

The temperature and pressure found here are both high in comparison to Ramgen claims. It is likely one of the assumptions for geometry is incorrect, but with no more information it is difficult to say which one. However, since both temperature and pressure are higher than the Ramgen claims, and since the assumptions were mostly conservative it is a reasonable conclusion to say that the Rampressor can feasibly achieve its stated pressure ratio and temperature gain.

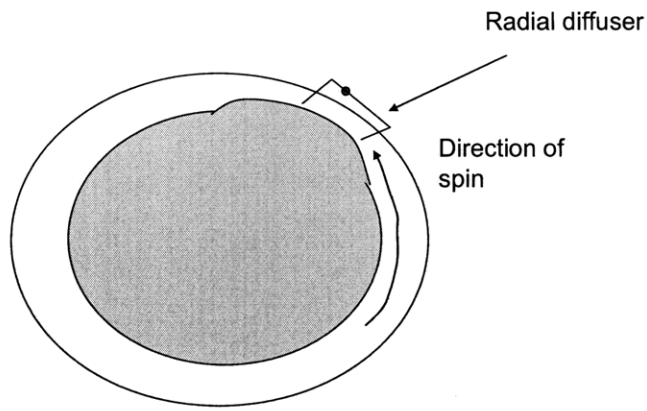

Estimated Molecule Properties:

T = 710 F

P = 258 psia

v = 0.7 M

Step 18: Radial diffuser deflects molecule to outlet

The radial diffuser is mentioned in the patent but its geometry and function are not clear. Theoretically the diffuser would increase static pressure even further, reducing radial velocity, and increasing axial velocity by deflecting the molecules axially. However, it was neglected in these calculations since its geometry was unknown.

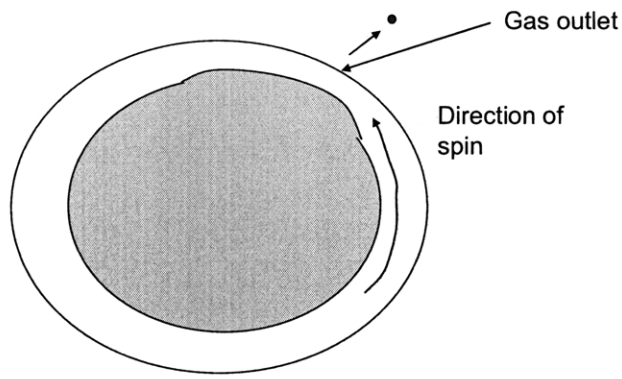

Estimated Molecule Properties:

T = 710 F

P = 258 psia

v = 0.7 M

Step 19: High pressure gas escapes axially

The supersonic rotor has an axial inlet and outlet. The radial diffuser in the previous slide serves to deflect the gas molecules in an axial direction, where they can then escape from the compressor entirely. Note that with these properties the gas stream will be in the supercritical phase.

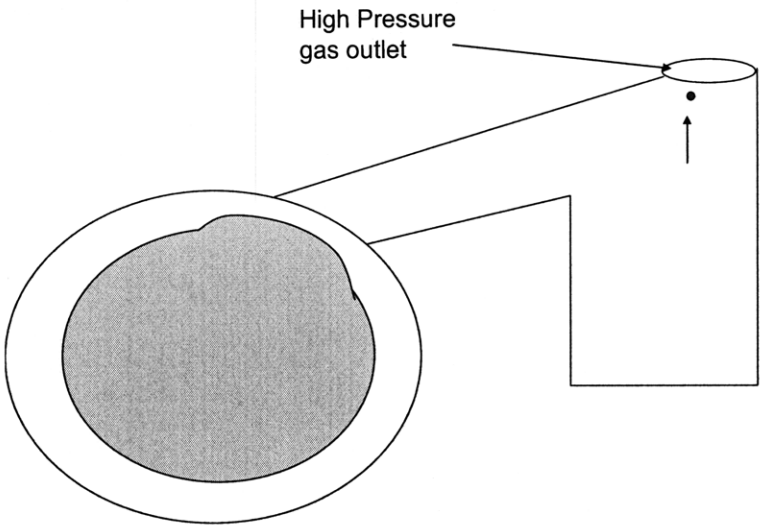

Step 20: Gas is removed from Rampressor

Hot compressed gas escapes from the compressor at low velocity. Some waste heat from the compression will inevitably remain within the compressor walls, however.

References

1. Stern, N. *The Stern Review*; The Office of Climate Change: 2006.

2. IPCC *Climate Change 2001: Third Assessment Report*; 2001.

3. NASA Clouds and the Earth's Radiant Energy System. http://eospso.gsfc.nasa.gov/ftp_docs/lithographs/CERES_litho.pdf

4. Wikipedia Climate Model. http://www.globalwarmingart.com/wiki/Wikipedia:Climate_model

5. Saha, K., *The Earth's Atmosphere: Its Physics and Dynamics*. Springer: 2008.

6. McCoy, S. T. The Economics of CO2 Transport by Pipeline and Storage in Saline Aquifers and Oil Reservoirs. Carnegie Mellon, 2008.

7. Ruether, J. A. *FETC Programs for Reducing Greenhouse Gas Emissions*; US Dept of Energy: 1998.

8. barackobama.com Campaign Issues. http://my.barackobama.com/page/content/newenergy

9. MIT The Future of Coal. http://web.mit.edu/coal/

10. Zachary, J., C02 Capture and Sequestration Options: Impact on Turbo-Machinery Design. In *Proceedings of ASME Turbo Expo 2008: Power for Land, Sea and Air*, Berlin, Germany, 2008.

11. CERIC Carbon Dioxide Pure Component Properties.
<http://www.cheric.org/research/kdb/hcprop/showprop.php?cmpid=1943>

12. PNNL About Supercritical Fluid.
<http://www.pnl.gov/supercriticalfluid/about.stm>

13. Shakhashiri Carbon Dioxide - Chemical of the week.
<http://scifun.chem.wisc.edu/chemweek/pdf/CarbonDioxide.pdf>

14. Moore, J., Novel Concepts for the Compression of
Large Volumes of CO2. *ASME Turbo Expo* **2007**.

15. McCollum, D. L., Techno-Economic Models for Carbon Dioxide Compression, Transport, and Storage & Correlations for Estimating Carbon Dioxide Density and Viscosity
2006.

16. Yang, J. L.; Ma, Y. T.; Liu, S. C., Performance investigation of transcritical carbon dioxide two-stage compression cycle with expander. *Energy* **2007,** 32, (3), 237-245.

17. Ludtke, K. H., *Process Centrifugal Compressors*. Springer: 2004.

18. Wilson, D. G.; Korakianitis, T., *The design of High-Efficiency Turbomachinery and Gas Turbines*. 2 ed.; 1998.

19. Brown, R., *Compressors: Selection and Sizing*. 3rd ed.; Elsevier: 2005.

20. Dresser-Rand Surge Control. http://www.dresser-rand.com/controls/sc0498.htm

21. Brun, K.; Kurz, R., Operating in 'Choke'. *Turbomachinery International* **2007**.

22. Gericke, B. Conceptual Solutions, Oxy-Fuel.
<http://www.netl.doe.gov/technologies/coalpower/turbines/refshelf/asme/Conceptual%20Solutions%20Regarding.pdf>

23. Statoil Sleipner CO2 Injection Compressor. <http://www.netl.doe.gov/technologies/coalpower/turbines/refshelf/asme/asmeturbo07STATOILCO2.pdf>

24. Figueroa, J. D., CO2 Capture Guidelines. *International journal of greenhouse gas control* **2007,** 2, (9).

25. Perry, M.; Eliason, D. CO2 Recovery and Sequestration at Dakota Gasification Company. <http://www.gasification.org/Docs/Conferences/2004/11ELIA_Paper.pdf>

26. Rostam-Abadi, M., Assessment of Carbon Dioxide Options for Power plants. In *Fourth Annual Conference on CCS.* , 2005.

27. Anderson Jr, J. D., *Fundamentals of Aerodynamics*. 3rd ed.; McGraw-Hill 2001.

28. Bar-Meir, G., *Fundamentals of Compressible Flow Mechanics*. Potto Project: 2007.

29. OCW Shock types. <http://ocw.mit.edu/NR/rdonlyres/Mechanical-Engineering/2-26Spring2004/21F13A93-9CC8-4F33-9CDB-0DC46385631F/0/lec6.pdf>

30. NASA Shock Waves. http://www.grc.nasa.gov/WWW/K-12/airplane/oblique.html

31. Ramgen Ramgen Overview www.ramgen.com (Sept 2008),

32. Lawlor, S. Supersonic Compressor. http://patft.uspto.gov/netacgi/nph-Parser?Sect1=PTO2&Sect2=HITOFF&p=1&u=/netahtml/PTO/search-bool.html&r=0&f=S&l=50&TERM1=supersonic+compressor&FIELD1=&co1=AND&TERM2=&FIELD2=&d=PTXT

33. MITEI Selexol Report. rpfield@mit.edu

34. Ciferno *CO2 Capture: Comparison of Cost & Performance of Gasification and Combustion-based Plants*; NETL: 2007.

35. Bossel, U., Well-to-Wheel Studies, Heating Values and the Energy Conversation Principle. **2003**.

36. Schlumberger Mineral: Bituminous Coal. http://www.slb.com/modules/mnemonics/MineralDetail.aspx?code=Bituminous%20Coal

37. Jacobs *Impact of CO2 removal on Coal Gasification Based Fuel Plants*; Jacobs Consultancy: 2006.

38. EIA Average Retail Price of Electricity to Ultimate Customers by End-Use Sector, by State. http://www.eia.doe.gov/cneaf/electricity/epm/table5_6_b.html